AD-A040 200 NAVAL POSTGRADUATE SCHOOL MONTEREY CALIF F/G 20/8
ELECTROEXCITATION OF THE T = 1 NUCLEUS NI58 AND THE T = 2 NUCLE--ETC(U)
MAR 77 J S BEACHY, S J KOWALICK

UNCLASSIFIED NL

1 OF 2
ADA
040200





AD A040200

NAVAL POSTGRADUATE SCHOOL
Monterey, California



THESIS

ELECTROEXCITATION OF THE
T = 1 NUCLEUS ^{58}Ni AND THE T = 2 NUCLEUS ^{60}Ni
UP TO 50 MeV EXCITATION ENERGY

by

John Scott Beachy
and
Stephen Joseph Kowalick Jr.

March 1977

Thesis Advisors: F.R. Buskirk
R. Pitthan

AD No.
DDC FILE COPY

DDC
JUN 6 1977
C

Approved for public release; distribution unlimited.

UNCLASSIFIED

SECURITY CLASSIFICATION OF THIS PAGE (When Data Entered)

REPORT DOCUMENTATION PAGE		READ INSTRUCTIONS BEFORE COMPLETING FORM
1. REPORT NUMBER	2. GOVT ACCESSION NO.	3. RECIPIENT'S CATALOG NUMBER
4. TITLE (and Subtitle) Electroexcitation of the T = 1 Nucleus ^{58}Ni and the T = 2 Nucleus ^{60}Ni Up to 50 MeV Excitation Energy.		5. TYPE OF REPORT & PERIOD COVERED Master's Thesis; March 1977 6. PERFORMING ORG. REPORT NUMBER
7. AUTHOR(s) John Scott Beachy Stephen Joseph Kowalick Jr.		8. CONTRACT OR GRANT NUMBER(s)
9. PERFORMING ORGANIZATION NAME AND ADDRESS Naval Postgraduate School Monterey, California 93940		10. PROGRAM ELEMENT, PROJECT, TASK AREA & WORK UNIT NUMBERS
11. CONTROLLING OFFICE NAME AND ADDRESS Naval Postgraduate School Monterey, California 93940		12. REPORT DATE March 1977 13. NUMBER OF PAGES 146
14. MONITORING AGENCY NAME & ADDRESS(if different from Controlling Office)		15. SECURITY CLASS. (of this report) Unclassified 15a. DECLASSIFICATION/DOWNGRADING SCHEDULE

16. DISTRIBUTION STATEMENT (of this Report)

Approved for public release; distribution unlimited.

17. DISTRIBUTION STATEMENT (of the abstract entered in Block 20, if different from Report)

18. SUPPLEMENTARY NOTES

19. KEY WORDS (Continue on reverse side if necessary and identify by block number)

inelastic electron scattering, giant resonances, multipole transitions, nuclear transitions, LINAC, line shape fitting, ^{58}Nickel, ^{60}Nickel

20. ABSTRACT (Continue on reverse side if necessary and identify by block number)

Giant multipole resonances and bound states in ^{58}Ni and ^{60}Ni were studied with inelastic scattering of electrons at 102 MeV incident energy and scattering angles of 45, 60, 75, 90, and 105 degrees. In the energy interval from 5 to 50 MeV excitation energy, eleven and thirteen states or resonances were →

next page

DD FORM 1 JAN 73 1473 (Page 1)

EDITION OF 1 NOV 65 IS OBSOLETE

S/N 0102-014-6601

UNCLASSIFIED

SECURITY CLASSIFICATION OF THIS PAGE (When Data Entered)

(20. ABSTRACT Continued)

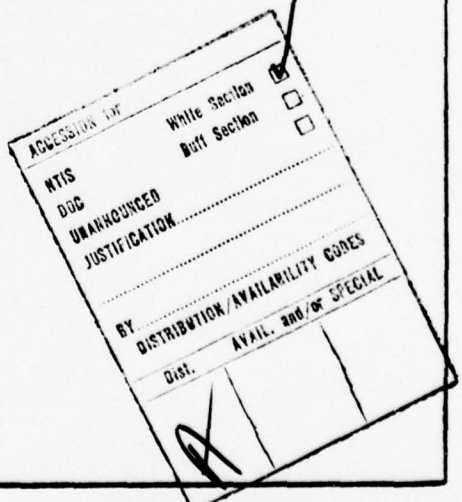
observed in ^{58}Ni and ^{60}Ni, respectively. ^{58}Ni resonances were observed at excitation energies of 6.0 (E2), 6.95 (E3), 9.6 (E4), 13.3 (E3), 15.1 (E4), 16.3 (E2), 18.3 (E1), 20.0 (E4), 21.75 (E1), 27.0 (E3), and 32.0 (E2) MeV. ^{60}Ni resonances were observed at excitation energies of 6.12 (E2), 7.05 (E3), 7.6 (E3), 8.7 (E3), 11.4 (E4), 12.8 (E3), 14.9 (E4), 16.2 (E2), 16.7 (E1), 18.6 (E4), 19.2 (E1), 27.1 (E3), and 32.0 (E2) MeV.

The following resonances were previously not known or differently classified:

^{58}Ni - 6.0 (E2), 9.6 (E4), 13.3 (E3), 15.1 (E4), 20.0 (E4), 27.0 (E3), and 32.0 (E2) MeV.

^{60}Ni - 6.12 (E2), 7.6 (E3), 8.7 (E3), 11.4 (E4), 12.8 (E3), 14.9 (E4), 18.6 (E4), 27.1 (E3), and 32.0 (E2) MeV.

Additionally, electroexcitation at low momentum transfer where the E1 cross section is predominantly excited shows a pronounced difference in cross section for ^{58}Ni when compared to ^{60}Ni and for (e,e') as compared to photon experiments.



Approved for public release; distribution unlimited.

Electroexcitation of the $T = 1$ Nucleus ^{58}Ni and the $T = 2$ Nucleus ^{60}Ni Up to 50 MeV Excitation Energy

by

John Scott Beachy
Lieutenant Commander, United States Navy
B.S., United States Naval Academy, 1966

and

Stephen Joseph Kowalick Jr.
Lieutenant Commander, United States Navy
B.S., United States Naval Academy, 1966

Submitted in partial fulfillment of the requirements for the degree of

MASTER OF SCIENCE IN PHYSICS

from the

NAVAL POSTGRADUATE SCHOOL
March 1977

Authors John Scott Beachy

Stephen Joseph Kowalick Jr.

Approved by: Fred R Buskirk
Thesis Co-Advisor

Rainer Pitthan
Thesis Co-Advisor

John M Dyer
Second Reader

K. E. Woehler
Chairman, Department of Physics and Chemistry

R R Fossum
Dean of Science and Engineering

ABSTRACT

Giant multipole resonances and bound states in ^{58}Ni and ^{60}Ni were studied with inelastic scattering of electrons at 102 MeV incident energy and scattering angles of 45, 60, 75, 90, and 105 degrees. In the energy interval from 5 to 50 MeV excitation energy, eleven and thirteen states or resonances were observed in ^{58}Ni and ^{60}Ni, respectively. ^{58}Ni resonances were observed at excitation energies of 6.0 (E2), 6.95 (E3), 9.6 (E4), 13.3 (E3), 15.1 (E4), 16.3 (E2), 18.3 (E1), 20.0 (E4), 21.75 (E1), 27.0 (E3), and 32.0 (E2) MeV. ^{60}Ni resonances were observed at excitation energies of 6.12 (E2), 7.05 (E3), 7.6 (E3), 8.7 (E3), 11.4 (E4), 12.8 (E3), 14.9 (E4), 16.2 (E2), 16.7 (E1), 18.6 (E4), 19.2 (E1), 27.1 (E3), and 32.0 (E2) MeV.

The following resonances were previously not known or differently classified:

^{58}Ni - 6.0 (E2), 9.6 (E4), 13.3 (E3), 15.1 (E4), 20.0 (E4), 27.0 (E3), and 32.0 (E2) MeV.

^{60}Ni - 6.12 (E2), 7.6 (E3), 8.7 (E3), 11.4 (E4), 12.8 (E3), 14.9 (E4), 18.6 (E4), 27.1 (E3), and 32.0 (E2) MeV.

Additionally, electroexcitation at low momentum transfer where the E1 cross section is predominantly excited shows a pronounced difference in cross section for ^{58}Ni when compared to ^{60}Ni and for (e,e') as compared to photon experiments.

TABLE OF CONTENTS

I. INTRODUCTION ---------- 11

II. BACKGROUND ---------- 13

III. THEORY ---------- 19

IV. DATA ACQUISITION ---------- 39

A. EXPERIMENTAL PROCEDURES ---------- 39

B. DATA ACCUMULATION ---------- 39

C. DATA REDUCTION ---------- 40

D. DATA ANALYSIS ---------- 41

E. ERRORS ---------- 43

V. RESULTS ---------- 45

A. THE GIANT DIPOLE RESONANCE (E1) ---------- 45

B. THE ISOSCALAR GIANT QUADRUPOLE RESONANCE (E2, $\Delta T = 0$) ---------- 48

C. THE ISOVECTOR GIANT QUADRUPOLE RESONANCE (E2, $\Delta T = 1$) ---------- 49

D. THE GIANT OCTUPOLE RESONANCE (E3) ---------- 51

E. OTHER STATES ---------- 57

VI. SUMMARY ---------- 60

LIST OF REFERENCES ---------- 141

INITIAL DISTRIBUTION LIST ---------- 146

LIST OF TABLES

I-A. Giant Dipole Resonances (E1) ---------- 63

I-B. Giant Isoscalar Quadrupole Resonances (E2, $\Delta T = 0$) ---------- 64

I-C. Giant Isovector Quadrupole Resonances (E2, $\Delta T = 1$) ---------- 65

I-D. Giant Resonances reported in the 13.0 MeV Excitation Energy Region ---------- 66

II. ^{58}Ni and ^{60}Ni Full Energy Weighted Sum Rules -- 67

III. ^{58}Ni Experimental Conditions ---------- 68

IV. ^{60}Ni Experimental Conditions ---------- 69

V. ^{58}Ni Resonances at 45° Scattering Angle ------- 70

VI. ^{60}Ni Resonances at 45° Scattering Angle ------- 70

VII. ^{58}Ni Resonances at 60° Scattering Angle ------- 71

VIII. ^{60}Ni Resonances at 60° Scattering Angle ------- 71

IX. ^{58}Ni Resonances at 75° Scattering Angle ------- 72

X. ^{60}Ni Resonances at 75° Scattering Angle ------- 72

XI. ^{58}Ni Resonances at 90° Scattering Angle ------- 73

XII. ^{60}Ni Resonances at 90° Scattering Angle ------- 73

XIII. ^{58}Ni Resonances at 105° Scattering Angle ------ 74

XIV. ^{60}Ni Resonances at 105° Scattering Angle ------ 74

XV. Collective Results for ^{58}Ni ---------- 75

XVI. Collective Results for ^{60}Ni ---------- 76

XVII. Shell model (RPA) predictions for excitation energy and strength of the E3 transitions ----- 77

LIST OF FIGURES

1. ^{58}Ni Full Inelastic Spectrum at 45° without background ---------- 78

2. ^{58}Ni Inelastic Spectra at 45° minus background and selected resonances ---------- 79

3. ^{58}Ni Full Inelastic Spectrum at 60° without background ---------- 80

4. ^{58}Ni Inelastic Spectra at 60° minus background and selected resonances ---------- 81

5. ^{58}Ni Full Inelastic Spectrum at 75° ---------- 82

6. ^{58}Ni Full Inelastic Spectrum at 75° without background ---------- 83

7. ^{58}Ni Inelastic Spectra at 75° minus background and selected resonances ---------- 84

8. ^{58}Ni Full Inelastic Spectrum at 90° ---------- 85

9. ^{58}Ni Full Inelastic Spectrum at 90° without background ---------- 86

10. ^{58}Ni Inelastic Spectra at 90° minus background and selected resonances ---------- 87

11. ^{58}Ni Full Inelastic Spectrum at 105° --------- 88

12. ^{58}Ni Full Inelastic Spectrum at 105° without background ---------- 89

13. ^{58}Ni Inelastic Spectra at 105° minus background and selected resonances ---------- 90

14. ^{60}Ni Full Inelastic Spectrum at 45° without background ---------- 91

15. ^{60}Ni Inelastic Spectra at 45° minus background and selected resonances ---------- 92

16. ^{60}Ni Full Inelastic Spectrum at 60° without background ---------- 93

17. ^{60}Ni Inelastic Spectra at 60° minus background and selected resonances ---------- 94

18. ^{60}Ni Full Inelastic Spectrum at 75° ---------- 95

19. ^{60}Ni Full Inelastic Spectrum at 75° without background ---------- 96

20. ^{60}Ni Inelastic Spectra at 75° minus background and selected resonances ---------- 97

21. ^{60}Ni Full Inelastic Spectrum at 90° ---------- 98

22. ^{60}Ni Full Inelastic Spectrum at 90° without background ---------- 99

23. ^{60}Ni Inelastic Spectra at 90° minus background and selected resonances ---------- 100

24. ^{60}Ni Full Inelastic Spectrum at 105° ---------- 101

25. ^{60}Ni Full Inelastic Spectrum at 105° without background ---------- 102

26. ^{60}Ni Inelastic Spectra at 105° minus background and selected resonances ---------- 103

27. Comparison of Total Cross Sections for ^{58}Ni and ^{60}Ni at 45° ---------- 104

28. Comparison of Total Cross Sections for ^{58}Ni and ^{60}Ni at 60° ---------- 105

29. E1 - E4 (Form Factors)^2 in comparison --------- 106

30. ^{58}Ni experimental inelastic form factors squared for state at 6.00 MeV ---------- 107

31. ^{58}Ni experimental inelastic form factors squared for state at 6.96 MeV ---------- 108

32. ^{58}Ni experimental inelastic form factors squared for state at 9.6 MeV ---------- 109

33. ^{58}Ni experimental inelastic form factors squared for state at 13.3 MeV ---------- 110

34. ^{58}Ni experimental inelastic form factors squared for state at 15.1 MeV ---------- 111

35. ^{58}Ni experimental inelastic form factors squared for state at 16.3 MeV ---------- 112

36. ^{58}Ni experimental inelastic form factors squared for state at 18.3 MeV ---------- 113

37. ^{58}Ni experimental inelastic form factors squared for state at 20.0 MeV ---------- 114

38. ^{58}Ni experimental inelastic form factors squared for state at 21.75 MeV ---------- 115

39. ^{58}Ni experimental inelastic form factors squared for state at 27.0 MeV ---------- 116

40. ^{58}Ni experimental inelastic form factors squared for state at 32.0 MeV ---------- 117

41. ^{60}Ni experimental inelastic form factors squared for state at 6.12 MeV ---------- 118

42. ^{60}Ni experimental inelastic form factors squared for state at 7.0 + 7.6 MeV ---------- 119

43. ^{60}Ni experimental inelastic form factors squared for state at 8.7 MeV ---------- 120

44. ^{60}Ni experimental inelastic form factors squared for state at 11.4 MeV ---------- 121

45. ^{60}Ni experimental inelastic form factors squared for state at 12.8 MeV ---------- 122

46. ^{60}Ni experimental inelastic form factors squared for state at 14.9 MeV ---------- 123

47. ^{60}Ni experimental inelastic form factors squared for state at 16.2 MeV ---------- 124

48. ^{60}Ni experimental inelastic form factors squared for state at 16.7 MeV ---------- 125

49. ^{60}Ni experimental inelastic form factors squared for state at 18.6 MeV ---------- 126

50. ^{60}Ni experimental inelastic form factors squared for state at 19.2 MeV ---------- 127

51. ^{60}Ni experimental inelastic form factors squared for state at 27.1 MeV ---------- 128

52. ^{60}Ni experimental inelastic form factors squared for state at 32.0 MeV ---------- 129

FIGURE CAPTIONS ---------- 130

ACKNOWLEDGEMENTS

As with many research projects of similar scope, the material of this publication has depended upon the efforts of many. We wish first to express our sincere appreciation to our advisors, Professors F.R. Buskirk and R. Pitthan. We have concluded that without their assistance and encouragement, our efforts in this work would have been futile. Professor Buskirk's able instruction in the classroom, coupled with his valuable suggestions during all phases of this project, has been fundamental to our knowledge and understanding of the theoretical physics associated with this work. Professor Pitthan's close association throughout our computer analysis and interpretation of results was essential to the completion of this research effort. His keen interest in our progress spurred our enthusiasm for this field of physics and scientific research in general. We wish to thank Professor J.N. Dyer for his able instruction in nuclear physics and for his valuable suggestions in the preparation of this manuscript.

We acknowledge the technical skill and ingenuity of Mr. H. McFarland and Mr. D. Snyder, who were responsible for the reliable operation of the Linac throughout our data acquisition.

Finally, we would like to thank our wives and families whose patience and encouragement gave us unmeasurable support during the course of this project.

I. INTRODUCTION

This work was conducted as part of an on-going research project which began at the Naval Postgraduate School's 120 MeV linear accelerator in 1973. Previous investigations of the giant resonance phenomena by inelastic electron scattering have been conducted in ^{197}Au, ^{208}Pb, ^{165}Ho, and ^{89}Y as reported in (WarW73), (FerW74), (Moor74), and (ShaS76). Our work is a continuation of that begun by DuBois and Bates (DuBB76) and is principally directed toward the comparison of the isotopes ^{58}Ni and ^{60}Ni in the giant resonance region.

$^{58,60}Ni$ isotopes are particularly interesting candidates for investigation since previous work with electron and hadron scattering and photonuclear reactions has revealed considerable structure in the giant resonance region. Additionally, isospin splitting of the isovector states has been predicted for nuclei such as $^{58,60}Ni$ with ground state isospin $T \neq 0$ (FalG65).

The first objective of this research was to identify the giant resonances in the 5 to 50 MeV region of ^{58}Ni. The second objective was to continue the analysis of the previously collected data for ^{60}Ni along with our additional data taken at 45° scattering angle with effort concentrated at the higher excitation energy regions of the spectra. Our third objective was to compare the two isotopes with

particular emphasis on the possible isospin splitting of isovector dipole (E1) and quadrupole (E2) transitions.

II. BACKGROUND

The elastic and inelastic scattering of high-energy electrons provides a means for the investigation of nuclear structure since the electro-magnetic interaction is known and the range of momentum transfer that can be produced by using primary electron energies of about 100 MeV and changing the scattering angle lead to cross sections that are sensitive to the spatial structure of the nuclear ground and excited states. The first major work involving the electron-scattering study of the nuclear levels in ^{58,60}Ni started with experiments done at the High Energy Physics Laboratory at Stanford University during 1960 (CraH61). Inelastic scattering of 183 MeV electrons through angles of 40°-90° was observed, leading to the excitation of discrete nuclear excited states in ^{58}Ni and ^{60}Ni. The excitation energies were below 8 MeV, and a Born approximation analysis of the measured inelastic form factors was used to determine the multipolarities. The important results of (CraH61) are: 1) the known E2 transitions, which in the even-even isotopes lead to the first excited states of ^{58}Ni and ^{60}Ni, were observed, 2) the form factors for the two isotopes of Ni (58 and 60) were found to be nearly identical for all momentum transfers investigated, including those in the regions where the measurements disagreed with the Born-approximation predictions, and 3) E4 transitions

in ^{58}Ni and ^{60}Ni were observed which had similar form factors.

In 1962, a study was made of the low-lying collective excitations in ^{58}Ni and ^{60}Ni at the Argonne National Laboratory (Broe63). Inelastic scattering of 43 MeV alpha particles was used to compare the relative strengths of the excited levels in both nickel isotopes at low excitation energies. Groups of states whose angular distributions resembled those of the collective E3 levels were seen at excitation energies of 6.8 MeV in ^{58}Ni and 6.2 MeV in ^{60}Ni.

In 1968, a study was made of the nuclear states of ^{58}Ni and ^{60}Ni at the Laboratory of Nuclear Science, Tohoku University, Sendai, Japan (Über71), where inelastic scattering of 183 and 250 MeV electron beams in the Tohoku 300 MeV linear accelerator produced data which were analyzed using the Born approximation and the Helm model to determine multipolarities and reduced transition probabilities. Working in the area from 1 to 8 MeV, Torizuka et al. found a total of fourteen states in ^{58}Ni located at excitation energies of 1.46(E2), 2.46(E4), 3.04(E2), 3.26(E2), 3.62(E4), 3.90(E2), 4.47(E4), 4.75(E4), 5.40(E4), 5.59(E4), 6.02(E3), 6.40(E3), 6.90(E3), and 7.20(E3) MeV. Eleven states in ^{60}Ni were identified at excitation energies of 1.33(E2), 2.16(E2), 2.50(E4), 3.12(E4), 3.67(E4), 4.04(E3), 4.86, 5.05(E4 + E6), 6.20(E3), 6.85(E3) and 7.05(E3) MeV. These low excitation energy results concurred quite favorably

with previous investigations of ^{60}Ni conducted by various research groups throughout the world using a variety of experimental procedures and data reduction techniques.

Also in 1968, experimental study in the giant resonance region above 10 MeV excitation energy was begun. Min and White (MinW68) reported measurements of photoneutron cross sections of separated ^{58}Ni and ^{60}Ni, and natural nickel samples in the excitation energy range from 10 to 26 MeV. These results suggested that in the theoretical treatment of the giant dipole resonance (E1) of the nickel isotopes in question, both in the absorption cross section and partial width calculations, it is necessary to take into account the different isospins since the cross sections of ^{58}Ni and ^{60}Ni determined were quite different in shape and integrated cross section. Min and White determined that the integrated (γ,n) cross section up to 25 MeV excitation energy exhausts 60% of the classical dipole (E1) sum rule in ^{60}Ni, but only 20% in ^{58}Ni. The results of Min and White (MinW68) were confirmed in 1974 by Fultz et al. (FulA74) where they determined that the total integrated (γ,n) cross section up to 33.5 MeV excitation energy exhausts 91% of the classical dipole (E1) sum rule in ^{60}Ni, but only 33% in ^{58}Ni.

For comparison to the results presented in this report, a survey was made of experiments since 1968 using ^{58,60}Ni targets where various methods were used to identify giant resonances above 10 MeV excitation energy. TABLE I (A

thru D) is divided into experimental results for the giant dipole resonances (E1), the giant quadrupole resonances (E2), both isoscalar and isovector, and resonances around 13 MeV reported from various experiments since 1968.

Miyase et al. investigated the isospin splitting of the E1 resonances in ^{58}Ni and ^{60}Ni by the (e,e'p) reaction in the excitation energy range between 10 and 34 MeV (MiyO73). Their findings are analogous to that of the (γ,p) reaction induced by bremsstrahlung; namely, that the sum of photon and neutron cross sections is equal for ^{58}Ni and ^{60}Ni. Fultz et al. (FulA74), however, point out that their results may be too large since both the (γ,Sn) and (γ,Xp) cross sections contain the (γ,pn) cross section, which may be counted twice and thus may constitute the dominant part of the high energy cross section in at least ^{58}Ni.

Gul'Karov et al. investigated the giant resonance region in ^{58}Ni and ^{60}Ni using electrons of about 200 MeV energy in the excitation energy region between 10 and 30 MeV (GulA69). Their results were found to be in agreement with the predictions of the dynamic collective model, (Drec68), and the giant resonance cross sections of both nickel isotopes were found to be about equal. This experiment, as we know now, was the first (e,e') experiment which excited the E2 giant resonance; but the identification of the multipolarity of this resonance was wrong.

The first in-depth studies of the E2 resonance by electron scattering were made at Darmstadt, Germany (PitW71, BusG72) and in Japan (FukT72). An interesting feature of these studies was that E2 (or E0) resonances were observed at an energy below the E1 resonance energy. Thus, in ^{90}Zr it turned out that E2 = 14.0 MeV, while E1 = 16.65 MeV, in ^{208}Pb, E2 = 10.7 MeV and E1 = 14.1 MeV, and in ^{139}La, ^{140}Ce, and ^{141}Pr, E2 = 12.0 MeV and E1 = 15.0 MeV. Gul'Karov et al. have reported an E1 resonance at 16.3 MeV in ^{60}Ni (GulA69, Gulk71, and Gulk73). Youngblood et al. and this report identify an E2 resonance in ^{60}Ni in the area of 16.4 MeV excitation energy with similar Γ and EWSR depletion values. TABLE I-B and FIGURE 47 refer.

Several papers, (TorK73, KocB73, ChaB75, and YouM76), have reported a resonance in the vicinity of 13 MeV excitation energy for $^{58,60}Ni$ as indicated in TABLE I-D, but except for (TorK73) and (Gulk73) no multipolarity has been assigned. FIGURES 33 and 45 of this work identify this resonance of ^{58}Ni and ^{60}Ni respectively as being E3. This result is of special importance, because a resonance at the corresponding energy of $53A^{-1/3}$ MeV has been proposed as a possible candidate for the E0 GR (breathing mode) in ^{208}Pb (PitB74), although an E2 assignment cannot be ruled out (SchF75).

The information from photoneutron cross sections as contained in (BerF75) coupled with the (α,α') measurements of (YouM76) were valuable aids in providing a starting

point for fitting the ^{58,60}Ni spectra, in particular, the E1 and E2 giant resonances.

III. THEORY

Inelastic electron scattering experiments are designed to study nuclear transitions by measuring the difference in energy between an incident electron beam and the electrons which are scattered from a target nucleus. While electrons are scattered by both elastic and inelastic collisions with the nucleus, it is the inelastically scattered electron which is of interest in experiments concerned with nuclear dynamics. During inelastic collisions, the momentum that is transferred to the nucleus excites it from the ground state to either a higher bound state or to an unbound state. The scattered electron loses an amount of momentum equal to that transferred to the nucleus; hence, an energy spectrum of the detected scattered electrons can determine the nuclear transitions which have occurred. If the transition is to a bound state, the nucleus will eventually decay to the ground state by emission of a photon. If the transition is to an unbound state, the nucleus may be transformed by particle emission.

The momentum transfer can be expressed by

$$\vec{q} = \vec{k}_1 - \vec{k}_2$$

where $\vec{q}$ is the momentum transfer vector and $\vec{k}_1$ and $\vec{k}_2$ are the incident and scattered electron momenta vectors,

respectively. Squaring both sides of the expression and neglecting the rest mass of the electron compared to the total energy leads to

$$c^2q^2 = 4E_iE_f \sin^2 (\theta/2)$$

or

$$q^2 = 4k_1k_2 \sin^2 (\theta/2)$$

where E_i and E_f are the energies of the incident and scattered electrons, and θ is the scattering angle. A significant advantage of electron scattering over photonuclear reactions for studying nuclear transitions is evident from this expression. The momentum transfer in electron scattering can be varied with incident electron energy or scattering angle. In this experiment, the incident energy was held constant while the scattering angle was changed. Varying momentum transfer permits exploration of transitions which may not be observed by photonuclear reaction and also permits an assignment of multipolarities to observed transitions by means of "form factors" which will be discussed later. Photonuclear reactions are limited to a momentum transfer q which is proportional to the nuclear excitation frequency ω of the excited state. It is, therefore, difficult to identify multipolarities of observed transitions, and the ground state of the nucleus cannot be probed. In

addition, photonuclear reactions do not significantly excite magnetic transitions.

Electron scattering enjoys two major advantages over hadron scattering (α,α'), (d,d'), (p,p'), etc. First, the interaction between the incident electron and the target nucleus is understood theoretically and can be treated with first order perturbation theory. Secondly, the interaction between the electron and the nucleus is not only a Coulomb interaction between charges but also an interaction of the current and magnetic moments of the nucleus with the electro-magnetic field of the passing electron. The electron, unlike the hadron, does not interact with the strong nuclear force of the nucleus. Analysis of electron scattering data, therefore, is unencumbered by approximations necessary in accounting for the imperfectly understood nuclear force. Another advantage of electron scattering over hadron scattering is the possibility of the excitation of the magnetic transitions at backward scattering angles (Fagg75).

One disadvantage of electron scattering is the appearance of the radiation tail which is caused mainly by photon emission from elastically scattered electrons. The strength of the radiation tail decreases with increasing scattering angle and incident energy. An additional source of background radiation is caused by electrons striking the slits of the analyzing magnet and the spectrometer walls. Since the inelastic spectrum is superimposed on this radiation tail, an accurate approximation of its effect must be made

in the line shape fitting program which resolves the inelastic resonances. The radiation tail in this experiment was calculated in the Born approximation (GinP64), but using correct elastic cross sections (FisR64). The approximation of the radiation tail constitutes the greatest uncertainty (10-30%) in inelastic scattering experiments in the continuum. The inelastic peaks also have radiation tails which are neglected for the Breit-Wigner line shape fits used in this analysis.

In order to describe theoretically electron scattering, one must solve the Dirac equation for the relativistic electron in the electrostatic field of the nucleus. For elastic electron scattering, the nucleus may be assumed to be a fixed and massive point charge without spin or magnetic moment. The electron is described as a Dirac free particle which accounts for its spin, magnetic moment, and its relativistic nature. By considering the interaction between the electron and nucleus in first order time-dependent perturbation theory (Born approximation), one can arrive at the familiar Mott scattering cross section for a point nucleus (See (Hofs63) for a complete development):

$$\left[\frac{d\sigma}{d\Omega}\right]_{\text{Mott}} = \left[\frac{Ze^2}{2E_i}\right]^2 \frac{\cos^2(\theta/2)}{\sin^4(\theta/2)} \qquad \text{(III-1)}$$

where

E_i = total energy of the incident electron

θ = scattering angle.

The effect of a finite nuclear charge distribution is to modify the cross section by a multiplication factor which is the Fourier transform of the charge distribution and is a function of momentum transfer q.

$$F(q) = \frac{1}{Ze} \int e^{-i\vec{K}\cdot\vec{r}} \rho(\vec{r}) \, d\tau \qquad \text{(III-2)}$$

where

$\vec{q} = \hbar \vec{K}$

r = nuclear radial coordinate

The Mott cross section is also corrected for recoil by including a recoil factor

$$R = \frac{1}{1 + \frac{2E_i}{Mc^2} \sin^2 (\theta/2)} \qquad \text{(III-3)}$$

where

M = mass of nucleus.

The differential cross section for elastic scattering now becomes

$$\frac{d\sigma_{el}}{d\Omega} = \left[\frac{Ze}{2E_i}\right]^2 \frac{\cos^2(\theta/2)}{\sin^4(\theta/2)} \frac{|F(q)|^2}{1 + \frac{2E_i}{Mc^2} \sin^2 (\theta/2)} \qquad \text{(III-4)}$$

The so-called elastic "form factor" F(q) can be expressed as the elastic cross section divided by the Mott cross section, corrected for recoil, or point charge cross section

$$|F(q)|^2_{2el} = \left| \frac{d\sigma_{el}}{d\Omega} \Big/ \frac{d\sigma}{d\Omega} \right|_{point} \qquad \text{(III-5)}$$

This expression was derived assuming a plane wave form for the incident and scattered electron. The Born approximation becomes increasingly inaccurate at higher Z. A more accurate approximation is used in this work. A phase shift analysis based on the partial wave expansion of the scattered wave function obtained from the Dirac equation was determined by Rawitscher (Rawi58). The calculation assumes that the potential acting on the electron is due to a static Coulomb interaction arising from a charge distribution. A complete description can be found in a thesis written by Dennis (Denn70). For the charge distribution of nuclei, a two parameter distribution is assumed (ZieP68):

$$\rho(r) = \rho_o \left[1 + \exp\left(\frac{r - c}{t/4.4}\right)\right]^{-1} \qquad \text{(III-6)}$$

where

ρ_o = normalized charge density

c = half-density radius

t = skin thickness measured between 10 and 90% of the charge distribution

r = nuclear radial coordinate.

The values of c and t were obtained from tabulated elastic electron scattering results in (deJd74). The elastic form factor squared, $|F(q)|^2_{el}$, can be determined from these values and is in turn used to obtain the inelastic form factor squared, $|F(q)|^2_{in}$, as follows. The ratio of the area of the inelastic peak, A_{in}, to the area of the elastic peak, A_{el}, is, with the exception of radiative corrections, equal to the ratio of the inelastic form factor squared to the elastic form factor squared. The computer code developed for fitting the experimental data determines the elastic and inelastic areas, uses the exact $|F(q)|^2_{el}$, calculated with the code of (FisR64) from the given values of c and t, and finally gives the inelastic cross sections (form factors):

$$|F(q)|^2_{in} = (A_{in}/A_{el}) \; |F(q)|^2_{el} \quad . \qquad \text{(III-7)}$$

The experimentally measured inelastic form factors must be compared with inelastic form factors which are calculated theoretically in order to determine multipolarities and transition strengths for observed resonances. It is, therefore, necessary to understand the theoretical development of inelastic electron scattering as well as elastic scattering.

In the plane wave Born approximation, the differential cross section $(d\sigma/d\Omega)_{PWBA}$ for nuclear excitation by inelastic

electron scattering can be written as a sum over cross-sections for electric (index E) and magnetic (index M) multipole transitions (Thei72),

$$(d\sigma/d\Omega)_{PWBA} = \sum_i (d\sigma/d\Omega)_{E\lambda} + \sum_i (d\sigma/d\Omega)_{M\lambda} \qquad \text{(III-8)}$$

where the cross sections for scattering of electrons of incident energy E_i (wave number k_i) through an angle θ into solid angle $d\Omega$, with momentum transfer q, is given by (IsaB63) as follows:

$$d\sigma_{E\lambda}/d\Omega = \frac{4\pi e^2(\lambda+1)}{\lambda[(2\lambda+1)!!]^2} \frac{q^{2\lambda}}{k_i^2} \left[\frac{\lambda}{\lambda+1} B(C\lambda,q,I_i \rightarrow I_f)V_L(\theta) + B(E\lambda,q,I_i \rightarrow I_f)V_T(\theta)\right] \qquad \text{(III-9)}$$

$$d\sigma_{M\lambda}/d\Omega = \frac{4\pi e^2(\lambda+1)}{\lambda[(2\lambda+1)!!]^2} \frac{q^{2\lambda}}{k_i^2} [B(M\lambda,q,I_i \rightarrow I_f)V_T(\theta)] \qquad \text{(III-10)}$$

where

λ = transition multipolarity

I_i and I_f = spins of the nuclear ground and excited states respectively.

The terms $V_L(\theta)$ and $V_T(\theta)$ depend only on the electron variables before and after scattering. When energy transfer is small compared with the initial and final electron energies ($k << k_1, k_2$), the angular distributions of

longitudinal and transverse virtual photons take the form

$$V_L(\theta) = \cos^2 \tfrac{1}{2}\theta / 4 \sin^4 \tfrac{1}{2}\theta \qquad \text{(III-11)}$$

$$V_T(\theta) = (1 + \sin^2 \tfrac{1}{2}\theta)/8 \sin^4 \tfrac{1}{2}\theta \qquad \text{(III-12)}$$

When the above expressions are substituted into equations for the electric and magnetic cross sections, (III-9) and (III-10), written in terms of Mott cross section, one obtains

$$d\sigma_{E\lambda}/d\Omega = \sigma_{Mott}[F_L^2(q) + (\tfrac{1}{2} + \tan^2 \tfrac{1}{2}\theta)\, F_T^2(q)] \qquad \text{(III-13)}$$

$$d\sigma_{M\lambda}/d\Omega = \sigma_{Mott}[\tfrac{1}{2} + \tan^2 \tfrac{1}{2}\theta]\, F_T^2(q) \qquad \text{(III-14)}$$

where $F_L^2(q)$ and $F_T^2(q)$ are the inelastic form factors for longitudinal and transverse photon absorption. It is evident that the magnetic cross section is expected to become increasingly more prominent as the scattering angle is increased towards 180°. The decomposition of the inelastic form factors is obtained from equations (III-9) and (III-10). The longitudinal form factor is a sum of terms of the electric type

$$|F_L^{E\lambda}(I_i \to I_f, q)|^2 = \frac{4\pi q^{2\lambda}}{Z^2[(2\lambda+1)!!]^2} B\,[C\lambda, q, I_i \to I_f] \qquad \text{(III-15)}$$

where λ can take integral values from 0 to ∞. The B values represent the reduced nuclear transition probabilities which

are an indication of the strength of the transition or resonance and are defined by Theissen (Thei72) in the more general case as

$$B(\lambda,q,I_i \rightarrow I_f) = (2I_i+1)^{-1} |\langle I_f || M(\lambda,q) || I_i \rangle|^2 \qquad \text{(III-16)}$$

where $M(\lambda,q)$ is the transition operator. The matrix element of the transition operator for the longitudinal electric or Coulomb interaction is related to the transition charge density $\rho_{tr}(\vec{r})$, through

$$\langle I_f | M(C\lambda,q) | I_i \rangle = \left[(2\lambda+1)!!\right] q^{-\lambda} \int d\vec{r} j_\lambda(qr) Y_{\lambda\mu}(\Omega) \rho_{tr}(\vec{r}) \qquad \text{(III-17)}$$

The matrix elements representing the transverse electric and magnetic interaction (denoted by *E* and *M*, respectively) are expressed in terms of the transition current density, $\vec{j}_{tr}(\vec{r})$, and the transition magnetization density, $\vec{\mu}_{tr}(\vec{r})$, as follows:

$$\langle I_f | M(E\lambda,q) | I_i \rangle = \left[(2\lambda+1)!!\right] q^{-\lambda-1} \int d\vec{r} [\nabla X j_\lambda(qr) \vec{Y}_{\lambda\lambda\mu}(\Omega) \vec{j}_{tr}(\vec{r}) + q^2 j_\lambda(qr) \vec{Y}_{\lambda\lambda\mu}(\Omega) \vec{\mu}_{tr}(r)] \qquad \text{(III-18)}$$

$$\langle I_f | M(M\lambda,q) | I_i \rangle = \left[(2\lambda+1)!!\right] q^{-\lambda} \int d\vec{r} [j_\lambda(qr) \vec{Y}_{\lambda\lambda\mu}(\Omega) \vec{j}_{tr}(\vec{r}) + (\nabla X j_\lambda(qr) \vec{Y}_{\lambda\lambda\mu}(\Omega)) \vec{\mu}_{tr}(\vec{r})] \qquad \text{(III-19)}$$

In equations (III-17) thru (III-19), $j_\lambda(qr)$ is the spherical Bessel function of the order λ, and where the terms $Y_{\lambda\mu}(\Omega)$ and $\vec{Y}_{\lambda\lambda\mu}(\Omega)$ are the spherical and vector spherical harmonic functions, respectively. If $qr < 1$, the spherical Bessel functions in the transition operators may be represented by a power series in qr. In this manner, reduced transition probabilities may be defined in the same way as the radiative transition probabilities and are obtained in this particular case by the substitution (IsaB63)

$$r_k^{\lambda} \rightarrow \frac{(2\lambda+1)!!}{q^{\lambda}} j_\lambda(qr_k) \qquad \text{(III-20)}$$

Thus in the limit of small qr (long wave limit),

$$B(C\lambda) = (2\lambda+1)\left|\int r^{\lambda} \rho_{tr}(\vec{r})\, r^2 dr\right|^2 . \qquad \text{(III-21)}$$

The $B(C\lambda)$ term gives the strength of the transitions occurring due to Coulomb interaction between the charges of the electron and nucleus, while $B(E\lambda)$ and $B(M\lambda)$ give strengths of convection current and magnetization contributions, respectively. However, the continuity equation relates transition charge density and convection current density. Therefore, often the $B(E\lambda)$ values are given instead of the $B(C\lambda)$ values. Both values are equal at the photon point according to the Siegert Theorem (Uber71), which is a direct consequence of the continuity equation. The B-values

given in this work are the $B(E\lambda, q = 0)$, which are less than one per cent different from the $B(E\lambda, q = k)$, e.g., for an El transition at 16 MeV. As indicated in (IsaB63), the magnetization and current contributions will be much smaller than the charge contribution for collective transitions, i.e., giant resonances. It is emphasized that at forward angles one should expect that the transitions in the giant resonance region are primarily due to Coulomb interaction.

The accuracy of the plane wave Born approximation is not sufficient for analysis of present-day inelastic scattering data from medium and heavy nuclei. The necessary improvement in accuracy of theoretical calculations of inelastic scattering can be obtained by accounting for the distorting effect that the Coulomb field has on the incident and scattered electron waves. This is done by the distorted wave Born approximation (DWBA). Phase shift analysis of wave functions obtained from numerical solutions of the Dirac equation is accomplished using a computer code such as that developed by Griffy, Biedenharn, Reynolds, Onley, and Wright, known as GBROW (Über71). Five conditions are assumed in the GBROW code:

(1) the transition is of an electric multipole character,

(2) the ground state is spherically symmetric,

(3) nuclear recoil energy is negligible compared to the excitation energy,

(4) the interaction involved is free of polarization or dispersion effects, and

(5) the excited state charge distribution is not significantly distorted from the ground state (ZieP68).

Since the transition potential of the nucleus has to be determined, one must resort to a model to calculate the nuclear potential in DWBA calculations. Giant resonance phenomena, which occur when nucleons are excited collectively within the nucleus, were first described by Goldhaber and Teller (GolT48), who made three alternative assumptions when proposing their model in 1948 (see also Migd44): (1) They assumed that the restoring forces for protons, displaced from their original positions, are proportional to the displacements and that the proportionality constant is the same for every proton in all nuclei. This implies that the frequency of dipole resonances is the same for all nuclei. (2) They assumed that protons and neutrons on the surface of the nuclei have fixed positions with respect to each other. Motion of protons and neutrons inside the nucleus causes density changes in proton fluid and neutron fluid. Restoring forces per unit mass will, therefore, are proportional to gradients of these densities. For a given displacement in the nucleus, the maximum density change is inversely proportional to $1/R^2$. Since the frequency of nuclear resonances must vary as the square root of the restoring force, it must be proportional to $1/R$ or the inverse cube root of the nuclear mass ($A^{-1/3}$). (3) They

assumed that protons and neutrons behave as two interpenetrating incompressible fluids. During dipole vibrations, the two fluids undergo relative displacements so that near the surface the two fluids no longer overlap. The total restoring force is proportional to R^2. Hence, the frequency of harmonic motion is proportional to the square root of the force over mass,

$$\omega \sim \left(\frac{R^2}{R^3}\right)^{1/3} = R^{-1/2}$$

or (III-22)

$$\omega \sim A^{-1/6}$$

It is the second alternative which is generally called the Goldhaber-Teller model and which was used in this work.

Überall notes that experimental data for the giant dipole resonance are described by $35.3\ A^{-1/6}$ MeV (Über71). Excitation energies in this paper are reported in units of $A^{-1/3}$ which are the more common units used for comparison between nuclei. The transition charge density assumed by the G-T model is given by

$$\rho_{tr}(r) = C_{GT} \cdot r^{\lambda-1} d\rho_o/dr \qquad \text{(III-23)}$$

where $\rho_o(r)$ = charge density of the ground state.

Überall generalized the G-T model by making two modifications to the original assumptions in order to permit the model to include magnetic transitions and the electric monopole transition. (1) Überall assumed that the nucleus contains four instead of two fluids, namely, neutrons with spin up, neutrons with spin down, protons with spin up, and protons with spin down. (2) He included a surface deformation scale factor, η, in the expression for the ground state charge density which could account for the electric monopole and other resonances of higher multipolarity which have been observed. The generalized G-T model gives a total charge density as

$$\rho(r) = \rho_o(r) + \rho_{tr}(r) \qquad \text{(III-24)}$$

where $\rho_{tr}(r) = -\eta r^{\lambda} \left[\frac{d\rho_o(r)}{dr} \right]$

η = surface deformation scale factor

λ = transition multipolarity

The transition charge density describes that part of the nucleus that takes part in the interaction. For example, surface oscillations would only affect those nucleons on or near the surface of the nucleus. The term ρ_{tr} would, in this case, have an appreciable amplitude only at a radius in the region of the surface. The rest of the nucleus would remain undisturbed, i.e., $\rho(r) \approx \rho_o(r)$ for single particle transitions (DuBB76).

It will be recalled that the objective of using DWBA and the G-T model was to calculate (model dependent) inelastic form factors. Plots of $|F(q)|^2_{DWBA}$ versus momentum transfer q were obtained from the GBROW computer code for electric dipole (E1), quadrupole (E2), etc., transitions as shown in figure 29. The inelastic form factors squared, $|F(q)|^2_{in}$, obtained from the solution of equation (III-7) in the analysis of the experimental data by the computer fitting program, were also plotted against momentum transfer. Comparison of the experimental plots with the theoretical curves is used to determine the multpolarity of the transitions as indicated in figures 30 through 52. Since the DWBA program normalizes the wave functions to a $B(E\lambda) = 1e^2fm^{2\lambda}$, $|F(q)|^2_{DWBA}$ is used as a divisor of $|F(q)|^2_{in}$ to yield the reduced electric transition probability, $B(E\lambda)$, as seen in the relation

$$B(E\lambda) = \frac{|F(q)|^2_{in}}{|F(q)|^2_{DWBA}} \quad . \qquad \text{(III-25)}$$

As stated previously, giant resonances are collective transitions. An indication of the relative degree of collectivity of observed transitions can be obtained by dividing the reduced transition probability values, $B(E\lambda)$, by the single particle reduced transition probability value, $B_{sp}(E\lambda)$. The value $B_{sp}(e\lambda)$ is defined by (SkoH66) as

$$B_{sp}(E\lambda)\uparrow = \frac{(2\lambda+1)}{4\pi}\left(\frac{3R_o^{\lambda}}{\lambda+3}\right)^2 \quad fm^{2\lambda} \qquad \text{(III-26)}$$

$$SPU = B(E\lambda)/B_{sp}(E\lambda)$$

where $R_o = 1.2A^{-1/3}$.

This single particle estimate, although model dependent, can provide an indication of strength of the collective excitation. The SPU values for the transitions observed in this work appear in the final results, TABLES XV and XVI.

A more general characterization of nuclear transition strength can be obtained by using the energy weighted sum rule (EWSR). The EWSR is preferred, in electron scattering analysis, over other sum rules because its theoretical limit essentially depends on the nuclear charge distribution in the ground state which is known (NatN66). Warburton and Weneser (WarW69) give the electric dipole (E1) EWSR as

$$S(E1) = E_x \cdot B(E1) = \frac{9\hbar^2}{8\pi M_p}\frac{NZ}{A} \qquad \text{(III-27)}$$

where M_p = mass of proton.

Nathan and Nilsson state the sum rule for isoscalar transitions of $\lambda > 1$ as

$$S(E\lambda) = E_x \cdot B(E\lambda) = \frac{\lambda(2\lambda+1)^2\hbar^2 Z}{8\pi M_p}\langle R^{2\lambda-2}\rangle \qquad \text{(III-28)}$$

where $\langle R^{2\lambda-2} \rangle$ was calculated by numerical integration from values of c and t obtained from (deJd74). The division of the strength between isoscalar ($\Delta T = 0$) and isovector ($\Delta T = 1$) transitions was based on the usual assumption that a fraction Z/A goes into the isoscalar transition and the remaining strength N/A goes into the isovector part. The accuracy of this assumption rests on the validity of the hydrodynamic model. The full EWSR values used in this work are found in the collected results, TABLES XV and XVI.

There has been considerable interest over the past decade in the effect of isospin splitting of isovector giant resonances. Isospin is the term which expresses the degree of symmetry of the nuclear wave function in the nucleus. Isospin for a nucleus in the ground state is determined by the expression $T = (N - Z)/2$ which gives $T = 1$ for ^{58}Ni and $T = 2$ for ^{60}Ni. The electric dipole (E1) selection rules for a nucleus with ground state isospin $T_o \neq 0$ allows transitions to states with $T = T^< \equiv T_o$ and $T = T^> \equiv T_o + 1$. A general assumption is that $T^<$ states in the E1 giant resonance decay preferentially via neutron emission since proton emission tends to be inhibited by the Coulomb barrier. For $T^>$ states, however, neutron decay to the $T = T_o - \frac{1}{2}$ ground state of the daughter nucleus is inhibited by isospin conservation. $T^>$ states should decay by proton emission, predominately, if the states involved are good isospin eigenstates (FulA74). The $T^>$ states are predicted to lie higher in energy than the $T^<$ states by an amount given by

$$\Delta E = E(T^{>}) - E(T^{<}) = U_D(1 + T_o^{-1}) \qquad \text{(III-29)}$$

where U_D is a symmetry energy for dipole states which Akyuz and Fallieros have expressed in (AkyF71) as

$$U_D \cong \bar{V}(T_o/A) = 60(T_o/A) \text{ MeV.} \qquad \text{(III-30)}$$

From experimental data collected on nuclei near nickel, Paul et al. have determined an empirical value of $\bar{V} = 58 \pm 5$ MeV (PauA71). The split in energy predicted by equation (III-25) is 2.1 MeV for ^{58}Ni and 3.0 MeV for ^{60}Ni.

Fallieros and Goulard have predicted the ratio of transition strengths between the $T^{>}$ and $T^{<}$ states in (FalG70).

$$I^{>}/I^{<} = \frac{T_o^{-1} - 3/2\ A^{-2/3}}{1 + 3/2A^{-2/3}} \qquad \text{(III-31)}$$

The relation leads to values of $I^{>}/I^{<} = 0.8$ for ^{58}Ni and $I^{>}/I^{<} = 0.36$ for ^{60}Ni. Fallieros and Goulard state, however, that their prediction is based on the shell model which does not accurately describe transitions which lie in the continuum above the threshold for particle emission. Neither does it account for normal isospin impurities induced directly by the residual Coulomb interaction. Both $T^{>}$ and $T^{<}$ states interact with the continuum proton states, which

implies that they effectively interact with each other (FalG70). This interaction of $T^>$ and $T^<$ gives rise to the possibility of mixing of the $T^>$ and $T^<$ resonances. The calculations of Ngo-Trong and Rowe (NgoR71) and Tanaka (Tana71) also indicate mixing of $T^>$ and $T^<$ dipole transitions in nickel isotopes. Tanaka, using various oscillator potentials for the shell model with multiple particle-hole interactions, concluded that: (1) Ratios of excitation strengths of the $T^>$ states relative to the $T^<$ states are unity in ^{58}Ni and $\frac{1}{2}$ in ^{60}Ni, independent of the potential assumed, (2) In ^{58}Ni, the $T^<$ state decays predominantly by proton emission with an exception in one case when one of the three potentials which Tanaka assumed is used. In ^{60}Ni, the $T^<$ state decays mostly be neutron emission with one exception noted in the model also. For the $T^>$ state, proton and neutron decay compete in both nuclei. The results of calculations by Ngo-Trong and Rowe are also based on the shell model and multiple particle-hole assumptions and are qualitatively similar to those of Tanaka.

IV. DATA ACQUISITION

A. EXPERIMENTAL PROCEDURE

The physical layout and operational procedures used during the data collection for this publication are contained in (BarC66) and (WarW73). Previous thesis works, (DuBB76) and (ShaS76), describe the major improvements made at the NPS Linac since 1973 which include the change from oil diffusion pumps to ion vacuum pumps and the use of a ten-channel scintillation counter ladder for the counting system.

Plateau curves for the entire counting system were measured and the delay curves were optimized. The energy calibration for the magnetic spectrometer was determined by two separate ^{12}C calibration runs where the know excitation energy of the 15.1 MeV state was used.

B. DATA ACCUMULATION

Self-supporting foils of ^{58}Ni and ^{60}Ni, with a target thickness of about 135.0 mg/cm^2 and enriched to more than 99%, obtained from the Oak Ridge National Laboratory at Oak Ridge, Tenn. were used. The target was placed in the scattering chamber and positioned for transmission geometry at an angle equal to one-half the scattering angle. In addition to the data measured by DuBois and Bates, (DuBB76), experiments were performed to have a complete data set at

45°, 60°, 75°, 90°, and 105° scattering angles for both isotopes.

The magnetic fields in both the accelerator deflection system and the spectrometer were saturated before the runs in order to ensure experimental reproducibility. Several trial runs were made prior to the actual data acquisition in an effort to check and reduce background in the counting system. In all experimental runs, the count rates were maintained below 50 counts per second per channel to avoid losses due to electronic dead time in the ladder counter system. Tables III and IV list the experimental conditions used for each run.

Additionally, prior to and at the completion of both the elastic and inelastic spectrum runs at all angles, in which the scattered electron energies were measured in 0.1 MeV steps, check points were established and measured in 2 MeV steps in order to determine if there were significant differences in the various spectra due to machine fluctuations during the course of the 36 to 48 hour data collection periods. The count rates were reproducible and thus showed the stability of the experimental conditions.

C. DATA REDUCTION

The single counter spectra for the ten counters of the counter ladder were written on a 7-track magnetic tape. Some preliminary data reduction was done on-line with the aid of an Altair 8800 micro-computer. The IBM 360/67'

on-line system was then used for text editing and final data reduction. All other calculations were performed on the IBM 360/67' off-line facility.

D. DATA ANALYSIS

In analyzing our data for ^{58,60}Ni, the following criteria were used to determine a reasonable fit:

(1) The data and calculated spectrum must coincide visually.

(2) The χ^2 per degree of freedom must be close to one. χ^2 is defined as

$$\chi^2 = \sum^{n} (x_i - x_o)^2/\sigma_i^2$$

where x_i is the calculated value of cross section, x_o is the measured value of the cross section, and σ_i is standard deviation associated with x_i. The errors are not strictly statistical because the detector momentum interval is larger than the momentum increment of the spectrometer field and hence correlations exist between energy bins.

(3) All observed resonances must consistently fit spectra for all angles.

When fitting the ^{58}Ni or ^{60}Ni data, each spectrum was fitted piecemeal; that is, our fittings started in the Giant Dipole Resonance (GDR) region from 12 to 24 MeV excitation energy and then they were expanded upward and downward as the fittings progressed.

For a given resonance, excitation energy (E_x), width (FWHM), and peak height (PH) were allowed to adjust (free fit) for a best fit in a given excitation energy range. The initial starting points for a given El or E2 resonance of ^{58}Ni or ^{60}Ni are contained in the Results section of this report. The plot section output from the fitting program was then examined, the fitted PH was recycled as starting values for the next fitting, and other parameters such as E_x or FWHM were freed as deemed necessary. This iterative technique was repeated, and various E_x, FWHM, and/or PH combinations were added and/or shifted with each fitting in an attempt to improve the χ^2 per degree of freedom.

Consistent improvement in the fit was best achieved by working with the data from several angles simultaneously. For a given isotope, one set of E_x, FWHM, and PH values was used for all angles, and changes in this combination at a given angle were made only when the χ^2 per degree of freedom improved for that particular angle. Examination of subsequent Fit Program printouts at a greater excitation energy range revealed positions and approximate widths of other resonances needed to fit the data for each spectrum. After numerous iterations, uniformly good χ^2 values were obtained and assignments of multipolarities were made. Tables V thru XIV contain the fitting results for each angle of the ^{58}Ni and ^{60}Ni spectra.

It is to be noted that a resonance located at ~8 MeV at all angles in both ^{58}Ni and ^{60}Ni has been identified as

a "ghost". This "ghost" occurs since the spectrometer does not have an open back thus producing an appreciable ghost peak. This peak is superimposed on any inelastic scattering spectrum, at a point where the magnetic field is low enough so that the numerous elastically-scattered electrons hit the inside of the spectrometer chamber and scatter indirectly into the counters. In our spectrometer, the ghost peak appears at an energy of 92% of that of the elastic peak, is known through measurements in ^{12}C, and thus can be accounted for in the evaluation, although this introduces an additional uncertainty for the cross sections in the 7-9 MeV region at forward angles. The area ratios of the ghost peaks (inelastic/elastic) were found to be $(2.1 \pm 0.1) \times 10^{-2}$ and $(1.3 \pm 0.2) \times 10^{-2}$ during the measurements of ^{58}Ni and ^{60}Ni, respectively.

E. ERRORS

As various E_x, FWHM, and PH combinations were fit to the five spectra of ^{58}Ni and ^{60}Ni at 45°, 60°, 75°, 90°, and 105°, obvious variations in E_x and FWHM were noted. These variations showed a systematic behavior as the fitting range was increased. A definite correlation was noted between background and the resulting transition strength. Our total background was described by the following functions of energy E_f of the outgoing electron:

$$(1) \quad BGR(E_f) = P_1 + P_2 \cdot 1/E_f + P_3 \cdot RT$$

or

$$(2) \quad BGR(E_f) = P_1 + P_2(E_f - E') + P_3 \cdot RT$$

with the P_i being fitting parameters, E' being the energy center of the fitting range, and RT being the calculated radiation tail (PitB77). Throughout the analysis of the data for the ^{58}Ni and ^{60}Ni spectra, it was found that similar results were obtained when either equation (1) or (2) was used in the fitting program to calculate total background for the limited fitting range of 10 to 50 MeV. More consistent EWSR depletion results were achieved in the full fitting range (5 to 50 MeV) when equation (2) was used. Thus, all experimental results for ^{58}Ni and ^{60}Ni listed in this report are based on equation (2) for the calculation of total background.

All the GRs evaluated in this experiment above 10 MeV were fit by a Breit-Wigner line shape. The total errors presented in this report and listed in Tables I(A thru D), XV, and XVI are the total estimated error obtained from the fluctuations in the B-values and excitation energies experienced during the fitting of ^{58}Ni and ^{60}Ni.

V. RESULTS

Eleven transitions in ^{58}Ni and thirteen transitions in ^{60}Ni have been identified in this report as summarized in Tables XV and XVI. The resonances are discussed below according to their assigned multipolarities.

A. THE GIANT DIPOLE RESONANCE (E1)

As indicated in the theory and background sections, there has been considerable investigation of ^{58}Ni and ^{60}Ni in the GR region. It will be evident from the following that the results are fairly contradictory. Transitions at 18.3 and 21.75 MeV in ^{58}Ni were identified as GDRs based on momentum transfer dependence (See Figures 36 and 38). It will be noted that the transition strengths of these resonances in the 90° and 105° spectra were fixed to the mean of the EWSR values obtained at the forward three angles (This is denoted by the symbol Δ in Figures 30 through 52.). This procedure is justified since the contribution of the GDR to the spectra of the backward two angles becomes increasingly insignificant as can be seen in Figure 29. Figures 2 and 4 demonstrate the effect of extricating the dipole resonances for ^{58}Ni from the spectra at 45° and 60°. The prominence of the 18.3 and 21.75 MeV resonances is evident from the lower plot in both figures. E1 resonances have been reported anywhere between 17.3 MeV and 21.9 MeV as indicated in the background summary

Table I-A. While Torizuka et al. report that 99% of the EWSR is exhausted by a resonance at 18.5 MeV, our EWSR exhaustion is 61 ± 6%. The energy of the 21.75 MeV resonance is in agreement with the excitation energy of the (γ,n) data of (GorI70), 21.9 MeV, which, however, is in disagreement with the (γ,n) results of (FulA74). Ishkhanov et al., finally report with (γ,p) a GDR at 21.4 MeV with a width of 10.0 MeV which exhausts 66% of the EWSR. The total EWSR depletion for GDR in ^{58}Ni observed in this report is 87%. The difference in energy between the GDRs is 3.45 MeV. This is significantly more than the predicted value of 2.1 MeV for isospin splitting of the $T^{>}$ and $T^{<}$ states (see equation III-29). The ratio of transition strengths between the 21.75 MeV and the 18.3 MeV resonances is 0.4 which is a factor of two lower than that predicted by Fallieros and Goulard (see equation III-31).

Transitions at 16.7 MeV and 19.2 MeV were identified as GDRs in ^{60}Ni based on momentum transfer dependence (Figures 48 and 50). Note that the transition strength of the GDR has been fixed in the 105° spectrum for the 16.7 MeV resonance and has been fixed in the 90° and 105° spectra for the 19.2 MeV resonances. The dominant contribution of the GDRs and the fit of the 16.7 and 19.2 MeV resonances is apparent from Figures 15 and 17. The GDRs reported in (FulA74) at 16.3 and 18.51 MeV were used as initial fitting values. Both excitation energy and width (FWHM) were fitted to obtain consistent results at all angles. The 16.3 MeV

transition strength is in agreement with the (γ,n) result of (FulA74) but totally in disagreement with the values reported for width and strength in (GulA69), (Gulk71), and (Gulk73). Gul'Karov et al. report a width of 4.1 MeV which is nearly a factor of two greater than either our results or those of Fultz et al. This explains partly the great difference in EWSR depletion, i.e., 16 ± 4% as reported herein, compared with 90 ± 15% reported in (Gulk73). The remainder of the difference is explained by the failure of (Gulk73) to recognize and subtract the E2 strength at 16.5 MeV. The excitation energy of the 19.2 MeV transition is in statistical agreement with the GDR reported in (Miy073), however, the strength is a factor of three larger in EWSR depletion than those reported by Miyase et al. The excitation energy of the GDR at 18.51 MeV reported in (FulA74), which was used as a starting value, agree with our results, but their strength is much larger. Of the two remaining experiments listed in Table I-A, the (γ,n) data of (GorI70) show a resonance at 20.7 MeV which expends 69% EWSR, and agree with our results, while the (γ,p) results of (IshK70) agree statistically with neither this work nor any other. The difference in energy for the two identified parts of the GDR in this report in ^{60}Ni is 2.5 MeV which is close to the 3.0 isospin splitting predicted by equation III-25. The ratio of transition strengths between the 19.2 and 16.3 MeV resonances is 3.1 which is not in agreement with the value of 0.36 predicted by equation III-31. It

is interesting to note that the higher energy GDR has about three times the strength of the lower GDR in ^{60}Ni, while the opposite is nearly true for ^{58}Ni. Our results yield a combined GDR transition strength of 68% EWSR depleted for ^{60}Ni, which is lower than the EWSR depletion of 80% reported in (FulA74) for the (γ,n) channel alone.

An interesting comparison is seen for the cross sections of ^{58}Ni and ^{60}Ni in the spectra of 45° and 60° in Figures 27 and 28, respectively. It is apparent that ^{58}Ni has a greater cross section than ^{60}Ni in the region of the GDRs (87% in ^{58}Ni compared with 68% in ^{60}Ni). The decreasing difference in cross section observed in, first the 45° and then the 60° spectrum, and the absence of such a significant difference at the backward angles also suggest that the effect is related to the GDRs which are most pronounced at the forward angles. This effect has not been seen in previous experiments.

B. THE ISOSCALAR GIANT QUADRUPOLE RESONANCE (E2, $\Delta T = 0$)

The isoscalar giant quadrupole resonance at an excitation energy of $63A^{-1/3}$ MeV, which is just below the GDR, has been found in numerous nuclei with $A > 40$. This resonance was identified in the work reported here in ^{58}Ni at 16.3 ($63A^{-1/3}$) MeV with a width (FWHM) of 4.5 ± 0.4 MeV and a transition strength of 50 ± 10% EWSR. Our results agree with the results reported in (YOUM76), which were used as starting values, as well as all other previous results (MoaB73, KocB73, TorK73, and ChaB75) as summarized in Table I-B. The cross sections plotted as a function of

momentum transfer (Figure 35) show the E2 character of this resonance. The transition strength was held constant at 45° which is justified by the small contribution of the E2 transition at 45° as seen in Figure 29. The lower spectrum of Figure 7 shows the excellent fit of the 16.3 MeV resonance.

The isoscalar quadrupole resonance in ^{60}Ni was identified at 16.2 ($63A^{-1/3}$) MeV with a width of 4.7 ± 0.3 MeV and a transition strength of 50 ± 10% EWSR. This result is close to the starting value taken from (YouM76) as indicated in Table I-B. The momentum transfer dependence (Figure 47) favors the quadrupole assignment. The lower plot of Figure 20 shows the 16.2 MeV resonance after the E1 and E3 resonances in the 75° spectrum, where Figure 29 indicates the quadrupole should be strongest, have been subtracted. Results for ^{58}Ni and ^{60}Ni are summarized in Table I-B.

C. THE ISOVECTOR GIANT QUADRUPOLE RESONANCE (E2, $\Delta T = 1$)

The giant quadrupole resonance predicted in (Mott60) at about $130A^{-1/3}$ MeV is less well known than the resonance at $63A^{-1/3}$ MeV. Isovector resonances are only weakly excited by proton scattering and not at all by α-particle scattering. Hence, the $T = 1$ transitions must be investigated mainly by radiative capture and electron scattering. A resonance at 32.0 ± 1.0 ($124A^{-1/3}$) MeV was identified in ^{58}Ni. The momentum transfer dependence (Figure 40) slightly favors a quadrupole assignment. An anomalous dip in the 60°

spectrum between 33 and 36 MeV (see Figure 3) required keeping the transition strength of this resonance constant. This limited the data to the three backward angles. The lower plot of Figure 7, however, reveals the distinct and broad resonance centered at 32.0 MeV. This is a good indication of the E2 character, since the quadrupole contribution is strongest at 75°. Our results are not in good agreement with previous results which have been reported for ^{58}Ni (Gulk74 and TorK73), as seen in Table I-C. The width is difficult to determine accurately for this resonance since it is both high in excitation energy and broad. If it is assumed to be 8.0 MeV wide, which is the smallest value found to fit the data, 28 ± 9 % of the EWSR is concentrated in this state. This value changes to 40 ± 11 % EWSR when the width is increased to 10.0 MeV, which is the value found to produce the most consistent fit at all angles.

A quadrupole resonance was also identified at 32.0 ($125A^{-1/3}$) MeV in ^{60}Ni. The form factors squared plot (Figure 52) favors a quadrupole assignment. It is noted, however, that the transition strength was fixed at 60° and 105°. A free fit of this resonance at 60° produced a consistently low EWSR depletion relative to the neighboring angles, particularly when the 27.0 MeV resonance was included. The EWSR depletion was consistently high at 105° when the 32.0 MeV resonance was permitted to be fit freely, as indicated in Figure 52. The broad resonance centered at

32.0 MeV is evident in the lower plot of Figure 20, which is the spectrum at 75° from which the quadrupole resonances have been subtracted. Again, the quadrupole assignment to the 32.0 MeV resonance is supported by its predominance at 75° which is where the quadrupole is expected to be strongest among all multipolarities. The EWSR depletion was 40 ± 15 % for a width of 9.0 ± 2.0 MeV which was found to produce the most consistent results at all angles. When the width was increased to 11.0 MeV, 45 ± 11 % EWSR depletion was obtained. While a quadrupole resonance was reported at 28.5 ± 0.3 MeV by Gul'Karov, no other information was presented (Gulk74). This excitation energy is too low to adequately fit our data as can be seen in Figures 18 and 19. It is interesting to note that the EWSR depletion is the same for both ^{58}Ni and ^{60}Ni in the case of both quadrupole resonances, i.e., 50% for $63A^{-1/3}$ MeV and 40% for $125A^{-1/3}$ MeV.

D. THE GIANT OCTUPOLE RESONANCE (E3)

Since low-lying octupole states in nuclei exhaust only a small fraction of the EWSR, it has been theorized that more strength should be expected at higher excitation energies (Mott60). In particular, additional $1\hbar\omega$ strength has been predicted to lie at about $30A^{-1/3}$ MeV in heavy nuclei by Hamamoto (Hama72). She, among others, has described the isoscalar and isovector strength based on the concepts of the Bohr-Mottelson self-consistent model. Her

results for a good shell model nucleus (i.e., magic configuration) are given in Table XVII. Since the shell model allows both $1\hbar\omega$ and $3\hbar\omega$ transitions for octupole excitations, the composite strength is more complex than in the case of quadrupole excitations for which only $2\hbar\omega$ is available for transitions into high-lying states. The E3 strength is, therefore, more widely distributed and more difficult to locate.

Figures 10 and 13 indicate the presence of a resonance centered at 27.0 ($105A^{-1/3}$) MeV excitation energy with a width of 6.0 ± 1.0 MeV (FWHM) in the ^{58}Ni spectra at 90° and 105°. The momentum transfer dependence of this resonance (see Figure 39) would be consistent with both an E2 and E3 assignment. The E3 assignment is favored instead of the E2 assignment, in view of the absence of the resonance at 45° and its very weak contribution at 60°, which required fixing the transition strength to obtain a consistent fit. Figure 29 illustrates this reasoning. It is interesting to note that this resonance was not detected until the full range spectra were analyzed carefully. Examination of Figures 8 and 11 indicate the difficulty of identification of broad resonances in the higher excitation energies at the backward angles. A surprising agreement of this resonance excitation energy with the isoscalar $3\hbar\omega$ octupole resonance predicted by Hamamoto is seen in Table XVII. The transition strength that we observed (13 ± 2 % EWSR exhausted) is much lower than the predicted value of 78%

EWSR expended. The shell model, upon which Hamamoto's predictions rest, is expected to yield accurate results for heavy magic nuclei, e.g., ^{208}Pb and ^{88}Sr. Failure of the shell model to describe adequately the semi-magic medium nuclei, ^{58,60}Ni, is a possible explanation for the difference in transition strength between observed and expected values.

A similar resonance was identified in ^{60}Ni at 27.1 ($106A^{-1/3}$) MeV excitation energy and with a width of 6.0 ± 1.2 MeV (FWHM). This transition is clearly evident in Figures 23 and 26 which are spectra of 90° and 105°. The momentum transfer dependence (see Figure 51) favors the E3 assignment, although neither an E2 nor an E4 assignment can be entirely discounted. Support for an E3 assignment is found in 1) the E3 assignment for similar resonance in ^{58}Ni, 2) the decreasing error bars at backward angles, and 3) the agreement with predicted values of excitation energy. The transition strength (23 ± 5 % EWSR expended) is nearly twice as great as that observed in ^{58}Ni but still less, by a factor of three, than that predicted in (Hama72) for the isoscalar ($105A^{-1/3}$) octupole resonance (see Table XVII). Naturally, there could be more non-resonant E3 strength in this area, which we could not detect by the evaluation method used.

As indicated in Table XVII, an isovector $1\hbar\omega$ state is predicted at $52A^{-1/3}$ MeV excitation energy. At 13.3 ± 0.2 ($51A^{-1/3}$) MeV excitation energy, we identified an E3 state

of relatively small width (Γ = 1.5 ± 0.2 MeV) in ^{58}Ni which carries 13 ± 1 % EWSR (E3, $\Delta T = 0$). The prominence of this well-defined transition is evident from Figures 8, 9, and 10 for the 90° spectra and Figures 11, 12, and 13 for the 105° spectra of ^{58}Ni. The E3 assignment is apparent from the fit of the experimental form factors squared plot in Figure 33. The constant value of transition strength is justified for an E3 state at 45°. The transition strength predicted by Hamamoto (see Table XVII) again is much stronger. Several reports have indicated the presence of a state at about 13.0 MeV excitation energy (see Table I-D). Torizuka et al. identified E2 states of very narrow widths (Γ = 0.6 in both cases) at 13.2 and 14.0 MeV excitation energy in their (e,e') results (TorK73) which are not in agreement with ours. A transition at about 13.5 MeV excitation energy and with a width of about 2.0 MeV was identified as an E2 or E0 in the (p,p') results of Kocher et al. (KocB73). This result agrees in excitation energy and width with both our results and the (d,d') results of Chang et al. (ChaB75), who mention a transition observed at about 13.0 MeV excitation energy and about 2.0 MeV in width. Additionally, the (α,α) results Youngblood et al. (YouM76) show indications of substructure at 13.3 MeV excitation energy in both ^{58}Ni and ^{56}Fe. It is interesting to note the variety of hadron scattering experiments which have detected this resonance. This must cast some doubt upon the isovector nature of this state.

A similar state in ^{60}Ni was identified at 12.8 ± 0.2 ($50A^{-1/3}$) MeV with a width of 1.5 ± 0.2 MeV which has a transition strength of 8 ± 2 % EWSR (E3, $\Delta T = 0$). This resonance is clearly indicated and well-defined in the spectra of 90° and 105° of ^{60}Ni (see Figures 21 thru 26) in a manner similar to ^{58}Ni. The momentum transfer dependence, Figure 45, favors an E3 assignment which is consistent with the multipolarity of the equivalent state in ^{58}Ni. This transition is in agreement with the excitation energy for the $1\hbar\omega$ (E3, $\Delta T = 1$) state predicted by Hamamoto but a factor of four greater in strength (see Table XVII). Again, the model dependence of transition strengths in Table XVII may be the reason for this difference. The (e,e') results of Gul'Karov (Gulk73) contain an E2 transition at 13.0 ± 0.3 MeV excitation energy, which agrees statistically with our results. The width (Γ = 4.1 ± 0.3 MeV), however, is in disagreement compared to all other results listed in Table I-D.

Lower in energy, we find a state at 6.96 ± 0.1 ($27A^{-1/3}$) MeV with a width of 0.8 ± 0.1 MeV and a strength of 12 ± 2 % EWSR in ^{58}Ni. This state first appears as a resolved peak in the spectrum at 60° (Figure 4) and becomes increasingly dominant in strength at the backward angles. It is particularly well-defined in the spectra of 90° and 105° (Figures 8 thru 13). The E3 assignment for this state conforms to the momentum transfer dependence as indicated in Figure 31. The excitation energy of this state agrees with the value

predicted by Hamamoto for the $1\hbar\omega$ state and with the E3 state at 6.9 MeV reported by Torizuka et al. (Über71). It must be noted, however, that Torizuka reported an additional E3 state at 7.2 MeV excitation energy which was not observed in our results.

In ^{60}Ni, the lower energy E3 strength is divided among three states at 7.05 ± 0.1 ($28A^{-1/3}$), 7.6 ± 0.2 ($30A^{-1/3}$), and 8.7 ± 0.2 ($34A^{-1/3}$) MeV respectively, all with narrow widths as seen in Table XVI. These states can be best located in Figures 19 and 22 where they are the second, third, and fourth narrow peaks in excitation energy. Since the 7.05 and 7.6 MeV states were hardly resolved in our data, the results for these two states were summed to yield the momentum transfer dependence seen in Figure 42 which favors an E3 assignment. The momentum transfer dependence of the state at 8.7 ($34A^{-1/3}$) MeV excitation energy, also, favors an E3 assignment (see Figure 43). Thus, the lower energy E3 strength (12 ± 2 % EWSR) is concentrated in a narrow state at about $27A^{-1/3}$ MeV excitation energy in ^{58}Ni, but the same strength (14 ± 3 % EWSR) is distributed among three narrow states, centered at a higher excitation energy of about $30A^{-1/3}$ MeV in ^{60}Ni. Octupole-octupole (0-0) coupling such as that suggested by Moss et al. to describe E3 states near $32A^{-1/3}$ MeV in nuclei from ^{90}Zr to ^{154}Sm (MosY76) is a possible explanation for this difference in structure between the nuclei ^{58}Ni and ^{60}Ni.

E. OTHER STATES

Several other states, which have not yet been discussed, are identified in our results (see Tables XV and XVI).

At 6.0 ± 0.1 ($23A^{-1/3}$) MeV excitation energy, we see a well-defined state in spectra of all five angles of ^{58}Ni. An E2 assignment was made based on the momentum transfer dependence depicted in Figure 30. It should be noted that the values for 45° was omitted from Figure 30 since it was much higher than in the remaining four angles due to the large effect of the ghost peak at 45° in this excitation energy region. A strength of 6 ± 1 % EWSR was determined for this state. Torizuka et al. reported a state at an excitation energy of 6.02 MeV, which is consistent with our results; however, an E3 assignment is given in their report (Über71).

A similar state is also seen at 6.12 ± 0.1 ($24A^{-1/3}$) MeV excitation energy in spectra of all five angles of ^{60}Ni. Figure 41 shows the momentum transfer dependence of this resonance which favors an E2 assignment. This state carries 5 ± 1 % EWSR which is consistent with the analogous E2 state in ^{58}Ni. An E3 state at an excitation energy of 6.2 MeV was reported by Torizuka et al., which is again consistent in excitation energy; however, an E3 assignment does not agree with our results (Über71).

Two resonances were identified in ^{58}Ni at excitation energies of 15.1 ± 0.2 ($58A^{-1/3}$) and 20.0 ± 0.7 ($77A^{-1/3}$) MeV. Plots of form factors squared, which were limited to

the two backward angles, favored an E4 assignment for each transition (see Figures 34 and 37). As indicated in Table XV, the resonance at 15.1 MeV was found to expend 37 ± 12 % EWSR, while the resonance at 20.0 MeV was found to contain 42 ± 13 % EWSR. Hence, a total of 79% EWSR is exhausted by these two resonances. It is recognized that this analysis, based on limited data, must be viewed cautiously. However, as indicated in Figures 10 and 13, additional structure, which cannot be accounted for by the resonances which have been discussed previously, is evident in the spectra of 90° and 105°. A consistent fit can be obtained for these angles, only, when the two resonances identified above are included. Neither of these resonances have been previously reported.

Examination of the spectra of ^{60}Ni at 75°, 90°, and 105°, from which the low multipolarity resonances have been subtracted, reveals two additional structures centered at about 15 MeV and 19 MeV excitation energy (see Figures 20, 23, and 26). Consistent results can be obtained in the 90° and 105° spectra only by fitting two resonances, one located at 14.9 ± 0.2 ($58A^{-1/3}$) MeV with a width of 2.1 ± 0.2 MeV and the other at 18.6 ± 0.2 ($73A^{-1/3}$) MeV with a width of 4.0 ± 0.4 MeV. In the 75° spectrum, the strength of these resonances had to be fixed to the mean value of their strengths at the backward angles to obtain a consistent fit. The momentum transfer dependence for these transitions indicate an E4 assignment for both (see Figures 46 and 49). The transition strength for the resonance

located at 14.9 MeV was determined to be 18 ± 5 % EWSR. The higher energy E4 resonance at 18.6 MeV was found to expend 38 ± 12 % EWSR. Neither of these resonances has been reported in previous literature.

A final state was detected in the 90° and 105° spectra of ^{60}Ni at 11.4 ± 0.2 ($45A^{-1/3}$) MeV excitation energy with a width of 1.2 ± 0.2 MeV. While limited to two data points, an assignment of E4 was given to this state based on the momentum transfer dependence (see Figure 44) and the association of this state with only the backward two angles. No previous evidence was found for this state. The total E4 strength found in ^{60}Ni was approximately 60% EWSR, whereas, the total E4 strength in ^{58}Ni was about 84% EWSR.

After the ghost peak was properly evaluated in the spectrum of ^{58}Ni at 45°, a structure was detected at an excitation energy of 11.5 MeV and a width of 4.7 MeV as indicated in Figures 1 and 2. An insignificant contribution from this structure was found in the spectra of 60° (the structure can be barely discerned by careful examination of the lower two spectra of Figure 4). While no evidence of this structure was seen in either the 75° or 90° spectra, it again was detected in the 105° spectrum with significant strength (see Figures 12 and 13). Since this behavior does not conform to that of any multipolarity considered (i.e., E1 thru E4), as indicated in Figure 29, this structure was evaluated as a possible magnetic transition for which our evaluation methods are not adequate.

VI. SUMMARY

We have analyzed the excitation range between 5 and 50 MeV in ^{58}Ni and ^{60}Ni. Our general objectives were two-fold, 1) to search for resonance structure in the continuum of both nuclei, and 2) to compare these nuclei, particularly with respect to possible isospin phenomena. Our collected results are found in Tables XV and XVI, respectively.

The following results deserve special emphasis:

1) Comparison of the total cross sections of ^{58}Ni and ^{60}Ni measured at low momentum transfer, where mainly E1 is excited, showed surprisingly different results compared with the total E1 cross sections which have been determined previously by summing (γ,n) and (γ,p) cross sections. The total ^{58}Ni cross section contains 87% EWSR and is centered in two resonances around 18 and 22 MeV. The total ^{60}Ni cross section composes 60% EWSR and is divided into structures at 17 and 19 MeV.

2) The isovector dipole (E1 strength was found to be divided into two resonances in both nuclei which may be attributable to isospin interaction. Our results, however, are not adequately explained by current theory. The isospin splitting phenomenon in medium-weight nuclei deserves further experimental investigation and theoretical work.

3) The giant isoscalar quadrupole (E2, $\Delta T = 0$) was identified at $63A^{-1/3}$ MeV excitation energy with a strength of about 50% EWSR in both nuclei. Our results agreed with previously reported results.

4) The giant isovector quadrupole (E2, $\Delta T = 1$) was identified at 32.0 MeV with a strength of about 40% in both nuclei. Our results are not in agreement with the limited previous data reported for this resonance in ^{58}Ni and ^{60}Ni.

5) A significant difference in the structure of the high-lying branch of the isoscalar ($1\hbar\omega$) E3 excitation at about $30A^{-1/3}$ MeV was observed in ^{58}Ni and ^{60}Ni. While strength of this lower energy E3 state remained nearly constant at about 13% for both nuclei, it was concentrated in a single narrow state at 6.96 MeV in ^{58}Ni and distributed among three states located at 7.05, 7.6, and 8.7 MeV in ^{60}Ni. This phenomenum had not previously been observed in ^{58}Ni or ^{60}Ni.

6) A state at about $50A^{-1/3}$ MeV was identified for the first time as E3 in both nuclei and found to agree in excitation energy with the predicted isovector E3 state.

7) A previously unknown resonance centered at about 27 MeV in both ^{58}Ni and ^{60}Ni was identified as E3 and found to agree in excitation energy, but not in strength with the predicted isoscalar E3 at $105A^{-1/3}$ MeV.

8) Two resonances located at $58A^{-1/3}$ MeV and $77A^{-1/3}$ MeV in ^{58}Ni were identified as E4 and found to

compose a total of 84% isoscalar EWSR. Three E4 resonances in ^{60}Ni were identified at $45A^{-1/3}$ MeV, $58A^{-1/3}$ MeV, and $73A^{-1/3}$ MeV and found to contain a total of about 60% EWSR. All of these resonances are reported here for the first time.

TABLE I-A. GIANT DIPOLE RESONANCES (E1)

ISO-TOPE	REFERENCE	EXCITATION ENERGY (MeV)	WIDTH (FWHM) (MeV)	EWSR DEPLETION (%)	REACTION
^{58}Ni	(GulA69)	17.3 ± 0.2	6.4 ± 0.3	----------	(e,e')
	(GorI70)	21.9 ± 0.3	----------	36 ± 3	(γ,n)
	(IshK70)	21.4 ± 0.3	10.0	66 ± 7	(γ,p)
	(MiyO73)	18.5	----------	55 ± 15	(e,e'p)
	(TorK73)	18.5	5.0	99 ± 10	(e,e')
	(FulA74)	17.3	----------	33	(γ,n)
	This Work	18.3 ± 0.2	4.2 ± 0.4	61 ± 6	(e,e')
		21.75 ± 1.0	5.0 ± 0.5	26 ± 7	(e,e')
^{60}Ni	(GulA69)	16.3 ± 0.2	5.9 ± 0.3	----------	(e,e')
	(GorI70)	20.7 ± 0.3	----------	69 ± 6	(γ,n)
	(IshK70)	22.6 ± 0.3	----------	36 ± 6	(γ,p)
	(Gulk71)	16.3 ± 0.2	----------	----------	(e,e')
	(Gulk73)	16.3 ± 0.2	4.1 ± 0.3	90 ± 15	(e,e')
	(FulA74)	16.3	2.44	91 { 15 }	(γ,n)
		18.51	6.37	{ 76 }	(γ,n)
	(MiyO73)	19.5	----------	23 ± 7	(e,e'p)
	This Work	16.7 ± 0.2	2.1 ± 0.2	16 ± 4	(e,e')
		19.2 ± 0.5	6.0 ± 0.8	52 ± 5	(e,e')

TABLE I-B. GIANT ISOSCALAR QUADRUPOLE RESONANCES (E2, $\Delta T = 0$)

ISO-TOPE	REFERENCE	EXCITATION ENERGY (MeV)	WIDTH (FWHM) (MeV)	EWSR DEPLETION (%)	REACTION
^{58}Ni	(MoaB73)	≈16.0	----------	----------	(3He,3He')
	(KocB73)	16.5 ± 0.5	4.2 ± 0.5	50 ± 10	(p,p')
	(TorK73)	16.3	≈4.5	57 ± 6	(e,e')
	(ChaB75)	16.0 ± 0.5	4.5 ± 0.3	45 ± 10	(d,d')
	(YouM76)	16.4 ± 0.3	4.9 ± 0.2	55 ± 15	(α,α')
	This Work	16.3 ± 0.2	4.5 ± 0.4	50 ± 10	(e,e')
^{60}Ni	(LewB72)	≈16.0	----------	----------	(p,p')
	(YouM76)	16.6 ± 0.3	5.0 ± 0.4	63 ± 15	(α,α')
	This Work	16.2 ± 0.2	4.7 ± 0.3	50 ± 10	(e,e')

TABLE I-C. GIANT ISOVECTOR QUADRUPOLE RESONANCES (E2, $\Delta T = 1$)

ISO-TOPE	REFERENCE	EXCITATION ENERGY (MeV)	WIDTH (FWHM) (MeV)	EWSR DEPLETION (%)	REACTION
^{58}Ni	(Gulk74)	28.3 ± 0.3	----------	----------	(e,e')
	(TorK73)	29.0	----------	11 ± 1	(e,e')
	This Work	32.0 ± 1.0	10.0 ± 2.0	40 ± 11	(e,e')
^{60}Ni	(Gulk74)	28.5 ± 0.3	----------	----------	(e,e')
	This Work	32.0 ± 1.0	9.0 ± 2.0	40 ± 15	(e,e')

TABLE I-D GIANT RESONANCES REPORTED IN THE 13 MeV EXCITATION ENERGY REGION

ISO-TOPE	REFERENCE	EXCITATION ENERGY (MeV)	WIDTH (FWHM) (MeV)	Eλ	EWSR DEPLETION (%)	REACTION
^{58}Ni	(TorK73)	13.2	0.6	E2	7.4 ± 0.7	(e,e')
	(TorK73)	14.0	0.6	E2	4.8 ± 0.7	(e,e')
	(KocB73)	≈13.5	≈2.0	--	----------	(p,p')
	(ChaB75)	≈13.0	≈2.0	--	----------	(d,d')
	(YouM76)	13.3	----------	--	----------	(α,α')
	This Work	13.3 ± 0.2	1.5 ± 0.2	E3	13 ± 1	(e,e')
^{60}Ni	(GulA69)	13.4 ± 0.3	----------	--	----------	(e,e')
	(Gulk73)	13.0 ± 0.3	4.1 ± 0.3	E2	----------	(e,e')
	This Work	12.8 ± 0.2	1.5 ± 0.2	E3	8 ± 2	(e,e')

TABLE II. ^{58}Ni and ^{60}Ni FULL ENERGY WEIGHTED SUM RULES

	^{58}Ni	^{60}Ni
$E\lambda$	$EWSR_{2\lambda}$ (MeV $fm^{2\lambda}$)	$EWSR_{2\lambda}$ (MeV $fm^{2\lambda}$)
E1	$2.16X10^{2}$	$2.23X10^{2}$
E2	$3.40X10^{4}$	$3.40X10^{4}$
E3	$2.10X10^{6}$	$2.10X10^{6}$
E4	$1.29X10^{8}$	$1.29X10^{8}$

Note: The E1 EWSR's listed above for ^{58}Ni and ^{60}Ni are isovector ($\Delta T = 1$). For the division of the sum rule strengths into isoscalar ($\Delta T = 0$) and isovector ($\Delta T = 1$) parts, the assumption was made that a fraction Z/A goes into the isoscalar and the remainder N/A goes into the isovector part. The values $\langle r^2 \rangle^{\frac{1}{2}} = 3.835$ fm, $\langle r^4 \rangle^{\frac{1}{4}} = 4.194$ fm, and $\langle r^6 \rangle^{1/6} = 4.528$ fm were used for the E2, E3, and E4 sum rules, respectively, in both isotopes.

TABLE III. ^{58}Ni EXPERIMENTAL CONDITIONS

^{58}Ni	Target Thickness = 134.6 mg/cm^2				Incident Energy = 102.0 MeV				
Spectrometer Angle in Degrees	Elastic Spectrum Spectrometer Energy Range	Inelastic Spectrum Spectrometer Energy Range	Capacitor Setting (μf)		Integrator Range Scale in Volts		Average Beam Current in Amperes		Elastic Momentum Transfer Squared (q^2) in fm^2
			Elastic	In-Elastic	Elastic	In-Elastic	Elastic	In-Elastic	
45	106.0 - 96.0 MeV	99.0 - 60.0 MeV	0.1	0.1	0.1	10.0	7.0×10^{-8}	1.4×10^{-7}	0.158
60	106.0 - 96.0 MeV	99.0 - 60.0 MeV	0.1	0.1	0.1	30.0	3.6×10^{-7}	7.0×10^{-7}	0.270
75	106.0 - 96.0 MeV	98.0 - 50.0 MeV	1.0	1.0	0.1	10.0	8.6×10^{-7}	1.0×10^{-6}	0.400
90	106.0 - 97.0 MeV	97.0 - 60.0 MeV	1.0	1.0	1.0	10.0	5.4×10^{-7}	1.0×10^{-6}	0.530
105	106.0 - 97.0 MeV	100.0 - 60.0 MeV	1.0	1.0	3.0	10.0	9.0×10^{-7}	1.1×10^{-6}	0.674

TABLE IV. ^{60}Ni EXPERIMENTAL CONDITIONS

^{60}Ni Target Thickness = 135.0 mg/cm^2									Incident Energy = 102.0 MeV
Spectrometer Angle in Degrees	Elastic Spectrum Spectrometer Energy Range	Inelastic Spectrum Spectrometer Energy Range	Capacitor Setting (μf)		Integrator Range Scale in Volts		Average Beam Current in Amperes		Elastic Momentum Transfer Squared (q^2) in fm^2
			Elastic	In-Elastic	Elastic	In-Elastic	Elastic	In-Elastic	
45	106.0 - 96.0 MeV	99.0 - 60.0 MeV	0.1	0.1	0.1	10.0	5.4×10^{-8}	1.6×10^{-7}	0.158
60	103.0 - 98.0 MeV	98.0 - 60.0 MeV	0.1	0.1	0.1	30.0	3.6×10^{-7}	8.6×10^{-7}	0.268
75	103.0 - 98.0 MeV	98.0 - 50.0 MeV	1.0	1.0	0.1	10.0	8.6×10^{-7}	9.3×10^{-7}	0.400
90	103.0 - 97.0 MeV	97.0 - 50.0 MeV	1.0	1.0	1.0	30.0	6.1×10^{-7}	1.6×10^{-6}	0.539
105	103.0 - 98.0 MeV	98.0 - 50.0 MeV	1.0	1.0	1.0	10.0	7.1×10^{-7}	1.3×10^{-6}	0.679

TABLE V. ^{58}Ni RESONANCES AT 45° SCATTERING ANGLE

E (MeV)	Q (fm^{-1})	MULTIPOLARITY (Eλ)	FORM FACTOR SQUARED	B VALUE ($fm^{2\lambda}$)
6.00	.387	E2	$6.70X10^{-4}$	$6.32X10^{2}$
6.95	.386	E3	$2.74X10^{-4}$	$7.51X10^{4}$
8.08	.384	Ghost	$7.08X10^{-3}$	--------
11.5	.379	----	$5.13X10^{-4}$	--------
13.3	.377	E3	$3.24X10^{-5}$	$9.97X10^{3}$
16.3	.374	E2	$4.93X10^{-4}$	$5.03X10^{2}$
18.3	.372	E1	$1.22X10^{-3}$	$3.51X10^{0}$
21.75	.370	E1	$3.60X10^{-4}$	$2.52X10^{0}$

TABLE VI. ^{60}Ni RESONANCES AT 45° SCATTERING ANGLE

E (MeV)	Q (fm^{-1})	MULTIPOLARITY (Eλ)	FORM FACTOR SQUARED	B VALUE ($fm^{2\lambda}$)
6.11	.387	E2	$1.40X10^{-4}$	$1.31X10^{2}$
8.08	.384	Ghost	$4.50X10^{-3}$	--------
16.2	.374	E2	$4.42X10^{-4}$	$4.46X10^{2}$
16.6	.374	E1	$3.01X10^{-4}$	$2.10X10^{0}$
20.0	.371	E1	$7.31X10^{-4}$	$5.13X10^{0}$
32.0	.368	E2	$1.63X10^{-4}$	$1.76X10^{2}$

TABLE VII. ^{58}Ni RESONANCES AT 60° SCATTERING ANGLE

E (MeV)	Q (fm^{-1})	MULTIPOLARITY (Eλ)	FORM FACTOR SQUARED	B VALUE ($fm^{2\lambda}$)
4.55	.508	----	$4.19X10^{-5}$	--------
5.98	.505	E2	$3.02X10^{-4}$	$1.68X10^{2}$
6.95	.503	E3	$1.95X10^{-4}$	$1.69X10^{4}$
8.08	.500	Ghost	$3.25X10^{-3}$	--------
11.5	.493	----	$2.06X10^{-5}$	--------
13.3	.489	E3	$9.90X10^{-5}$	$9.71X10^{3}$
16.3	.483	E2	$7.87X10^{-4}$	$4.68X10^{2}$
18.3	.480	E1	$8.47X10^{-4}$	$6.37X10^{0}$
21.75	.474	E1	$3.00X10^{-4}$	$2.24X10^{0}$
27.0	.466	E3	$4.87X10^{-5}$	$5.66X10^{3}$
32.0	.460	E2	$3.71X10^{-4}$	$2.41X10^{2}$

TABLE VIII. ^{60}Ni RESONANCES AT 60° SCATTERING ANGLE

E (MeV)	Q (fm^{-1})	MULTIPOLARITY (Eλ)	FORM FACTOR SQUARED	B VALUE ($fm^{2\lambda}$)
6.12	.503	E2	$2.34X10^{-4}$	$1.30X10^{2}$
7.12	.501	E3	$1.34X10^{-4}$	$1.18X10^{4}$
7.95	.499	Ghost	$2.54X10^{-3}$	--------
12.9	.489	E3	$4.89X10^{-5}$	$4.75X10^{3}$
16.2	.482	E2	$5.97X10^{-4}$	$3.57X10^{2}$
16.6	.482	E1	$1.91X10^{-4}$	$1.44X10^{0}$
19.0	.477	E1	$9.62X10^{-4}$	$7.18X10^{0}$
27.0	.465	E3	$8.63X10^{-5}$	$1.03X10^{4}$
32.0	.459	E2	$3.20X10^{-4}$	$2.06X10^{2}$

TABLE IX. ^{58}Ni RESONANCES AT 75° SCATTERING ANGLE

E (MeV)	Q (fm^{-1})	MULTIPOLARITY ($E\lambda$)	FORM FACTOR SQUARED	B VALUE ($fm^{2\lambda}$)
6.0	.615	E2	$3.77X10^{-4}$	$1.81X10^{2}$
7.0	.612	E3	$3.40X10^{-4}$	$1.61X10^{4}$
8.08	.609	Ghost	$1.44X10^{-3}$	--------
9.58	.604	E4	$2.18X10^{-5}$	$2.12X10^{5}$
13.3	.594	E3	$1.99X10^{-4}$	$1.01X10^{4}$
16.3	.586	E2	$1.03X10^{-3}$	$5.01X10^{2}$
18.3	.581	E1	$7.27X10^{-4}$	$7.49X10^{0}$
21.75	.572	E1	$3.12X10^{-4}$	$3.08X10^{0}$
27.0	.560	E3	$7.22X10^{-5}$	$4.40X10^{3}$
32.0	.549	E2	$5.87X10^{-4}$	$2.97X10^{2}$

TABLE X. ^{60}Ni RESONANCES AT 75° SCATTERING ANGLE

E (MeV)	Q (fm^{-1})	MULTIPOLARITY ($E\lambda$)	FORM FACTOR SQUARED	B VALUE ($fm^{2\lambda}$)
6.11	.614	E2	$3.26X10^{-4}$	$1.57X10^{2}$
7.1	.612	E3	$2.04X10^{-4}$	$9.67X10^{3}$
7.7	.610	E3	$1.77X10^{-4}$	$8.45X10^{3}$
8.08	.609	Ghost	$8.44X10^{-4}$	--------
8.8	.607	E3	$5.36X10^{-5}$	$2.55X10^{3}$
12.7	.596	E3	$1.11X10^{-4}$	$5.62X10^{3}$
14.9	.590	E4	$6.49X10^{-5}$	$7.06X10^{5}$
16.3	.586	E2	$8.09X10^{-4}$	$3.90X10^{2}$
16.7	.585	E1	$1.37X10^{-4}$	$1.43X10^{0}$
18.6	.580	E4	$8.40X10^{-5}$	$1.00X10^{6}$
19.0	.579	E1	$5.83X10^{-4}$	$5.95X10^{0}$
27.0	.560	E3	$1.18X10^{-4}$	$7.14X10^{3}$
32.0	.549	E2	$4.12X10^{-4}$	$2.10X10^{2}$

TABLE XI. ^{58}Ni RESONANCES AT 90° SCATTERING ANGLE

E (MeV)	Q (fm^{-1})	MULTIPOLARITY (Eλ)	FORM FACTOR SQUARED	B VALUE ($fm^{2\lambda}$)
6.0	.707	E2	$3.15X10^{-4}$	$1.70X10^{2}$
6.95	.704	E3	$4.42X10^{-4}$	$1.61X10^{4}$
8.08	.700	Ghost	$5.18X10^{-4}$	--------
9.6	.695	E4	$6.67X10^{-5}$	$3.49X10^{5}$
13.3	.682	E3	$2.36X10^{-4}$	$8.91X10^{3}$
15.0	.677	E4	$2.38X10^{-4}$	$1.38X10^{6}$
16.3	.672	E2	$9.13X10^{-4}$	$4.59X10^{2}$
18.3	.666	E1	$3.96X10^{-4}$	$7.08X10^{0}$
20.5	.659	E4	$1.87X10^{-4}$	$1.16X10^{6}$
21.75	.655	E1	$1.51X10^{-4}$	$2.48X10^{0}$
27.0	.639	E3	$1.28X10^{-4}$	$5.46X10^{3}$
32.0	.624	E2	$3.72X10^{-4}$	$1.79X10^{2}$

TABLE XII. ^{60}Ni RESONANCES AT 90° SCATTERING ANGLE

E (MeV)	Q (fm^{-1})	MULTIPOLARITY (Eλ)	FORM FACTOR SQUARED	B VALUE ($fm^{2\lambda}$)
6.17	.713	E2	$3.00X10^{-4}$	$1.63X10^{2}$
6.98	.710	E3	$1.49X10^{-4}$	$5.32X10^{3}$
7.39	.708	E3	$2.52X10^{-4}$	$9.00X10^{3}$
8.08	.706	Ghost	$2.89X10^{-4}$	--------
8.6	.704	E3	$5.50X10^{-5}$	$2.00X10^{3}$
11.4	.695	E4	$2.45X10^{-5}$	$1.29X10^{5}$
12.7	.691	E3	$1.59X10^{-4}$	$5.87X10^{3}$
14.9	.683	E4	$1.31X10^{-4}$	$7.35X10^{5}$
16.2	.679	E2	$8.81X10^{-4}$	$4.46X10^{2}$
16.7	.677	E1	$1.29X10^{-4}$	$2.52X10^{0}$
18.6	.671	E4	$1.86X10^{-4}$	$1.12X10^{6}$
19.0	.670	E1	$3.26X10^{-4}$	$6.04X10^{0}$
27.5	.644	E3	$1.42X10^{-4}$	$5.98X10^{3}$
32.0	.631	E2	$3.85X10^{-4}$	$1.86X10^{2}$

TABLE XIII. ^{58}Ni RESONANCES AT 105° SCATTERING ANGLE

E (MeV)	Q (fm^{-1})	MULTIPOLARITY (Eλ)	FORM FACTOR SQUARED	B VALUE ($fm^{2\lambda}$)
6.0	.797	E2	$2.10X10^{-4}$	$1.57X10^{2}$
6.97	.793	E3	$6.42X10^{-4}$	$2.15X10^{4}$
8.08	.789	Ghost	$1.78X10^{-4}$	--------
9.69	.783	E4	$1.05X10^{-4}$	$3.69X10^{5}$
11.5	.776	----	$1.53X10^{-4}$	--------
13.3	.769	E3	$2.66X10^{-4}$	$8.87X10^{3}$
15.2	.762	E4	$4.41X10^{-4}$	$1.68X10^{6}$
16.3	.757	E2	$8.19X10^{-4}$	$5.12X10^{2}$
18.3	.750	E1	$1.83X10^{-4}$	$7.05X10^{0}$
19.5	.745	E4	$3.49X10^{-4}$	$1.42X10^{6}$
21.75	.737	E1	$7.29X10^{-5}$	$2.47X10^{0}$
27.0	.718	E3	$1.11X10^{-4}$	$3.90X10^{3}$
32.0	.700	E2	$3.59X10^{-4}$	$1.89X10^{2}$

TABLE XIV. ^{60}Ni RESONANCES AT 105° SCATTERING ANGLE

E (MeV)	Q (fm^{-1})	MULTIPOLARITY (Eλ)	FORM FACTOR SQUARED	B VALUE ($fm^{2\lambda}$)
6.11	.800	E2	$2.88X10^{-4}$	$1.23X10^{2}$
7.0	.796	E3	$3.05X10^{-4}$	$1.02X10^{4}$
7.6	.794	E3	$2.12X10^{-4}$	$7.08X10^{3}$
8.08	.792	Ghost	$9.99X10^{-5}$	--------
8.8	.789	E3	$7.81X10^{-5}$	$2.60X10^{3}$
11.4	.779	E4	$5.42X10^{-5}$	$1.93X10^{5}$
12.9	.774	E3	$2.20X10^{-4}$	$7.33X10^{3}$
14.9	.766	E4	$2.10X10^{-4}$	$7.86X10^{5}$
16.2	.761	E2	$9.38X10^{-4}$	$5.96X10^{2}$
16.7	.759	E1	$4.50X10^{-5}$	$1.96X10^{0}$
18.6	.752	E4	$3.85X10^{-4}$	$1.53X10^{6}$
19.0	.750	E1	$1.56X10^{-4}$	$5.99X10^{0}$
27.0	.721	E3	$2.87X10^{-4}$	$1.01X10^{4}$
32.0	.703	E2	$6.66X10^{-4}$	$3.52X10^{2}$

TABLE XV. COLLECTED RESULTS FOR ^{58}Ni

ENERGY (MeV)	Γ (MeV)	B VALUE ($fm^{2\lambda}$)	$E\lambda$	EWSR (%)	ΔT	B (SPU)	ENERGY ($A^{-1/3}$MeV)
6.0 $\pm$ 0.1	1.09$\pm$0.1	$1.69X10^{2}$	E2	6 $\pm$ 1	0	3	23
6.96 $\pm$ 0.1	0.8$\pm$0.1	$1.77X10^{4}$	E3	12 $\pm$ 2	0	13	27
9.6 $\pm$ 0.1	0.7$\pm$0.2	$3.10X10^{5}$	E4	5 $\pm$ 2	0	11	37
13.3 $\pm$ 0.2	1.5$\pm$0.2	$9.51X10^{3}$	E3	13 $\pm$ 1	0	7	51
15.1 $\pm$ 0.2	4.3$\pm$0.4	$1.28X10^{6}$	E4	37 $\pm$ 12	0	45	58
16.3 $\pm$ 0.2	4.5$\pm$0.4	$4.66X10^{2}$	E2	50 $\pm$ 10	0	7	63
18.3 $\pm$ 0.2	4.2$\pm$0.4	$7.30X10^{0}$	E1	61 $\pm$ 7	1	3	71
20.0 $\pm$ 0.7	5.0$\pm$0.5	$1.29X10^{6}$	E4	42 $\pm$ 13	0	45	77
21.75 $\pm$ 1.0	5.0$\pm$0.5	$2.56X10^{0}$	E1	26 $\pm$ 7	1	1	84
27.0 $\pm$ 1.0	6.0$\pm$1.0	$4.86X10^{3}$	E3	13 $\pm$ 5	0	3	105
32.0 $\pm$ 1.0	10.0$\pm$2.0	$2.23X10^{2}$	E2	40 $\pm$ 11	1	3	124

TABLE XVI. COLLECTED RESULTS FOR ^{60}Ni

ENERGY (MeV)	Γ (MeV)	B VALUE ($fm^{2\lambda}$)	$E\lambda$	EWSR (%)	ΔT	B (SPU)	ENERGY ($A^{-1/3}$MeV)
6.12 ± 0.1	0.7±0.2	$1.41X10^{2}$	E2	5 ± 1	0	2	24
7.05 ± 0.1	0.7±0.2	$9.25X10^{3}$	E3	6 ± 2	0	6	28
7.6 ± 0.2	0.95±0.1	$8.73X10^{3}$	E3	6 ± 1	0	6	30
8.7 ± 0.2	0.97±0.1	$2.38X10^{3}$	E3	2 ± 1	0	2	34
11.4 ± 0.2	1.2±0.2	$1.61X10^{5}$	E4	3 ± 2	0	5	45
12.8 ± 0.2	1.5±0.2	$5.89X10^{3}$	E3	8 ± 2	0	4	50
14.9 ± 0.2	2.1±0.2	$7.42X10^{5}$	E4	18 ± 5	0	24	58
16.2 ± 0.2	4.7±0.3	$4.47X10^{2}$	E2	50 ± 10	0	6	63
16.7 ± 0.2	2.1±0.2	$1.95X10^{0}$	E1	16 ± 4	1	1	65
18.6 ± 0.2	4.0±0.4	$1.22X10^{6}$	E4	38 ± 12	0	39	73
19.2 ± 0.5	6.0±0.8	$6.12X10^{0}$	E1	52 ± 5	1	2	75
27.1 ± 1.0	6.0±1.2	$8.38X10^{3}$	E3	23 ± 7	0	6	106
32.0 ± 1.0	9.0±2.0	$2.26X10^{2}$	E2	40 ± 15	1	3	125

TABLE XVII. Shell model (RPA) predictions for excitation energy and strength of the E3 transitions. The numbers were taken from Ref. (Hama72) using $\hbar\omega = 40A^{-1/3}$ MeV.

	CLASSIC		$\Delta T = 0$		$\Delta T = 1$	
$E_x [\hbar\omega]$	$E_x [A^{-1/3} MeV]$	EWSR	$E_x [A^{-1/3} MeV]$	EWSR	$E_x [A^{-1/3} MeV]$	EWSR
1	40	0.14	24	0.28	52	0.02
3	120	0.86	105	0.72	192	0.98

FIGURE 1. ^{58}Ni FULL INELASTIC SPECTRUM AT 45° WITHOUT BACKGROUND.

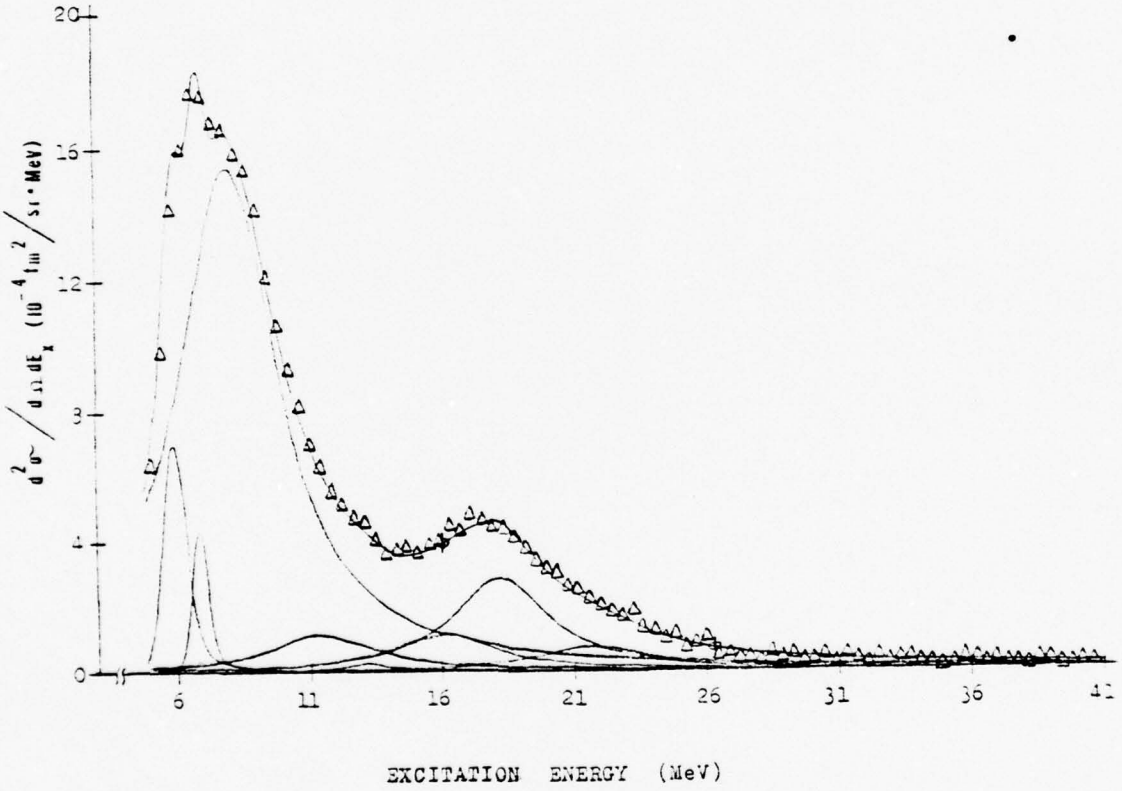


FIGURE 2. ^{58}Ni INELASTIC SPECTRA AT 45° MINUS BACKGROUND AND SELECTED RESONANCES.

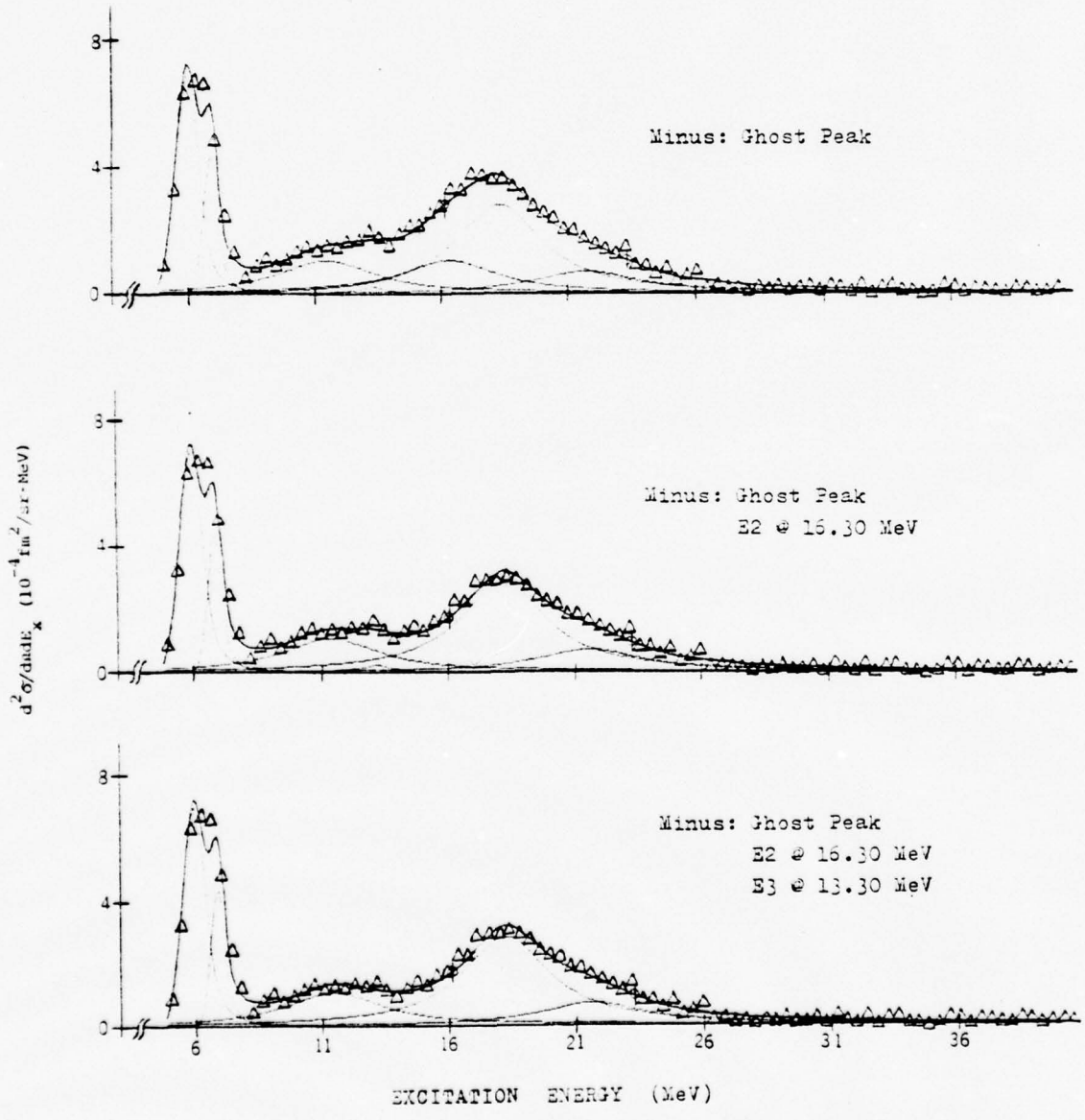


FIGURE 3. ^{58}Ni FULL INELASTIC SPECTRUM AT 60° WITHOUT BACKGROUND.

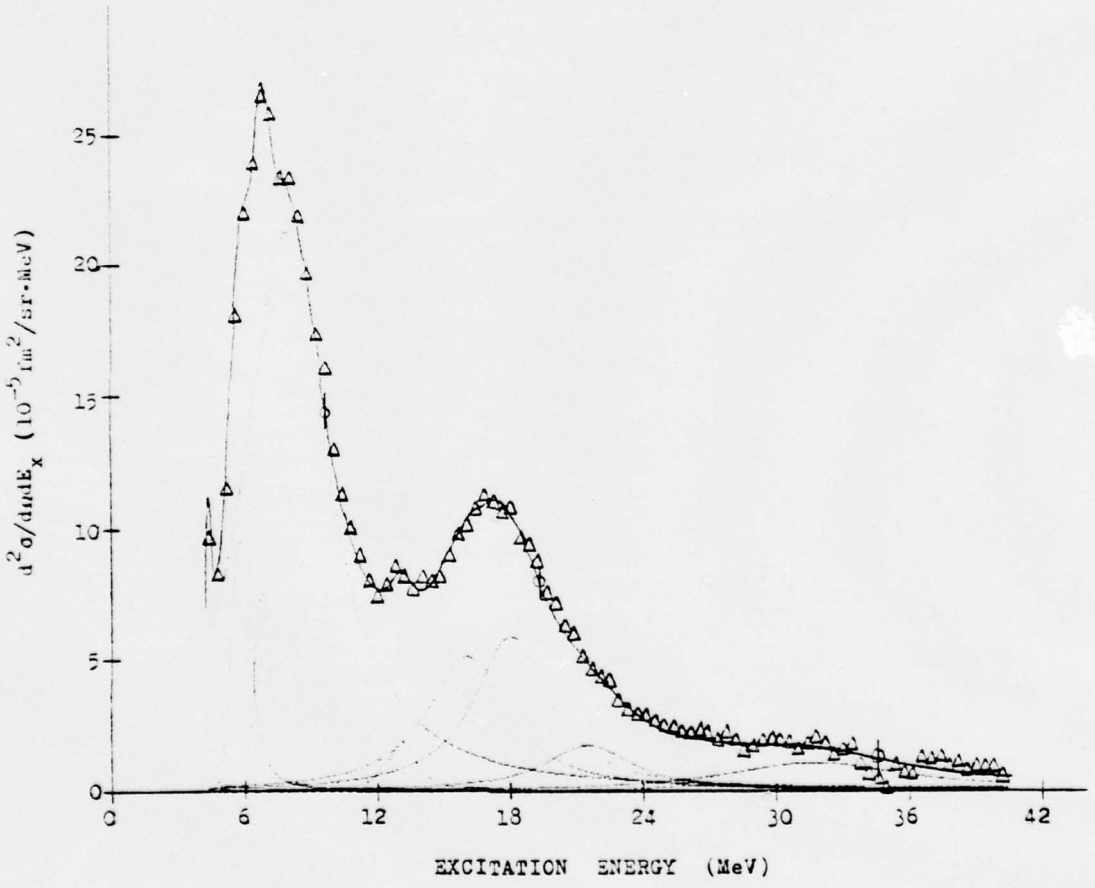


FIGURE 4. ^{58}Ni INELASTIC SPECTRA AT 60° MINUS BACKGROUND AND SELECTED RESONANCES.

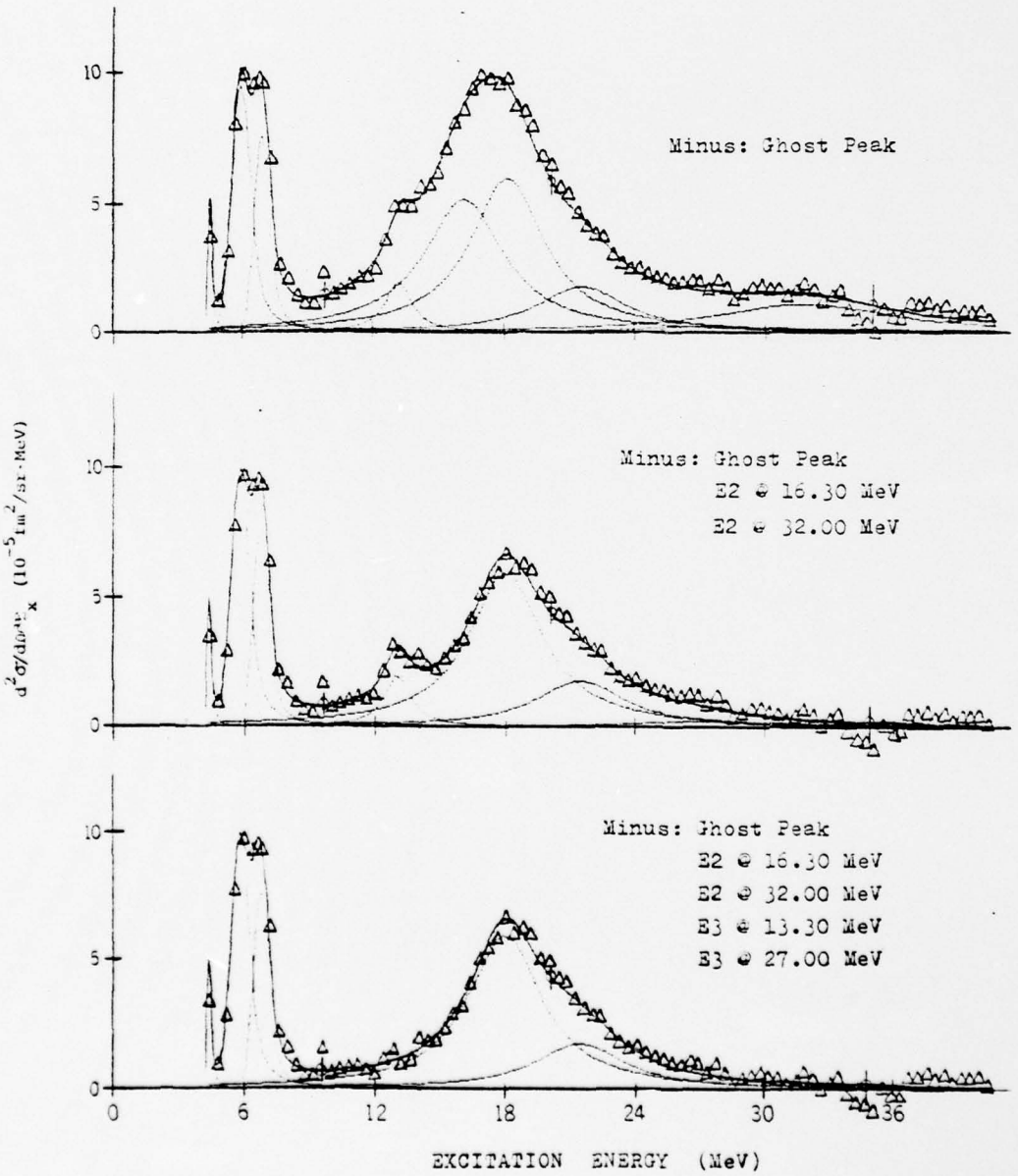


FIGURE 5. ^{58}Ni FULL INELASTIC SPECTRUM AT 75°.

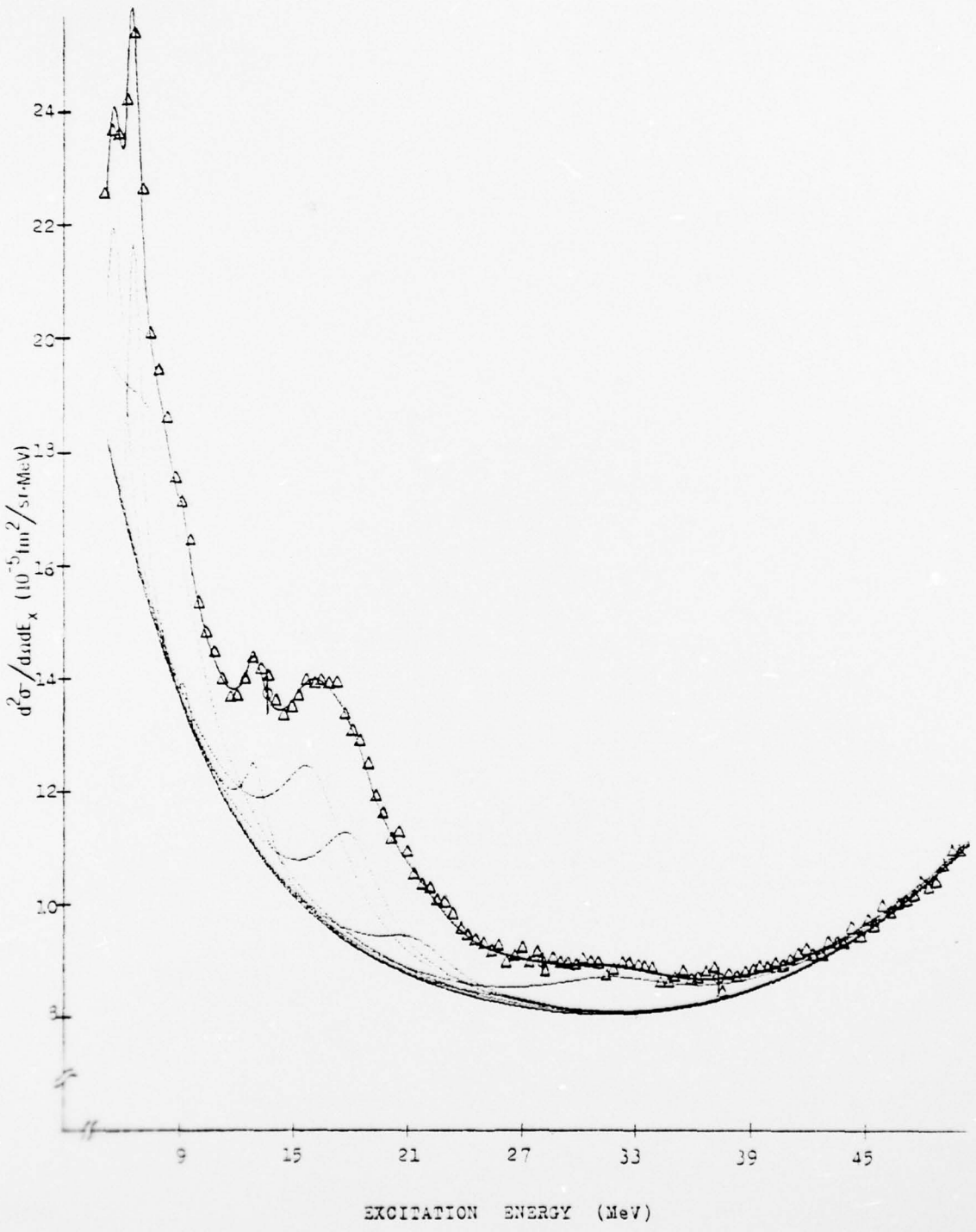


FIGURE 6. ^{58}Ni FULL INELASTIC SPECTRUM AT 75°
WITHOUT BACKGROUND.

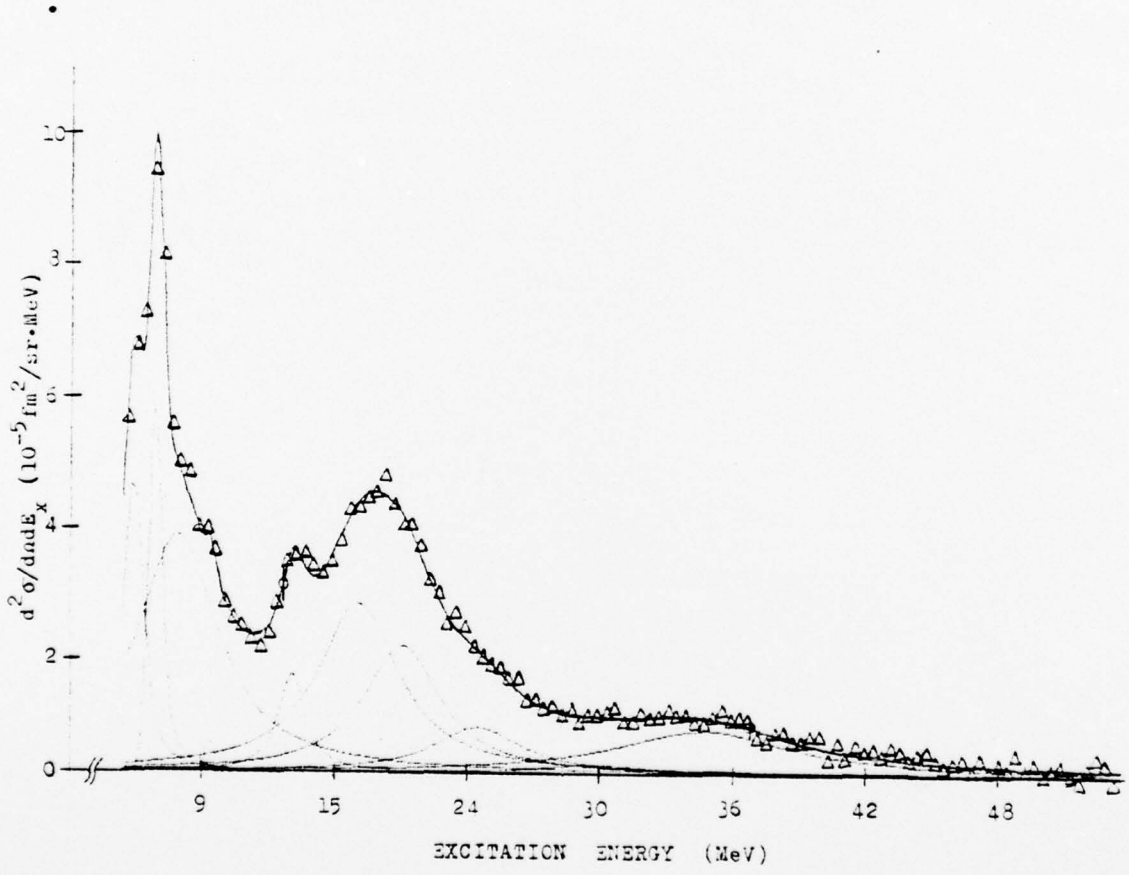


FIGURE 7. ^{58}Ni INELASTIC SPECTRA AT 75° MINUS BACKGROUND AND SELECTED RESONANCES.

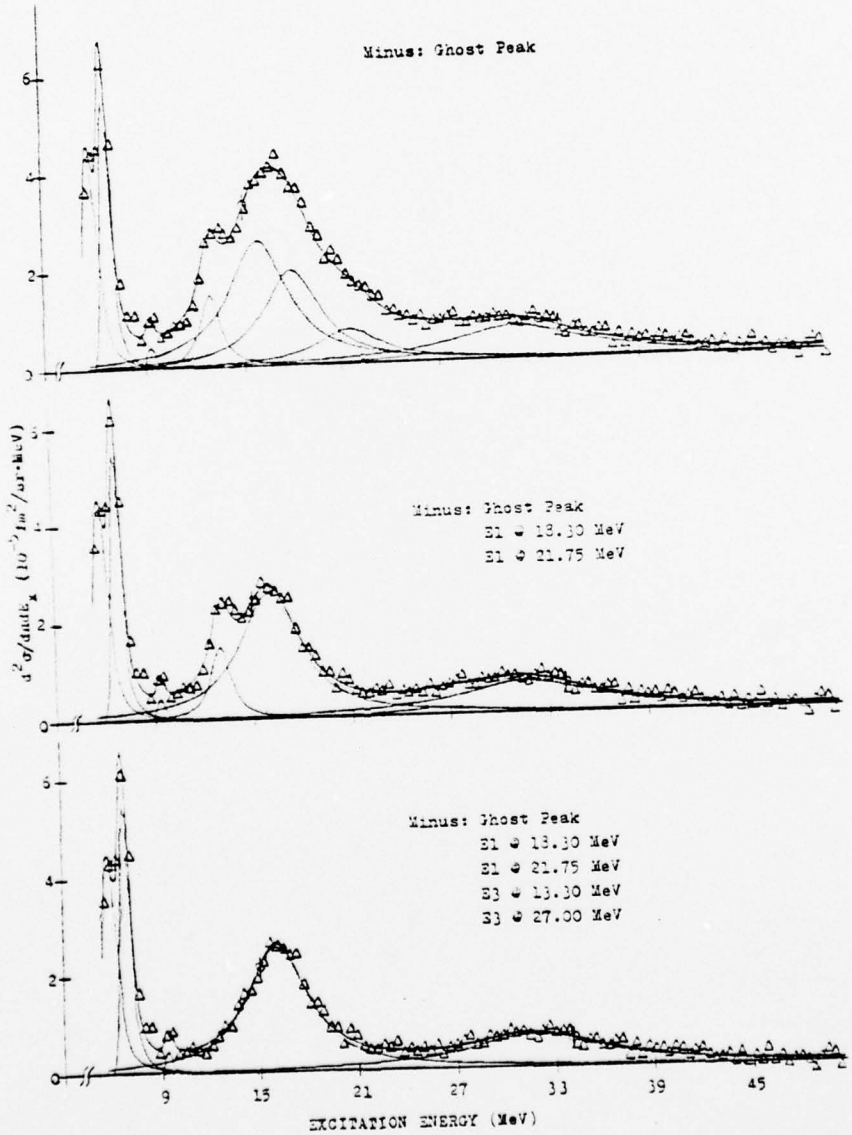


FIGURE 8. ^{58}Ni FULL INELASTIC SPECTRUM AT 90°.

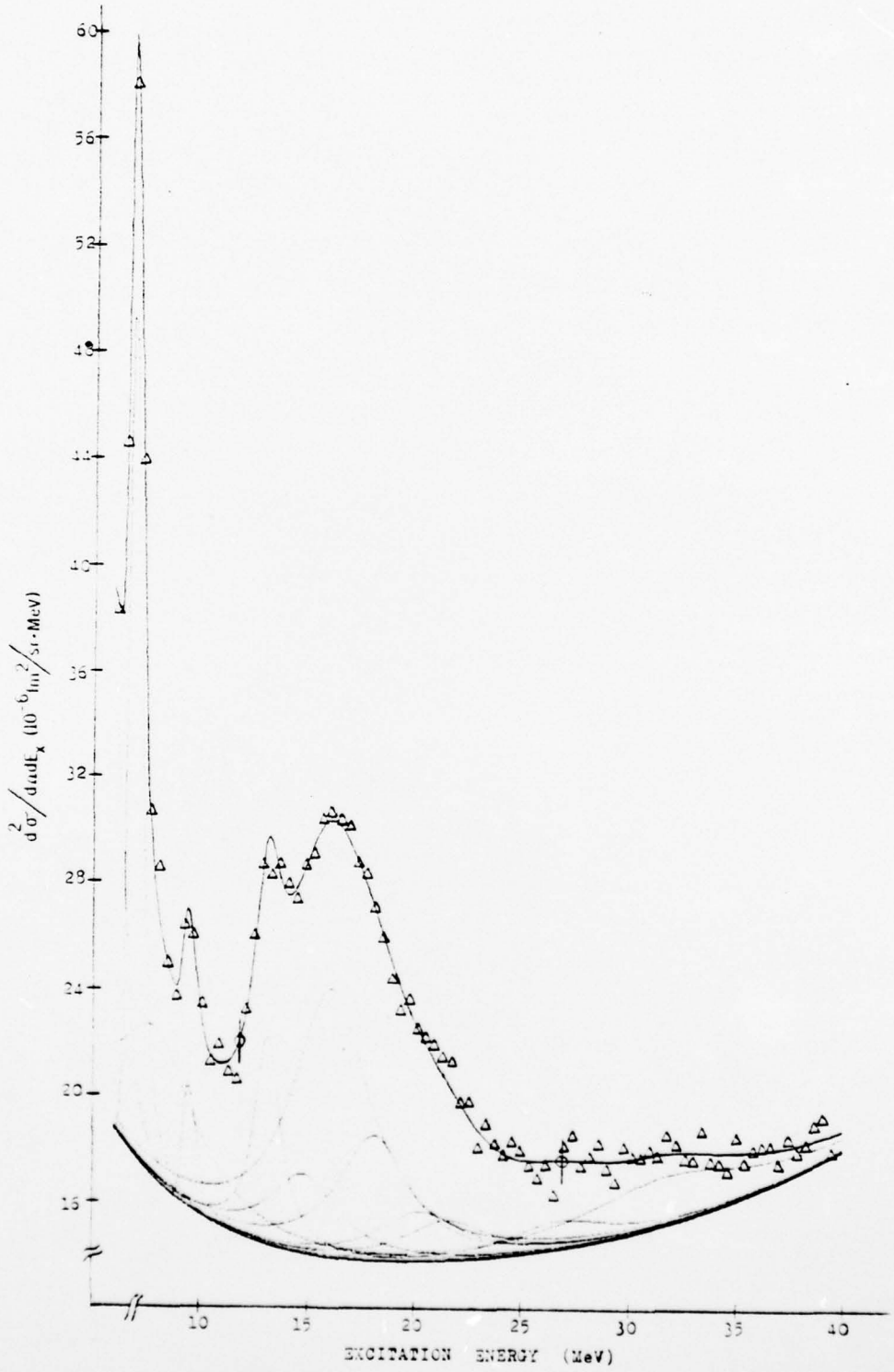


FIGURE 9. ^{58}Ni FULL INELASTIC SPECTRUM AT 90° WITHOUT BACKGROUND.

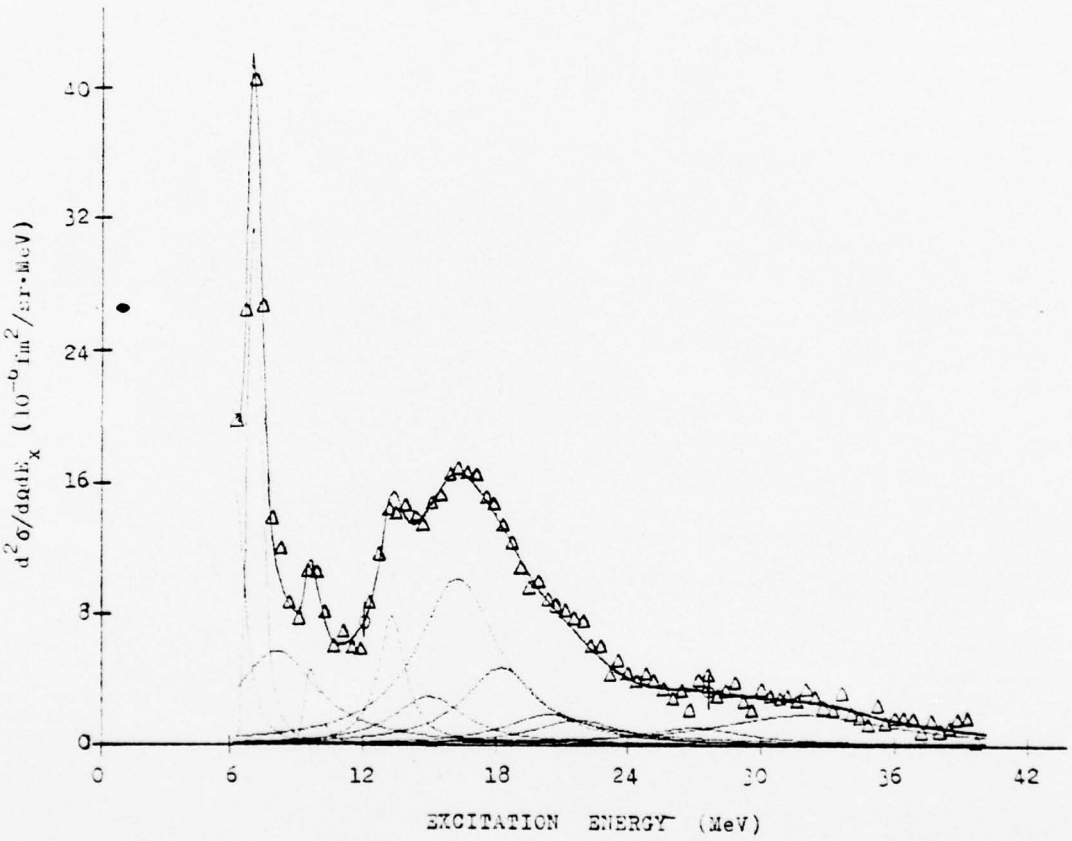


FIGURE 10. ^{58}Ni INELASTIC SPECTRA AT 90° MINUS BACKGROUND AND SELECTED RESONANCES.

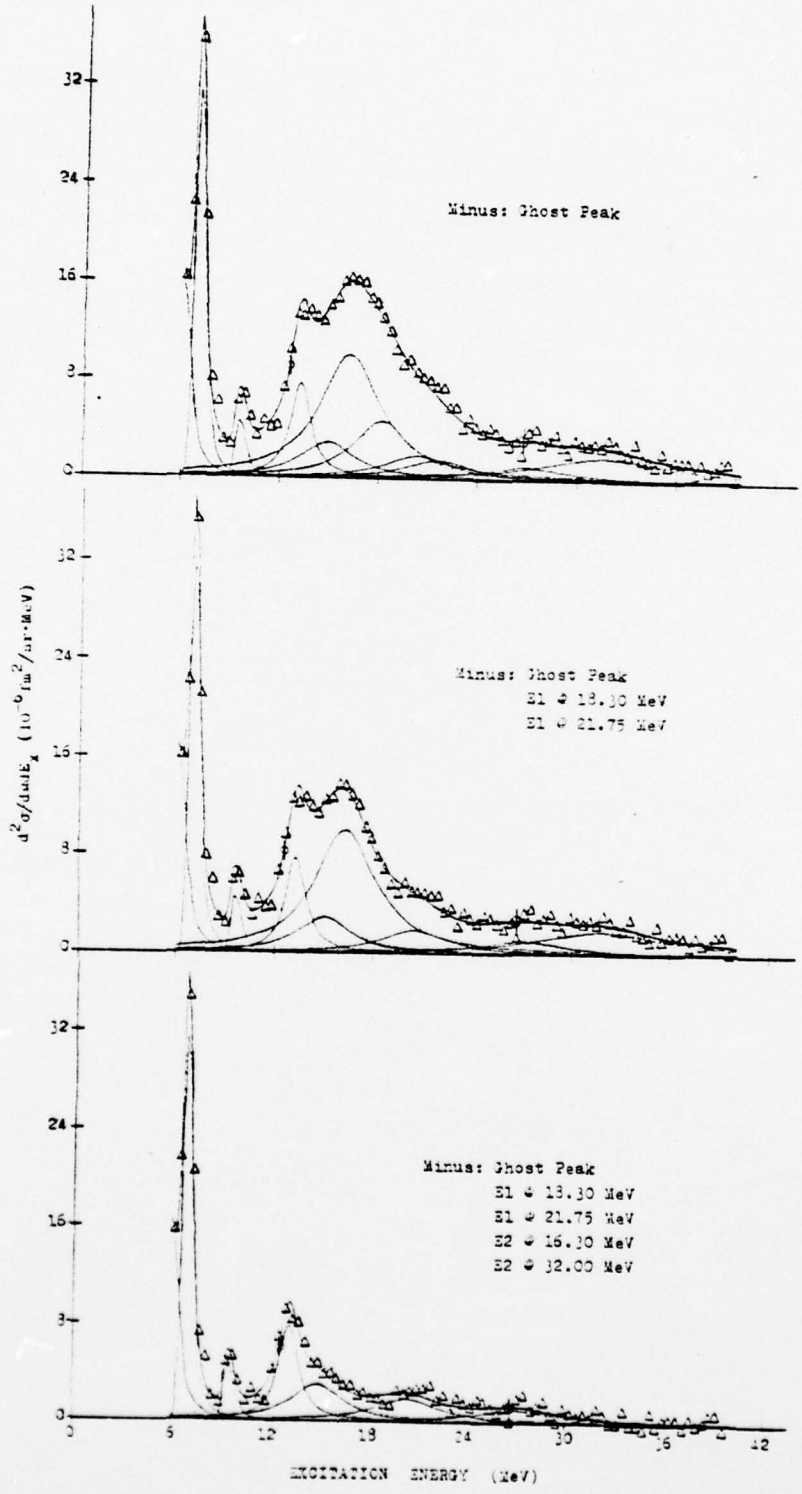


FIGURE 11. ^{58}Ni FULL INELASTIC SPECTRUM AT 105°.

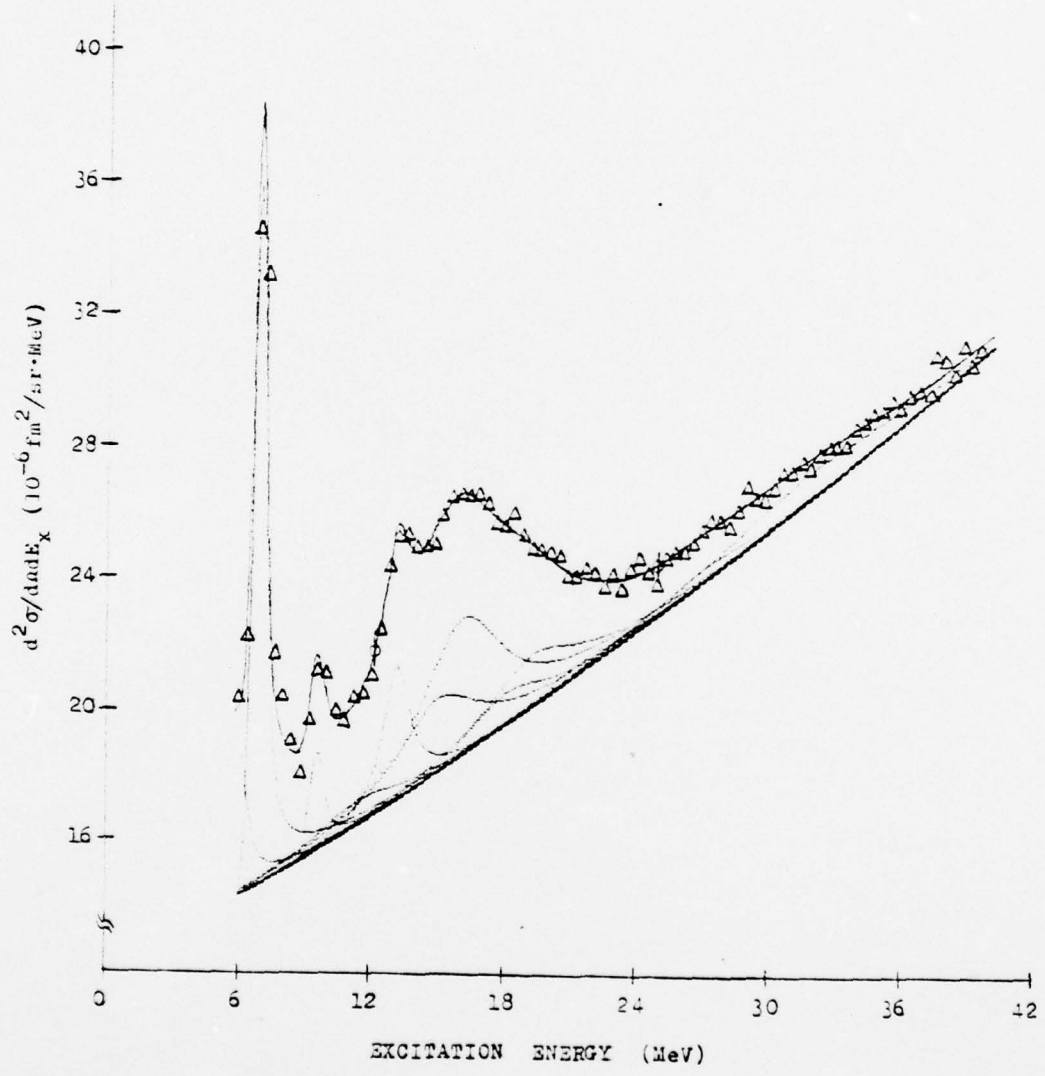


FIGURE 12. ^{58}Ni FULL INELASTIC SPECTRUM AT 105° WITHOUT BACKGROUND.

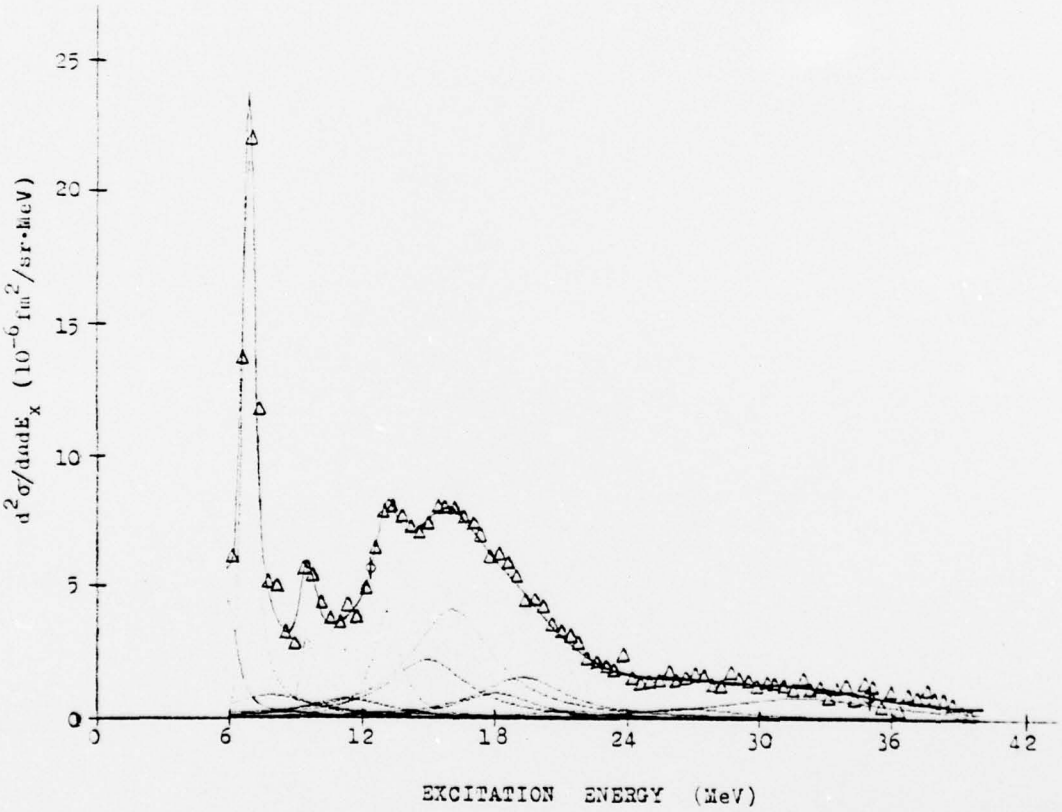


FIGURE 13. ^{58}Ni INELASTIC SPECTRA AT 105° MINUS BACKGROUND AND SELECTED RESONANCES.

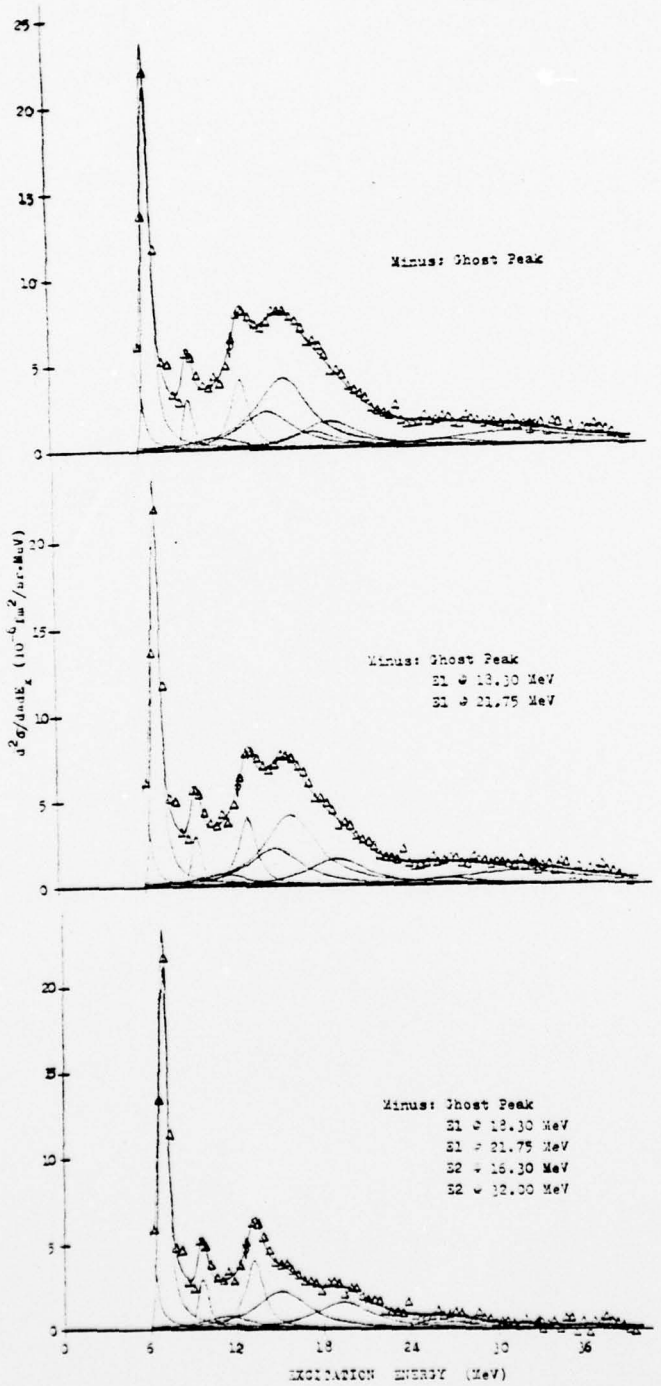


FIGURE 14. ^{60}Ni FULL INELASTIC SPECTRUM AT 45° WITHOUT BACKGROUND.

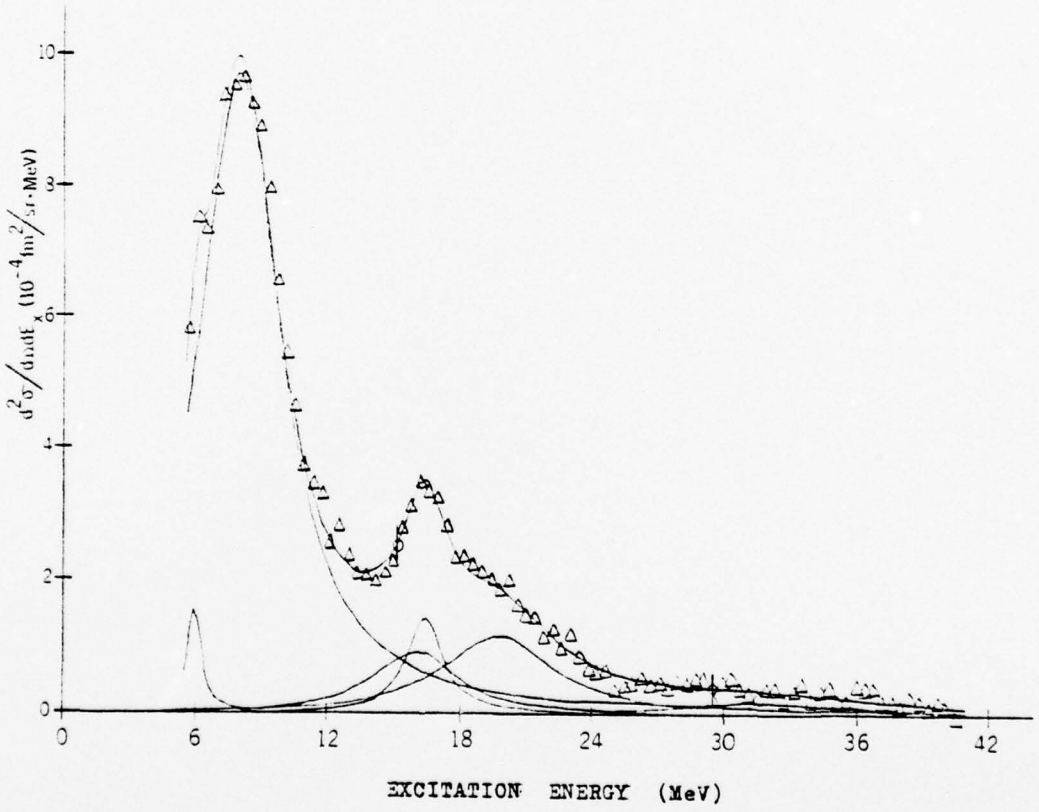


FIGURE 15. ^{60}Ni INELASTIC SPECTRA AT 45° MINUS BACKGROUND AND SELECTED RESONANCES.

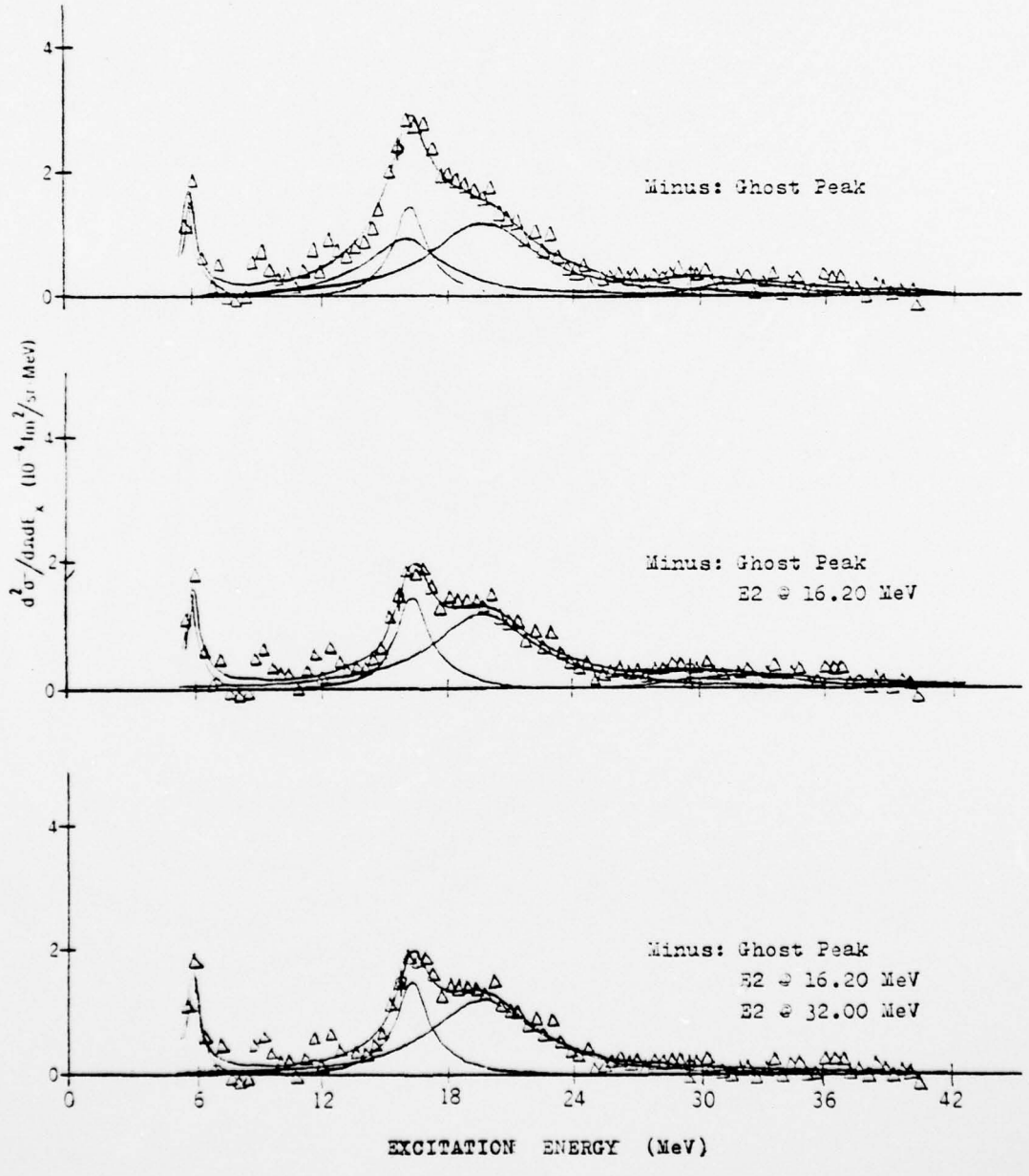


FIGURE 16. ^{60}Ni FULL INELASTIC SPECTRUM AT 60° WITHOUT BACKGROUND.

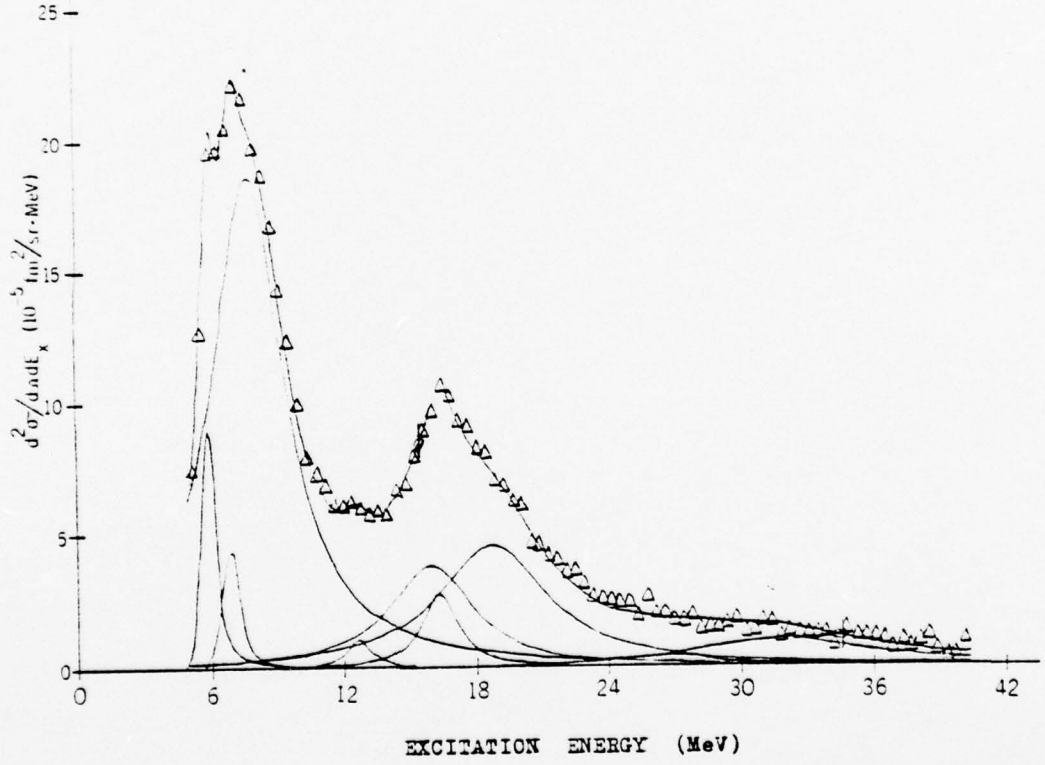


FIGURE 17. ^{60}Ni INELASTIC SPECTRA AT 60° MINUS BACKGROUND AND SELECTED RESONANCES.

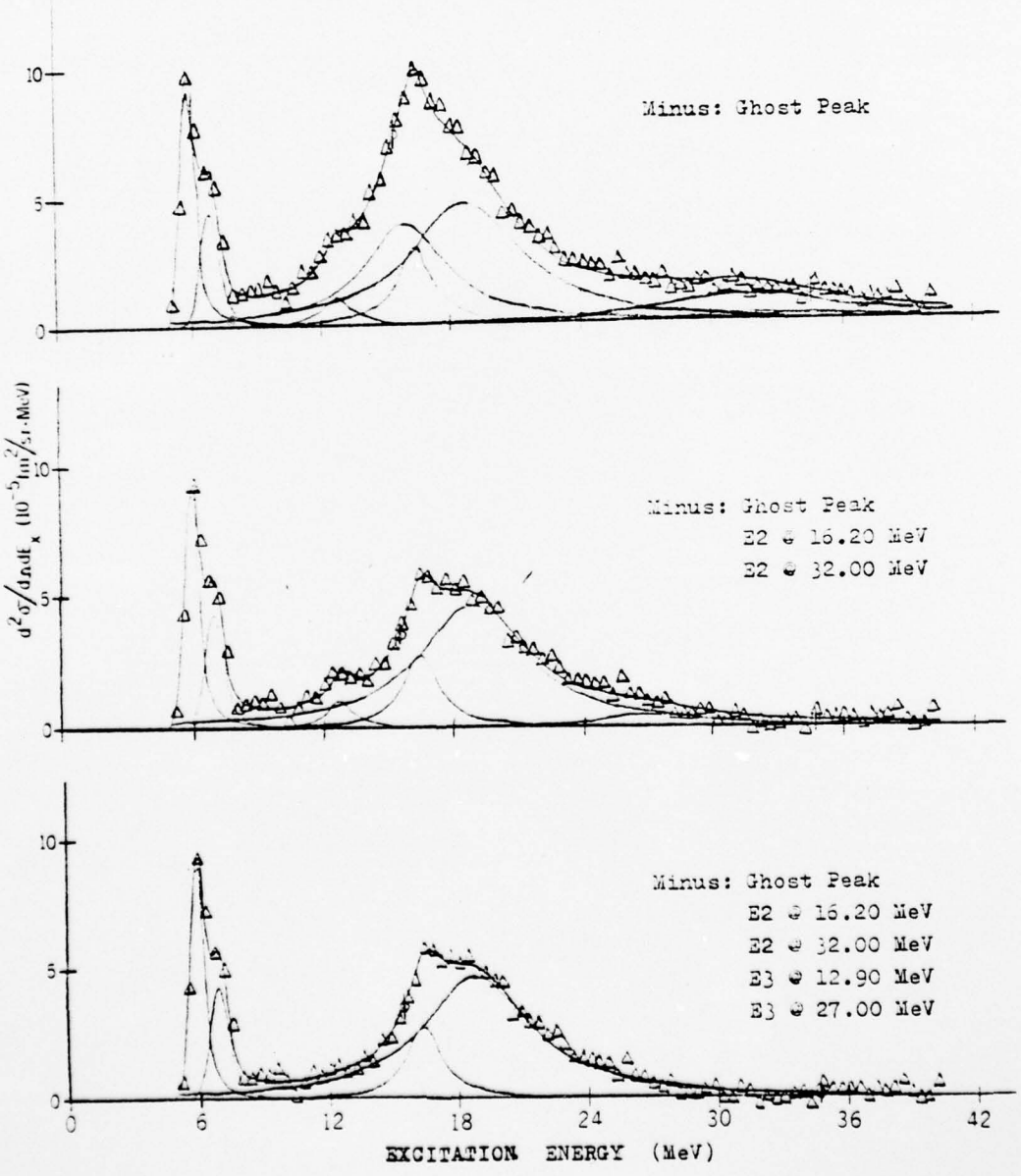
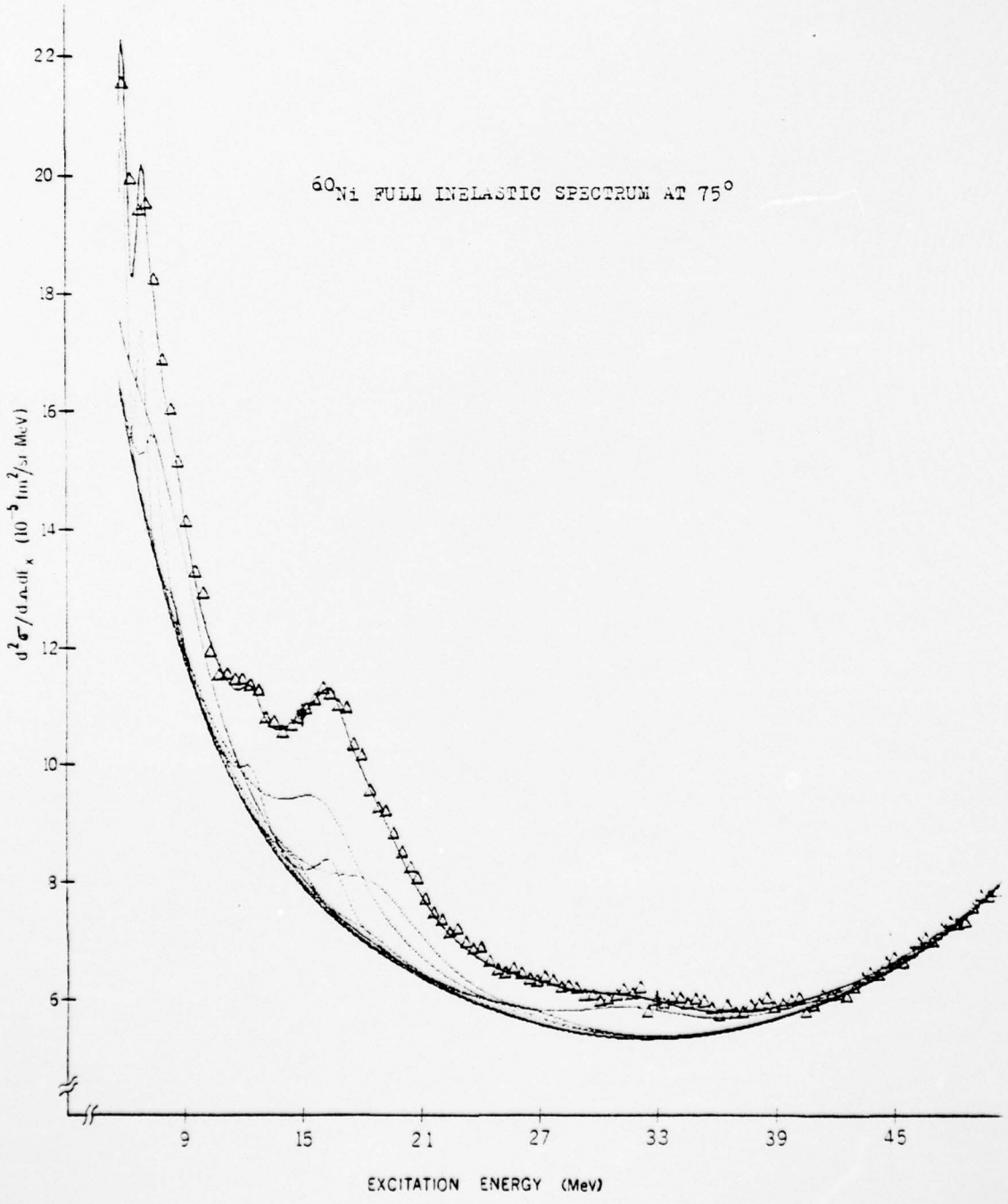


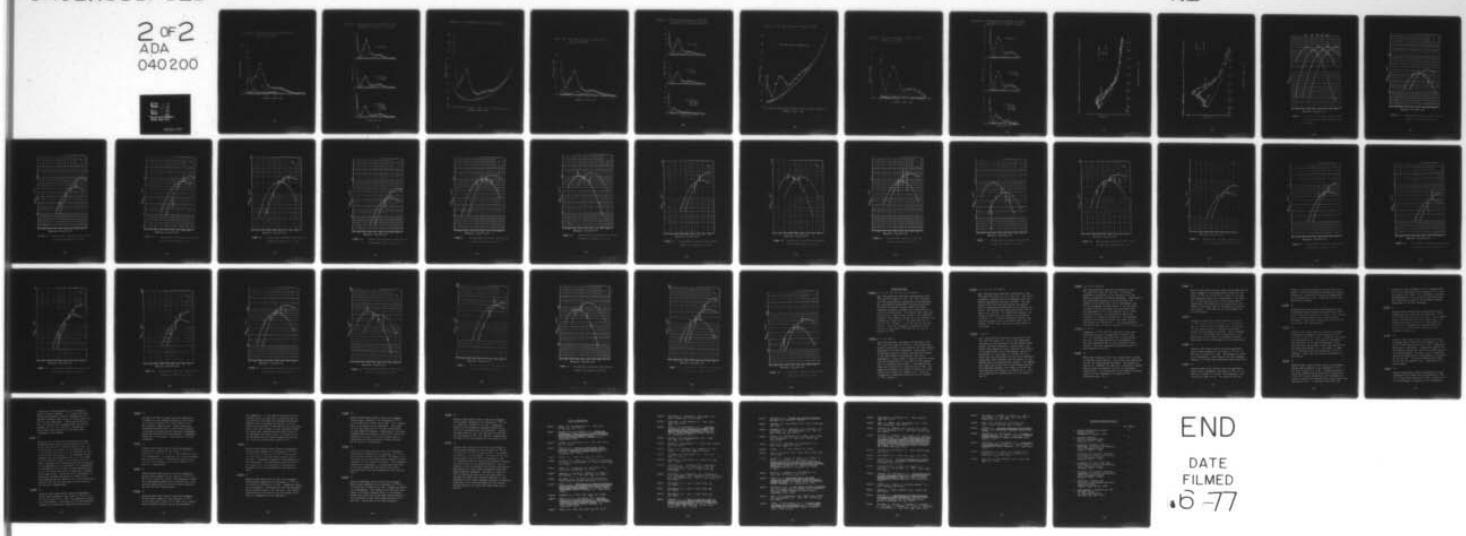
FIGURE 18. ^{60}Ni FULL INELASTIC SPECTRUM AT 75°.



AD-A040 200 NAVAL POSTGRADUATE SCHOOL MONTEREY CALIF F/G 20/8
ELECTROEXCITATION OF THE T = 1 NUCLEUS NI58 AND THE T = 2 NUCLE--ETC(U)
MAR 77 J S BEACHY, S J KOWALICK

UNCLASSIFIED NL

2 OF 2
ADA
040200



END

DATE
FILMED
6-77

FIGURE 19. ^{60}Ni FULL INELASTIC SPECTRUM AT 75° WITHOUT BACKGROUND.

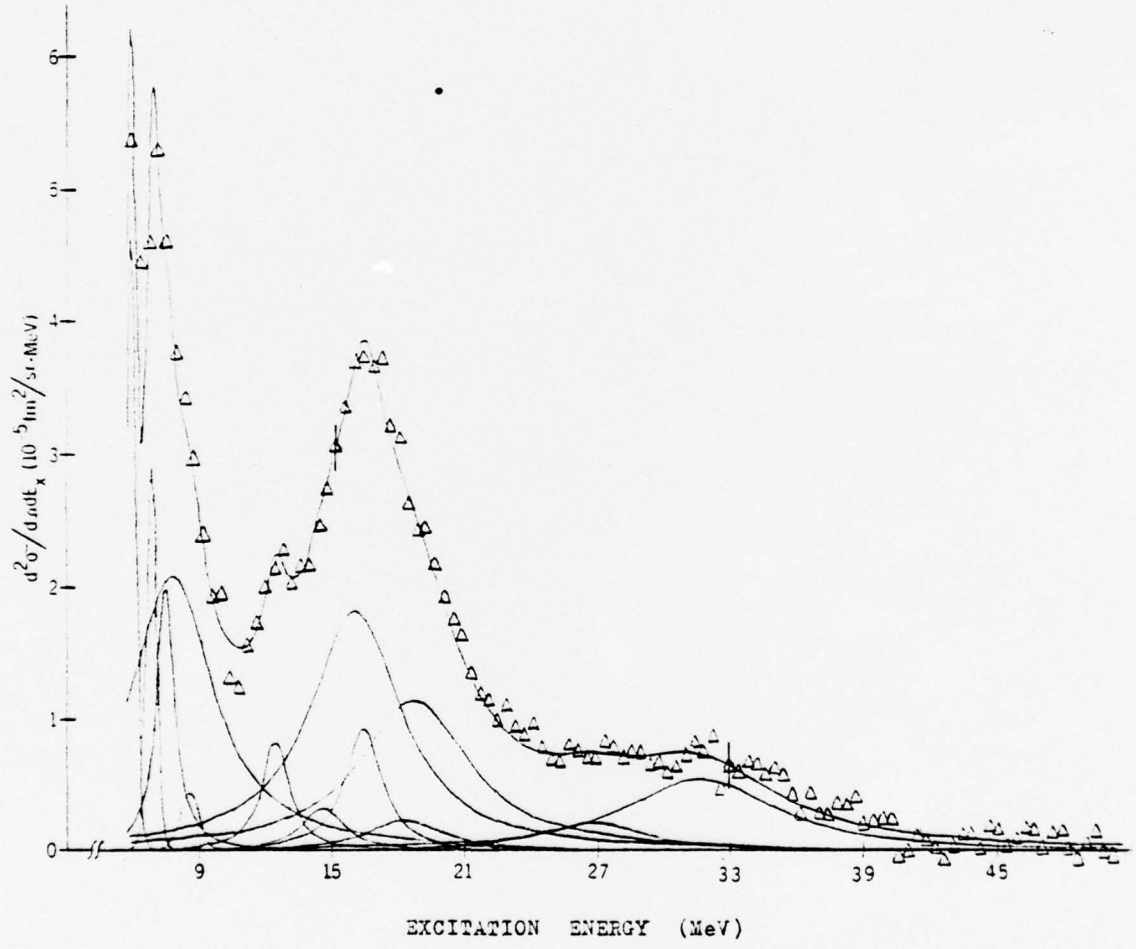


FIGURE 20. ^{60}Ni INELASTIC SPECTRA AT 75° MINUS BACKGROUND AND SELECTED RESONANCES.

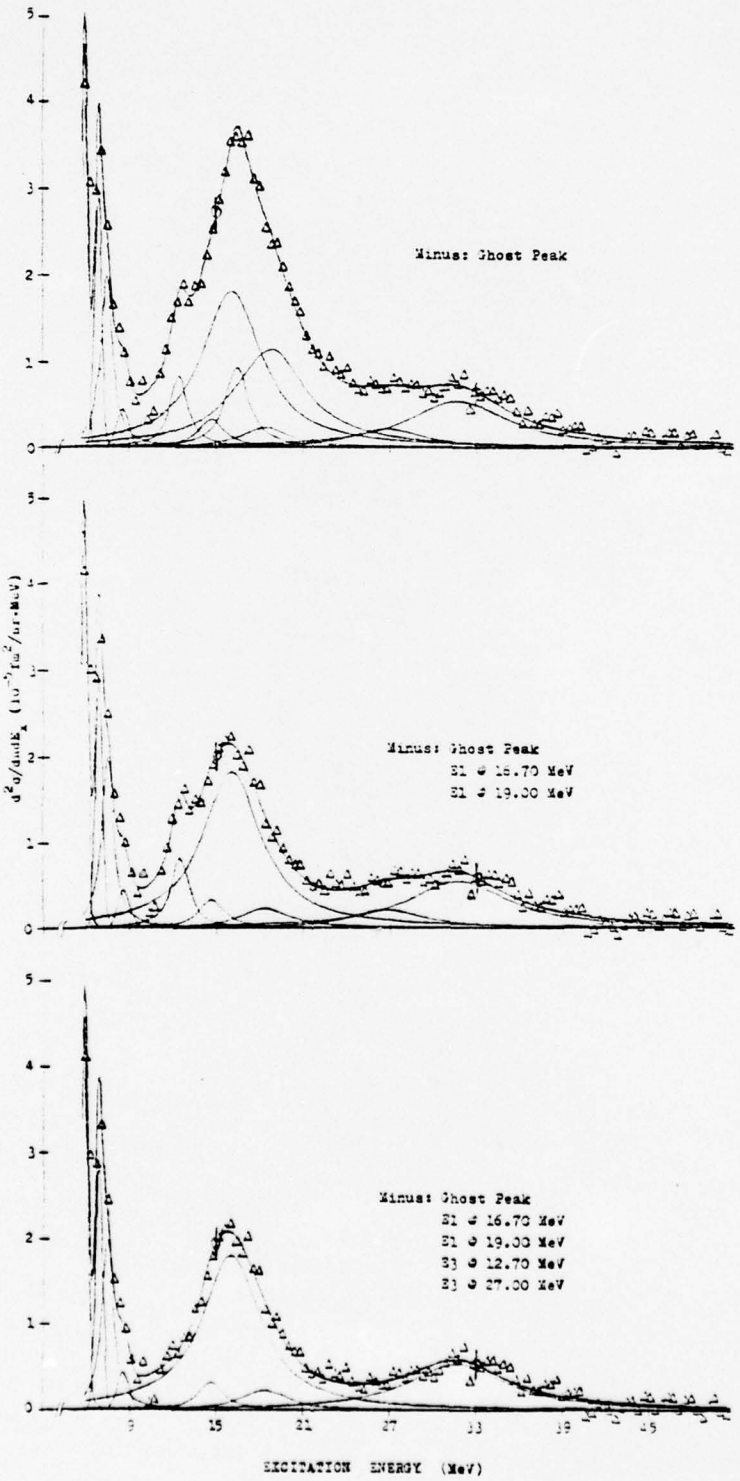


FIGURE 21. ^{60}Ni FULL INELASTIC SPECTRUM AT 90°.

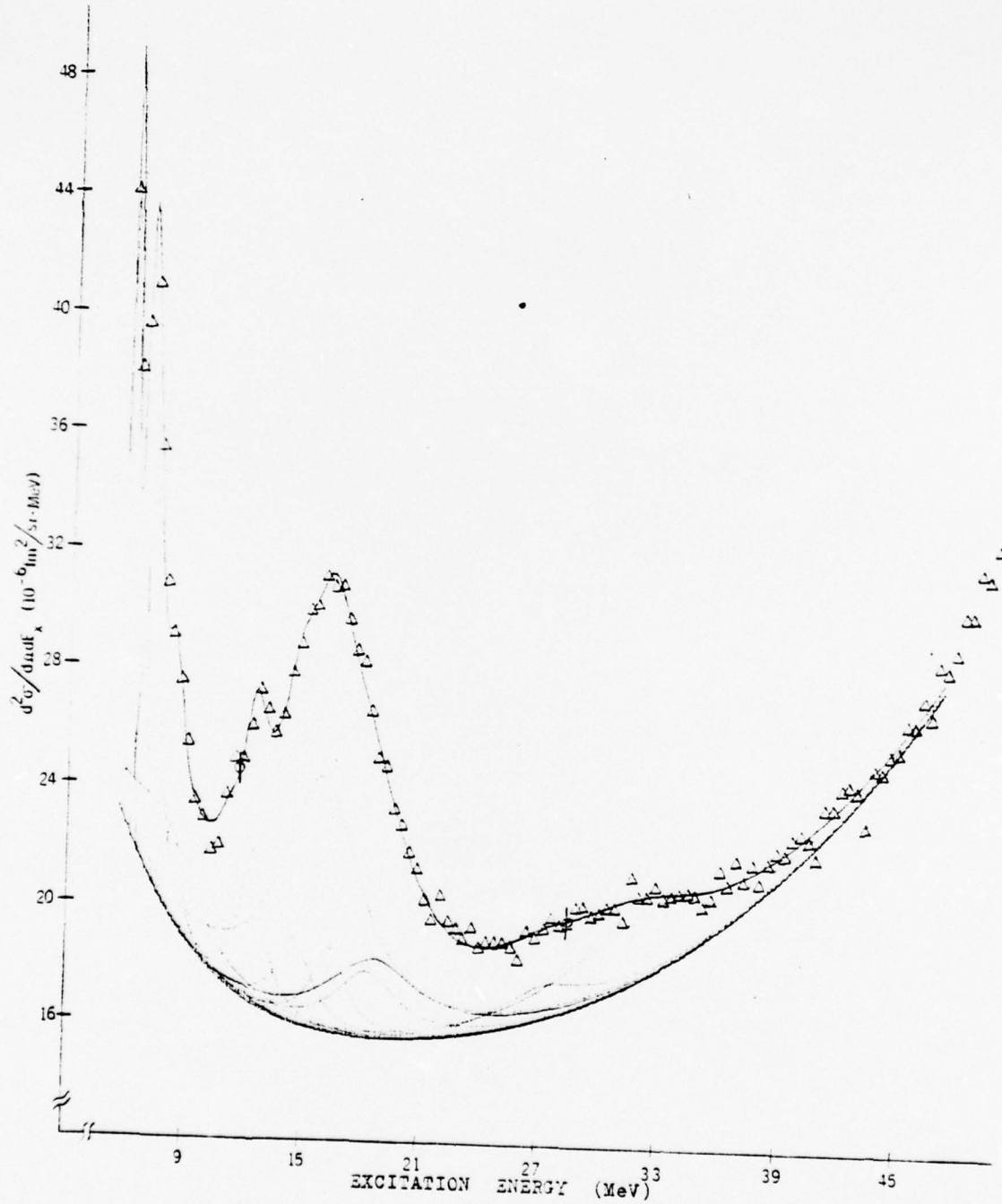


FIGURE 22. ^{60}Ni FULL INELASTIC SPECTRUM AT 90° WITHOUT BACKGROUND.

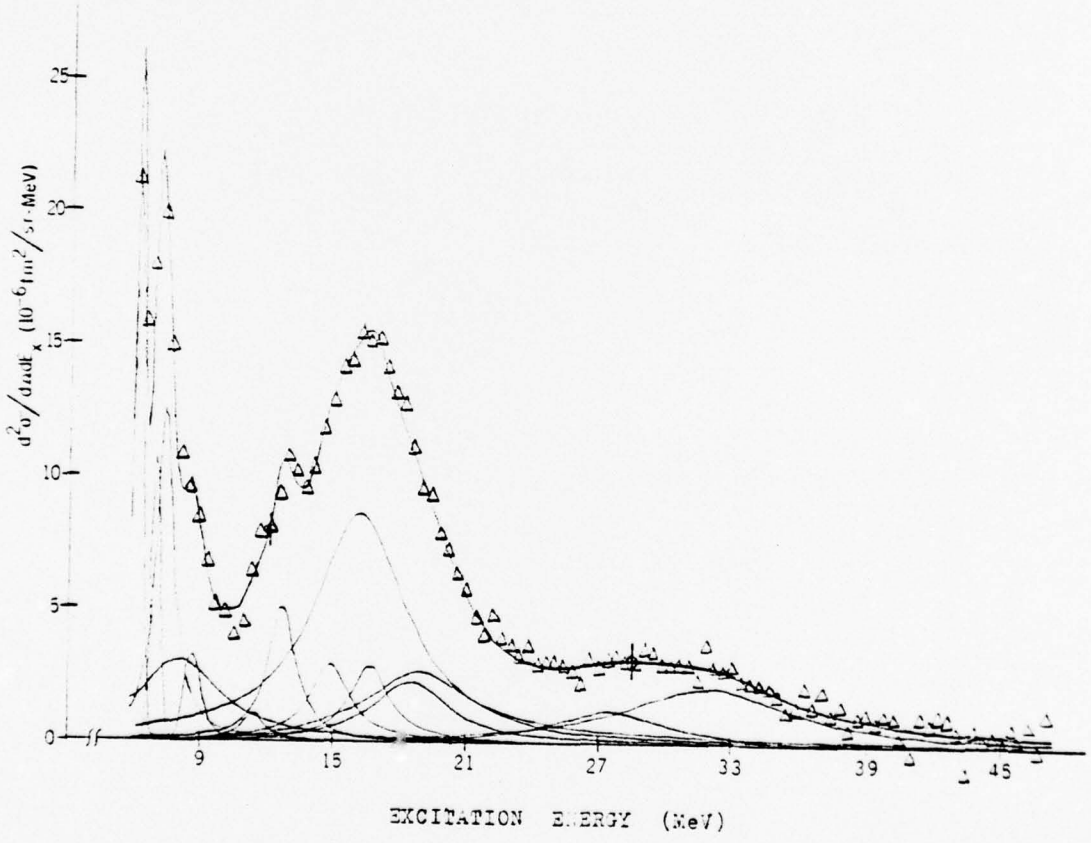


FIGURE 23. ^{60}Ni INELASTIC SPECTRA AT 90° MINUS BACKGROUND AND SELECTED RESONANCES.

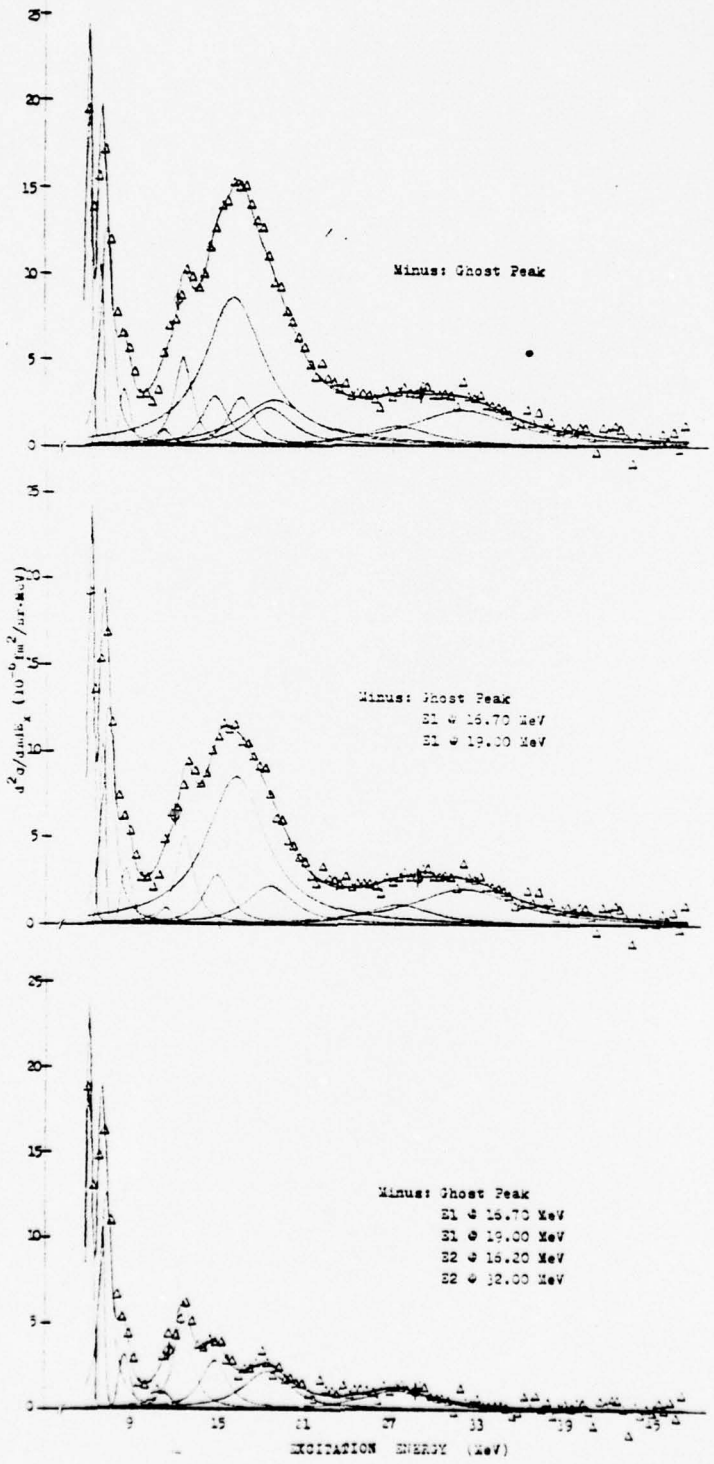


FIGURE 24. ^{60}Ni FULL INELASTIC SPECTRUM AT 105°.

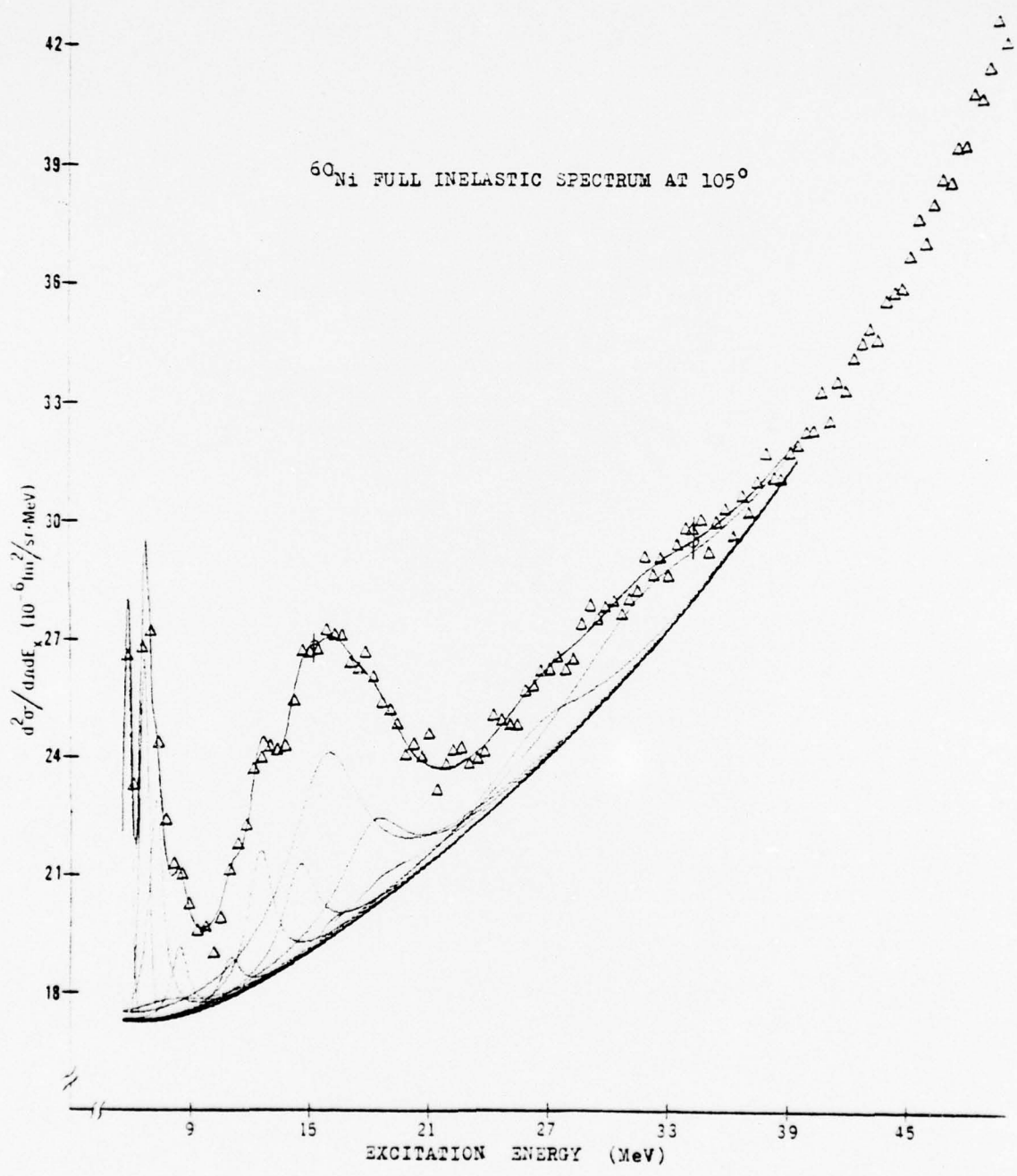


FIGURE 25. ^{60}Ni FULL INELASTIC SPECTRUM AT 105° WITHOUT BACKGROUND.

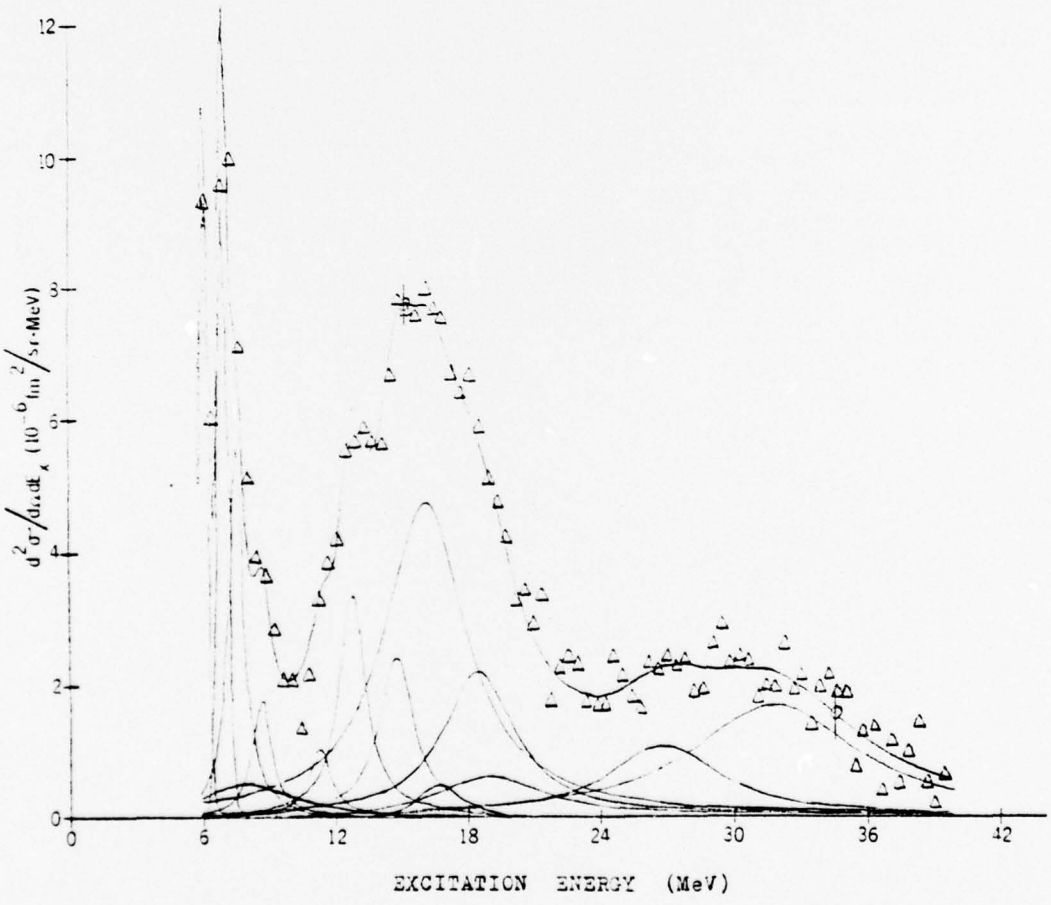


FIGURE 26. ^{60}Ni INELASTIC SPECTRA AT 105° MINUS BACKGROUND AND SELECTED RESONANCES.

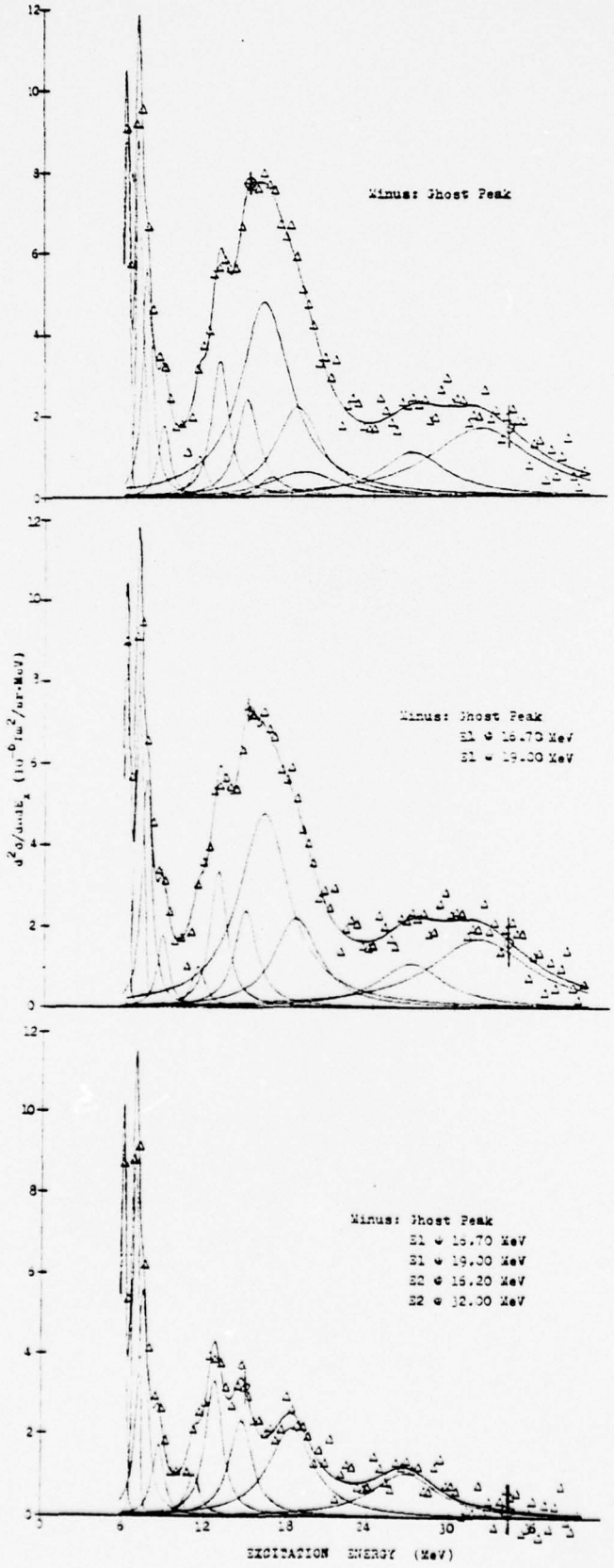


FIGURE 27. COMPARISON OF TOTAL CROSS SECTIONS FOR ^{58}Ni AND ^{60}Ni AT 45°

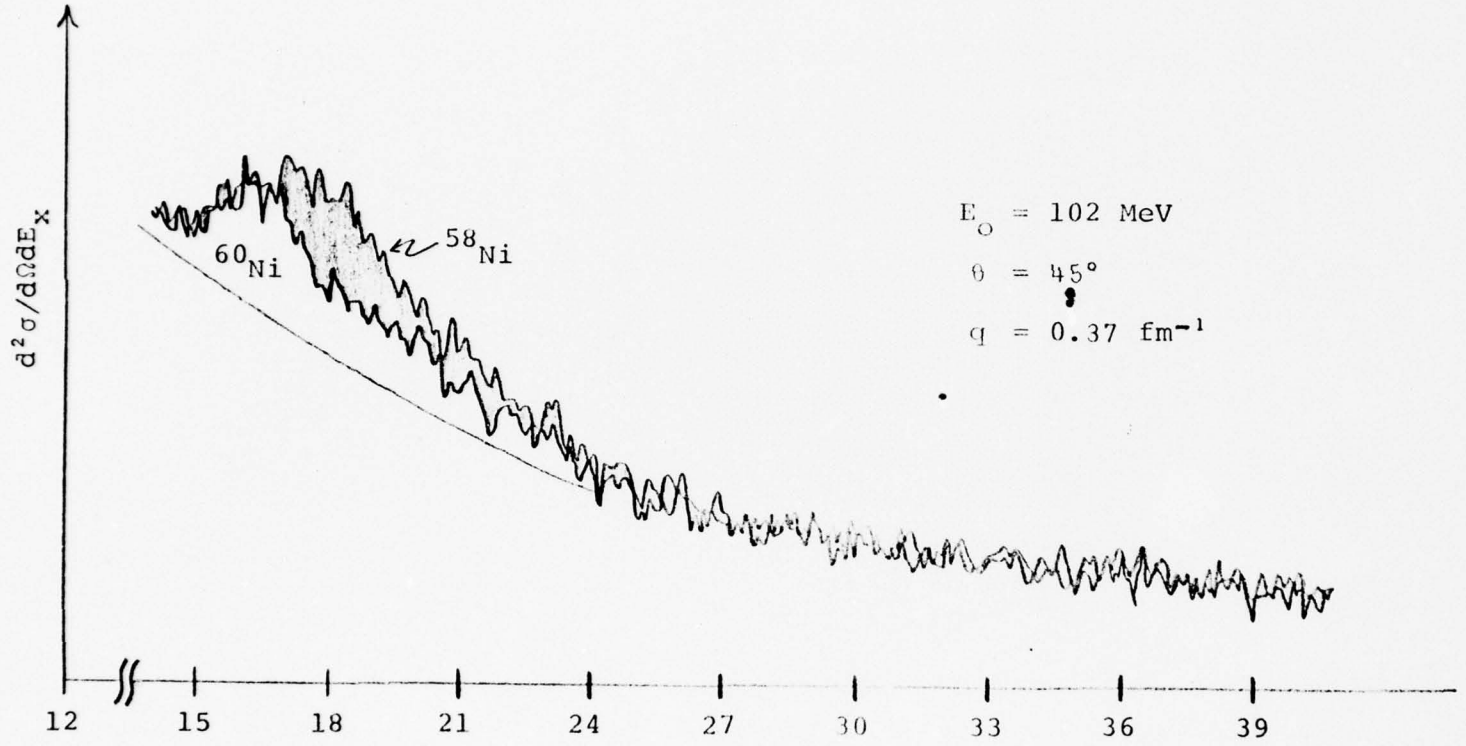
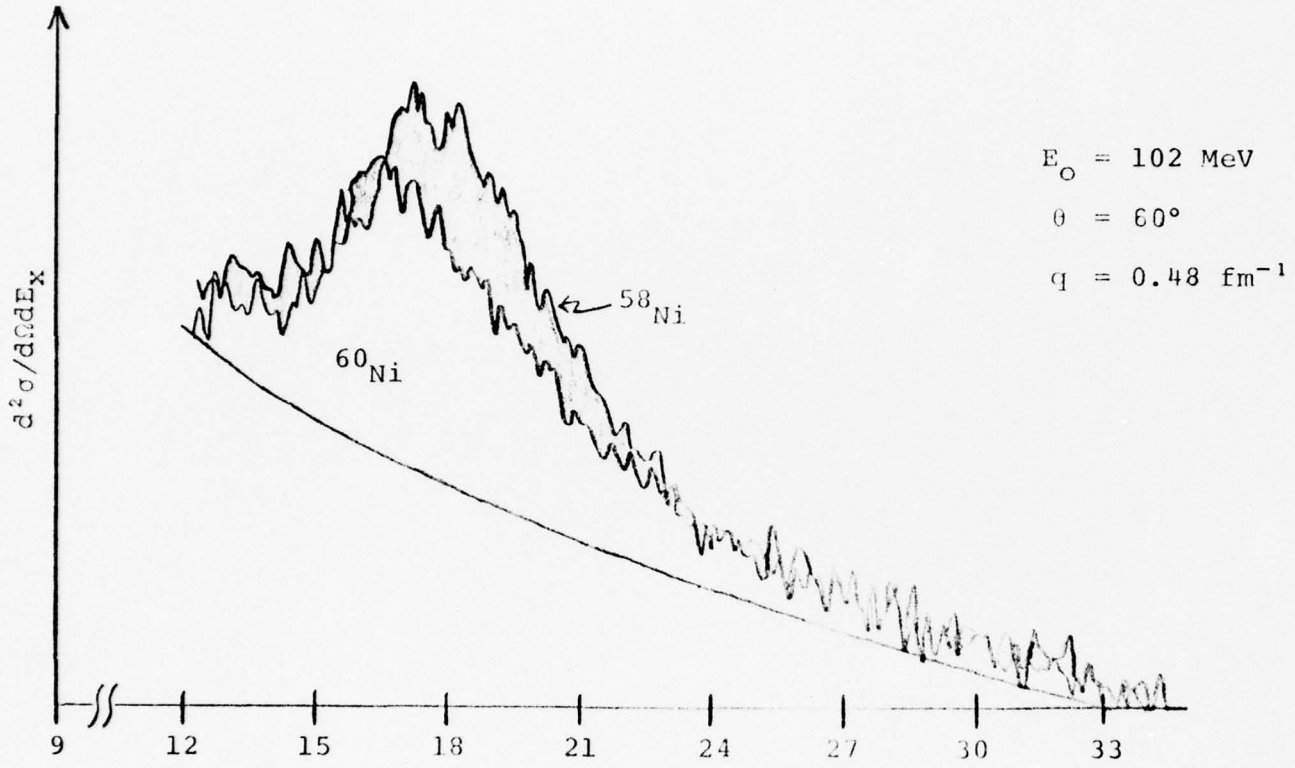


FIGURE 28. COMPARISON OF TOTAL CROSS SECTIONS FOR ^{58}Ni AND ^{60}Ni AT 60^{o}



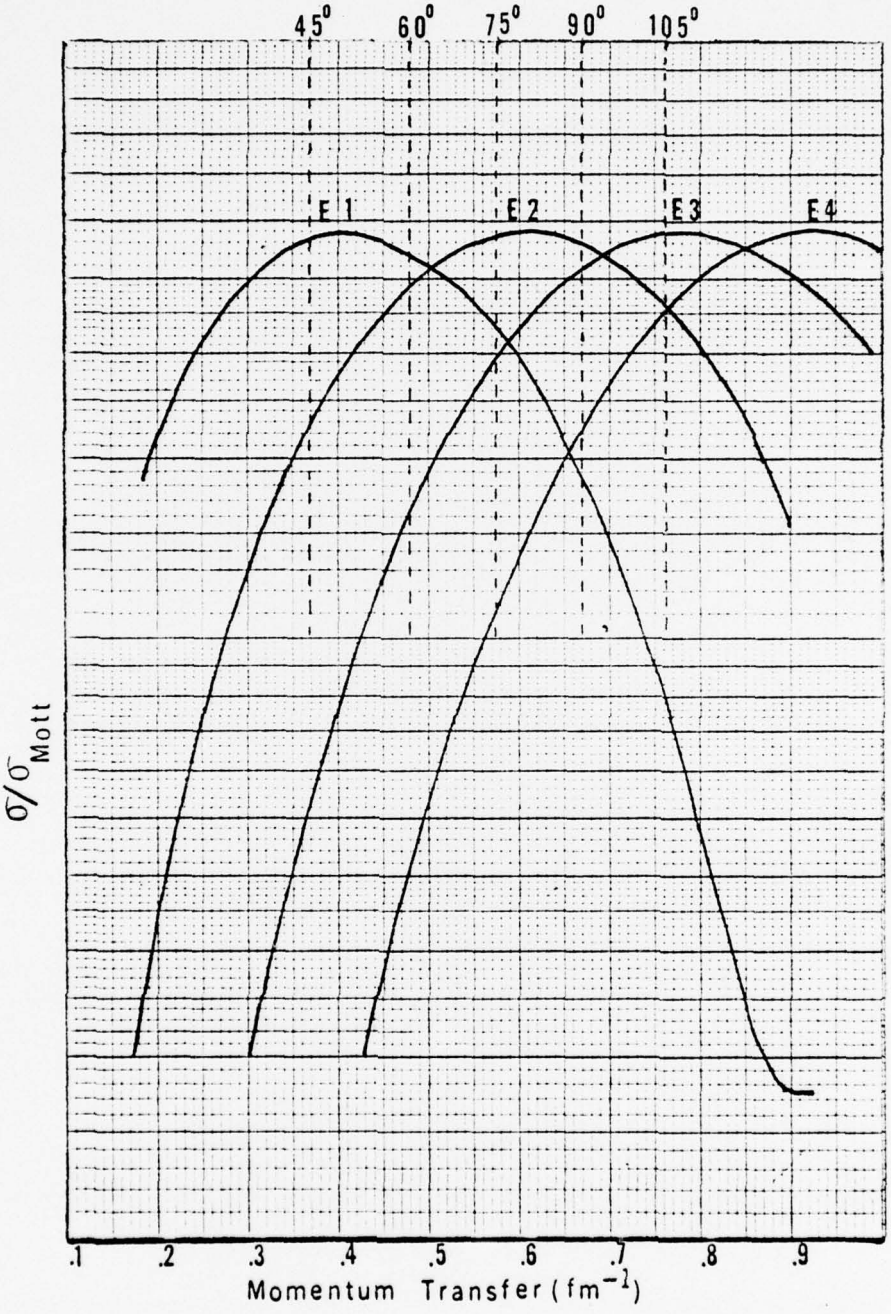


FIGURE 29. Normalized DWBA Cross Sections for E1 to E4 Transitions (Form Factors Squared)

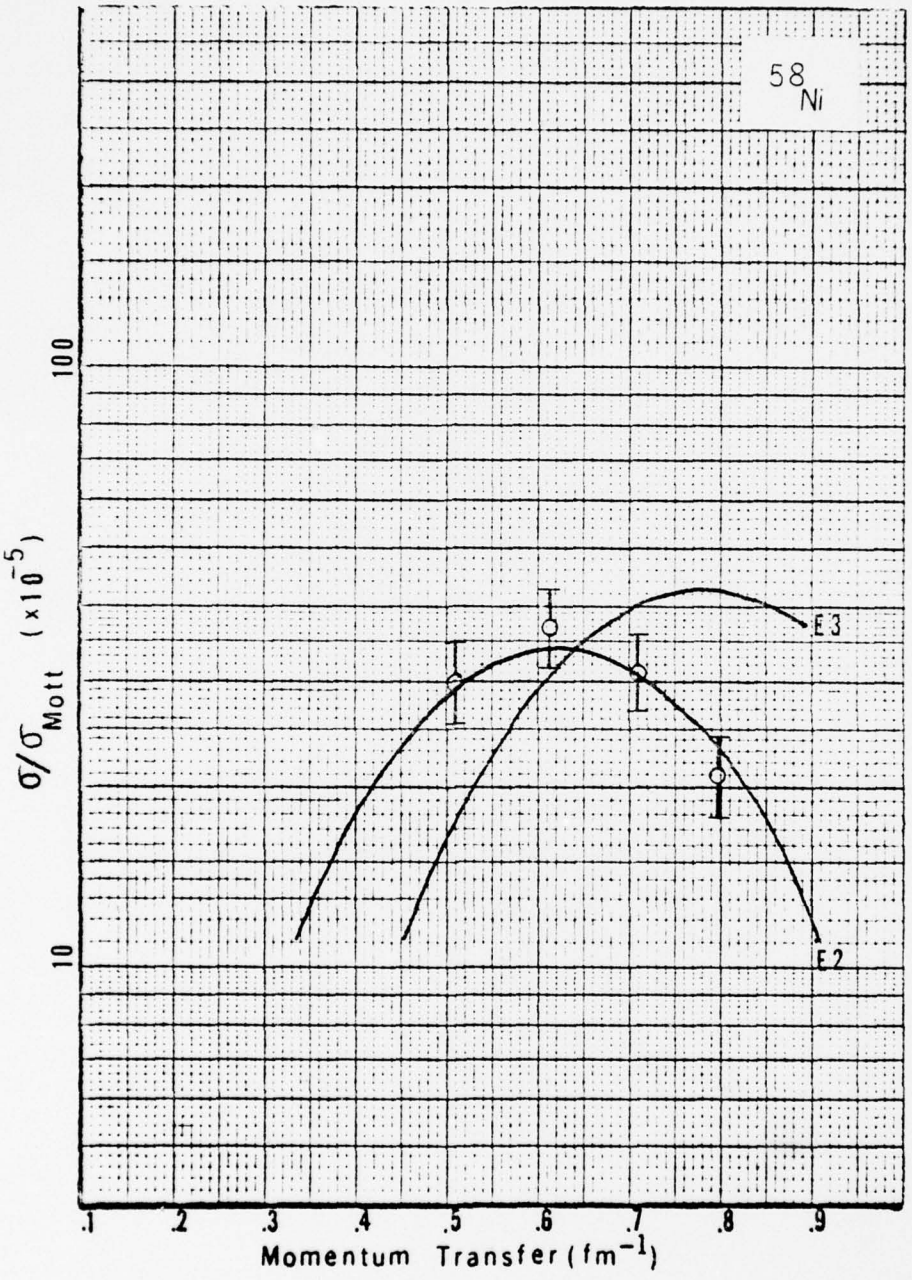


FIGURE 30. Experimental inelastic form factors squared for state at 6.00 MeV

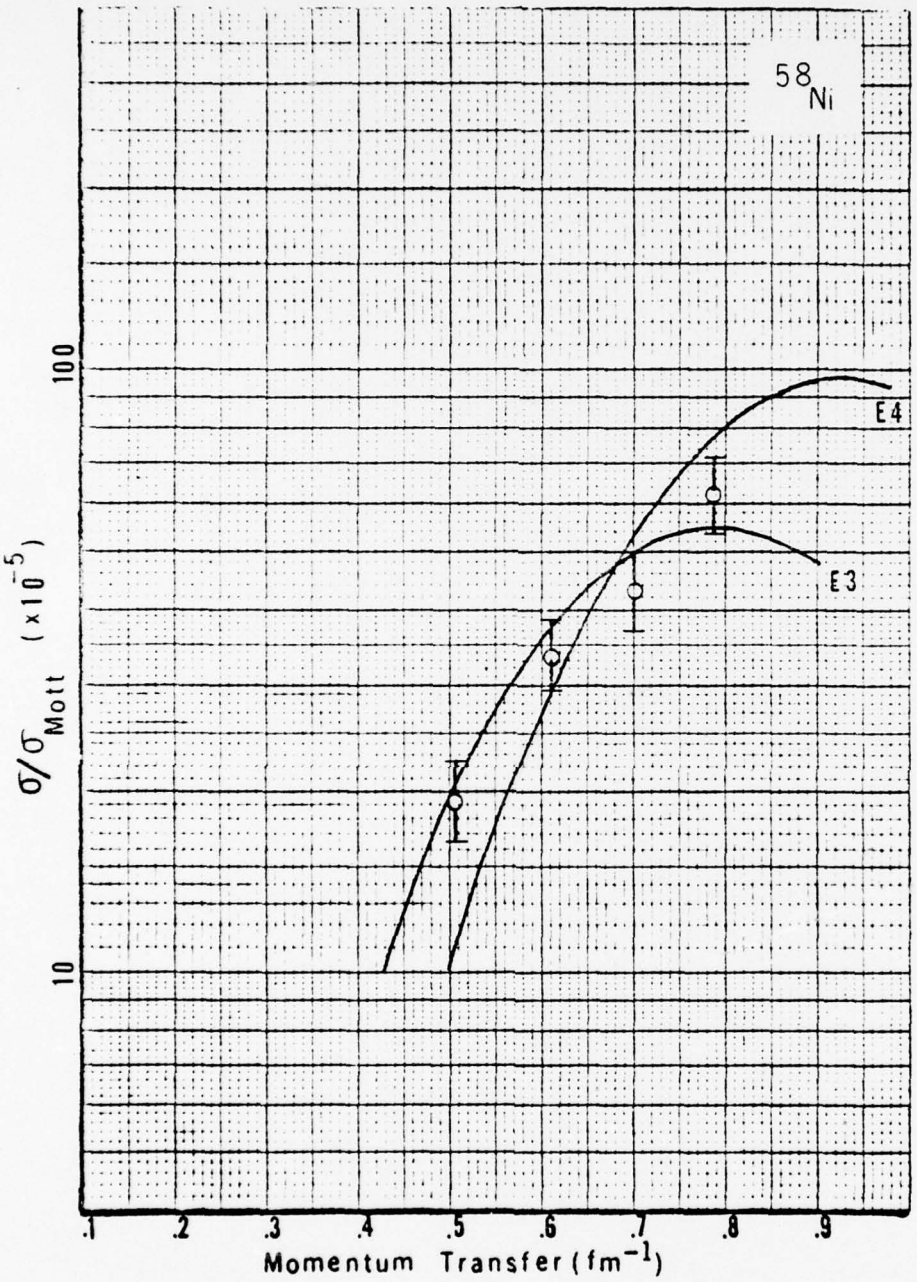


FIGURE 31. Experimental inelastic form factors squared for state at 6.96 MeV

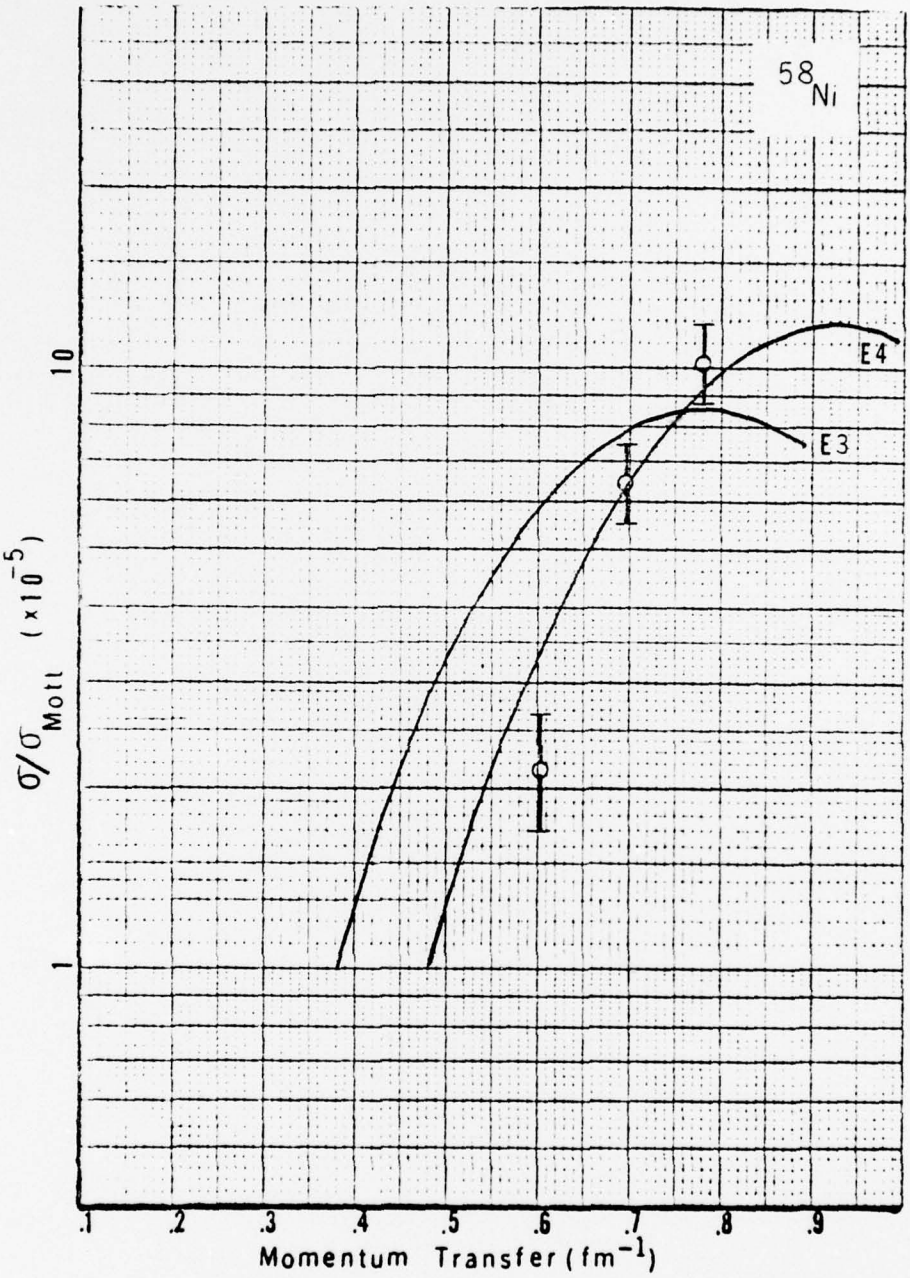


FIGURE 32. Experimental inelastic form factors squared for state at 9.6 Mev

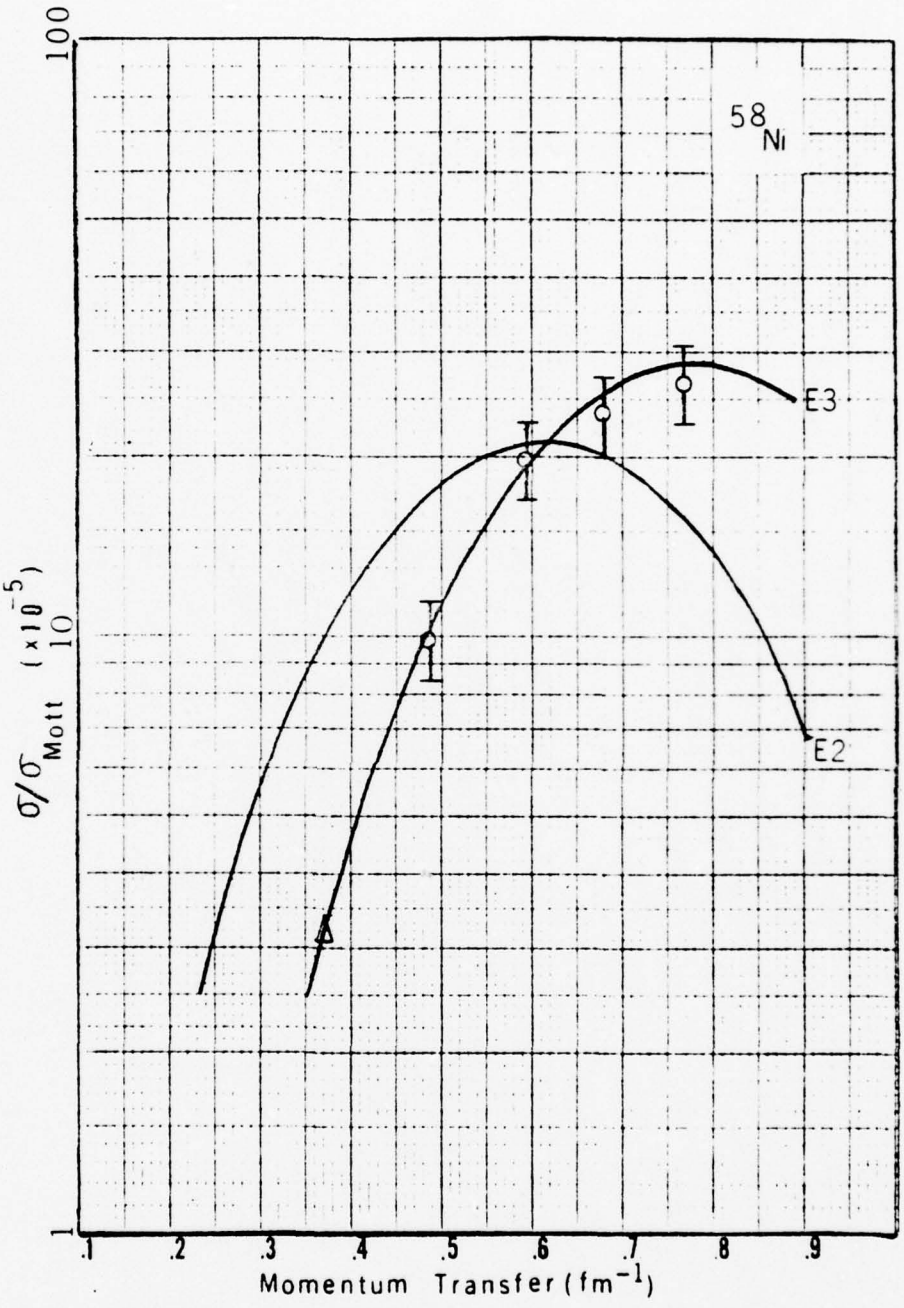


FIGURE 33. Experimental inelastic form factors squared for state at 13.3 MeV

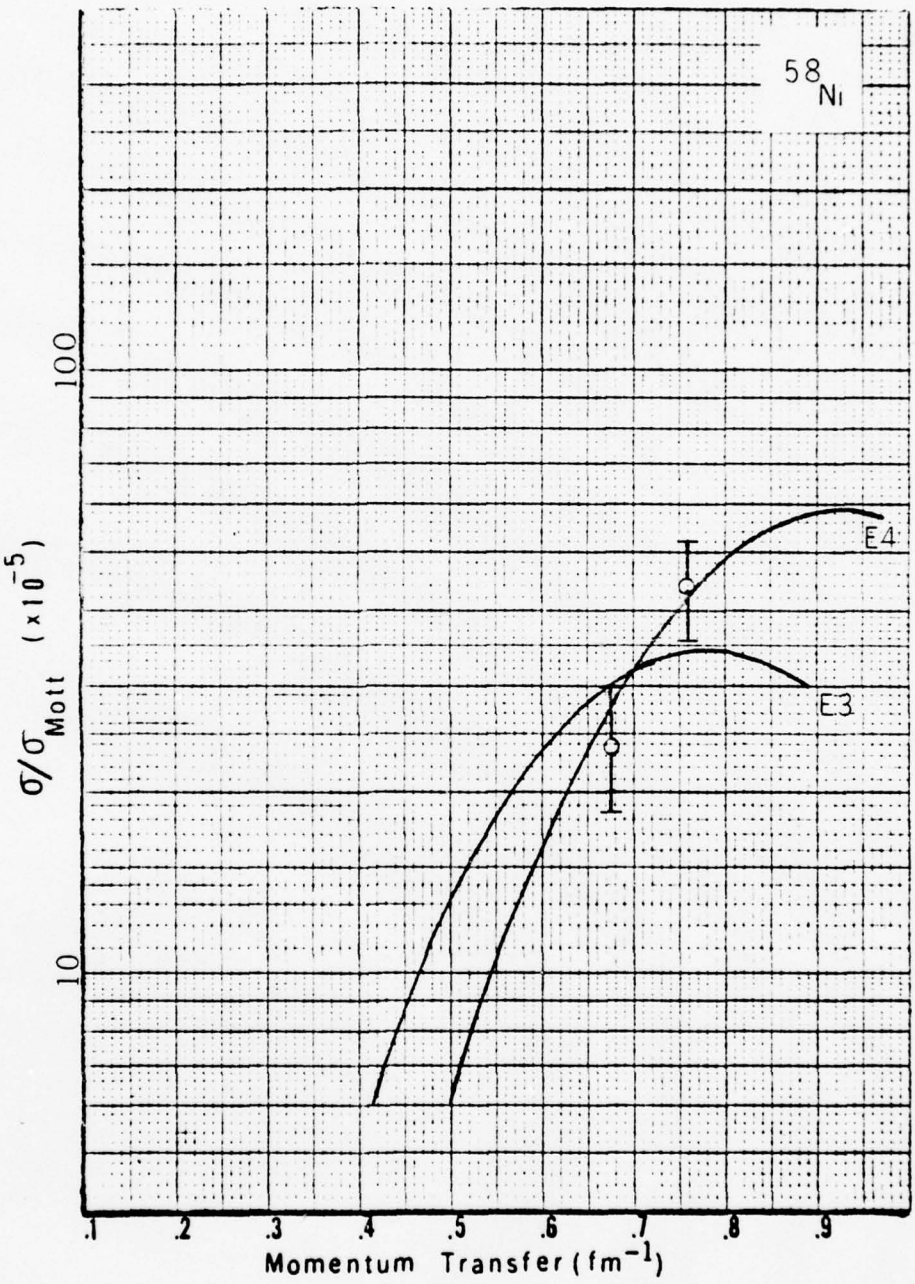


FIGURE 34. Experimental inelastic form factors squared for state at 15.1 MeV

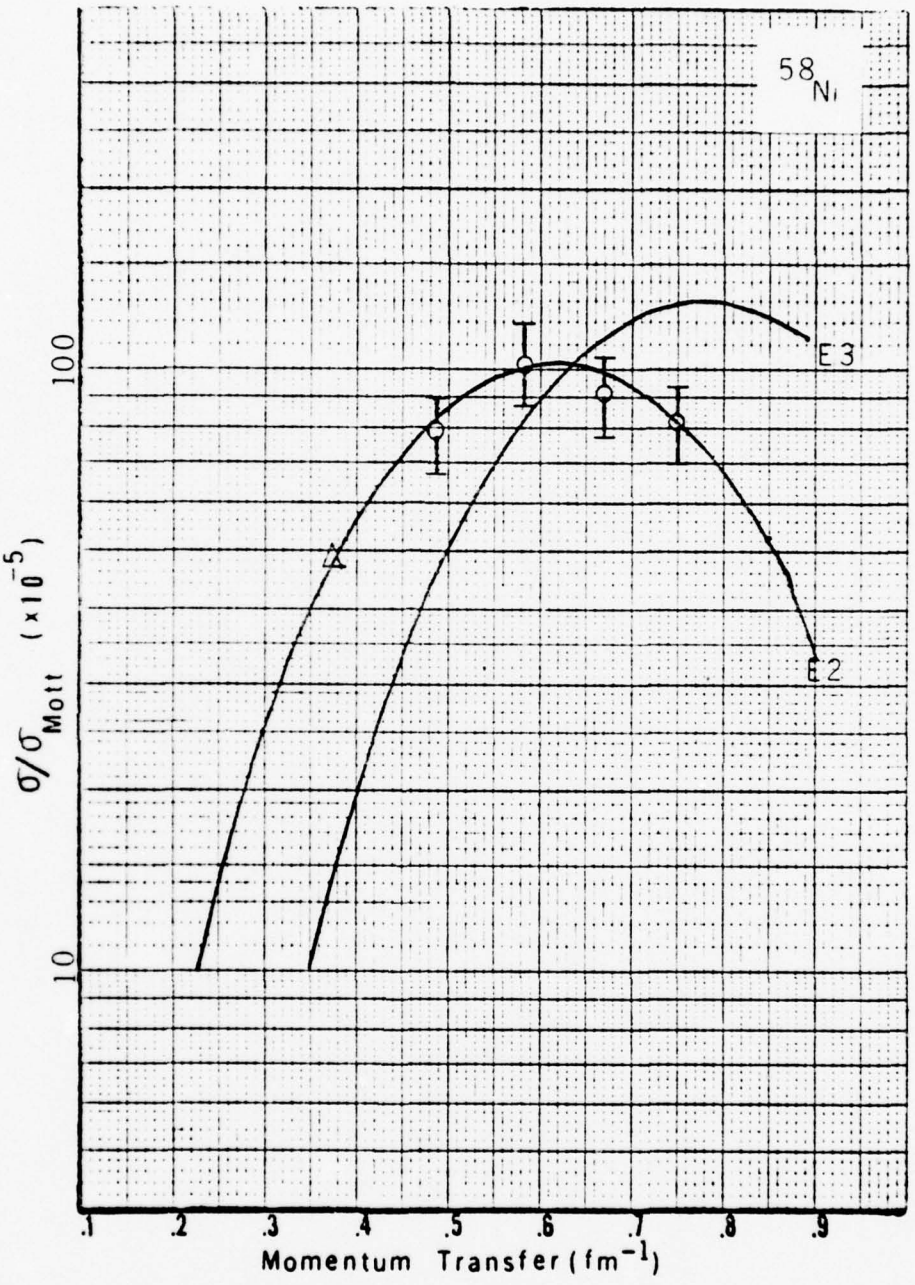


FIGURE 35. Experimental inelastic form factors squared for state at 16.3 MeV

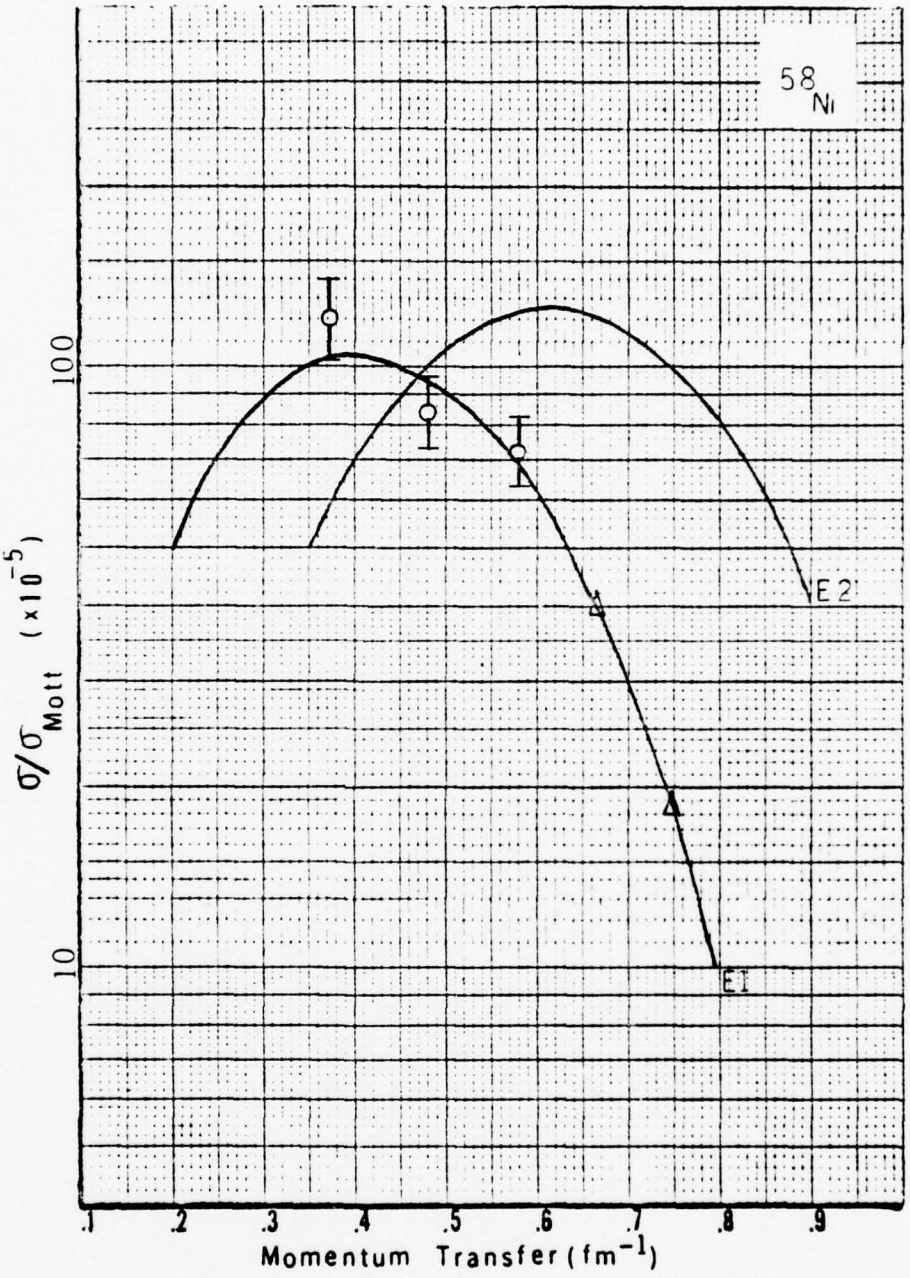


FIGURE 36. Experimental inelastic form factors squared for state at 18.3 MeV

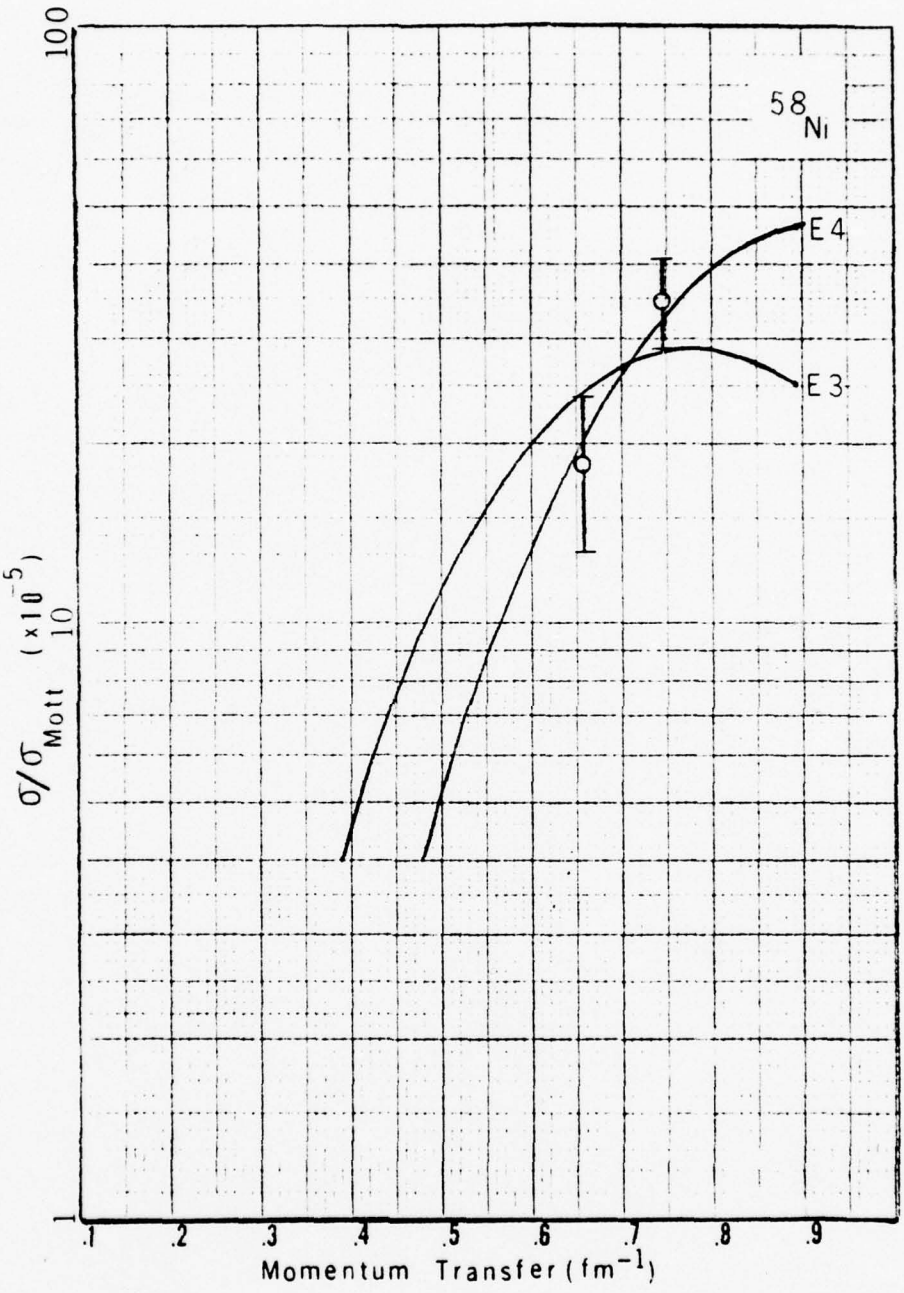


FIGURE 37. Experimental inelastic form factors squared for state at 20.0 MeV

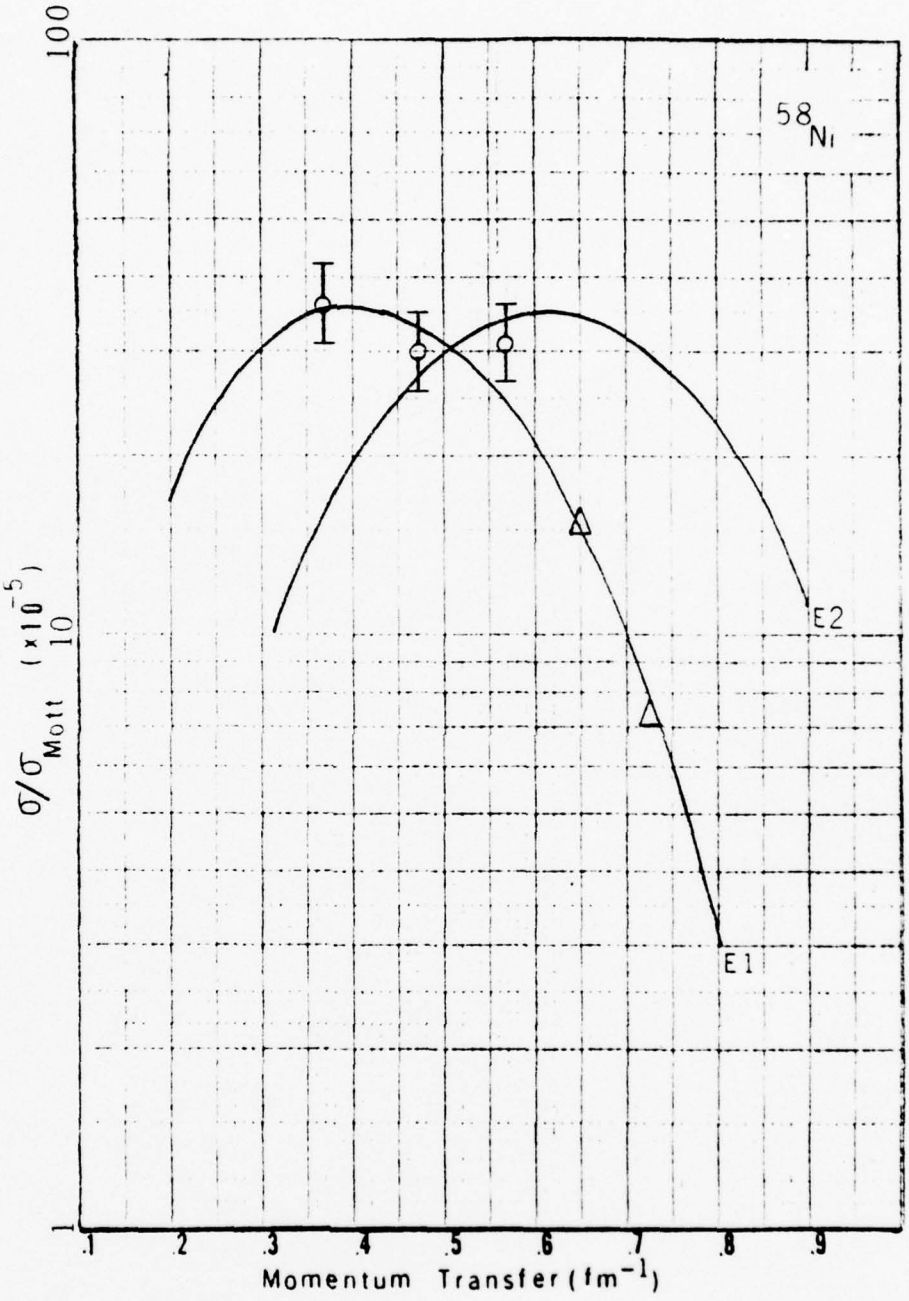


FIGURE 38. Experimental inelastic form factors squared for state at 21.75 MeV

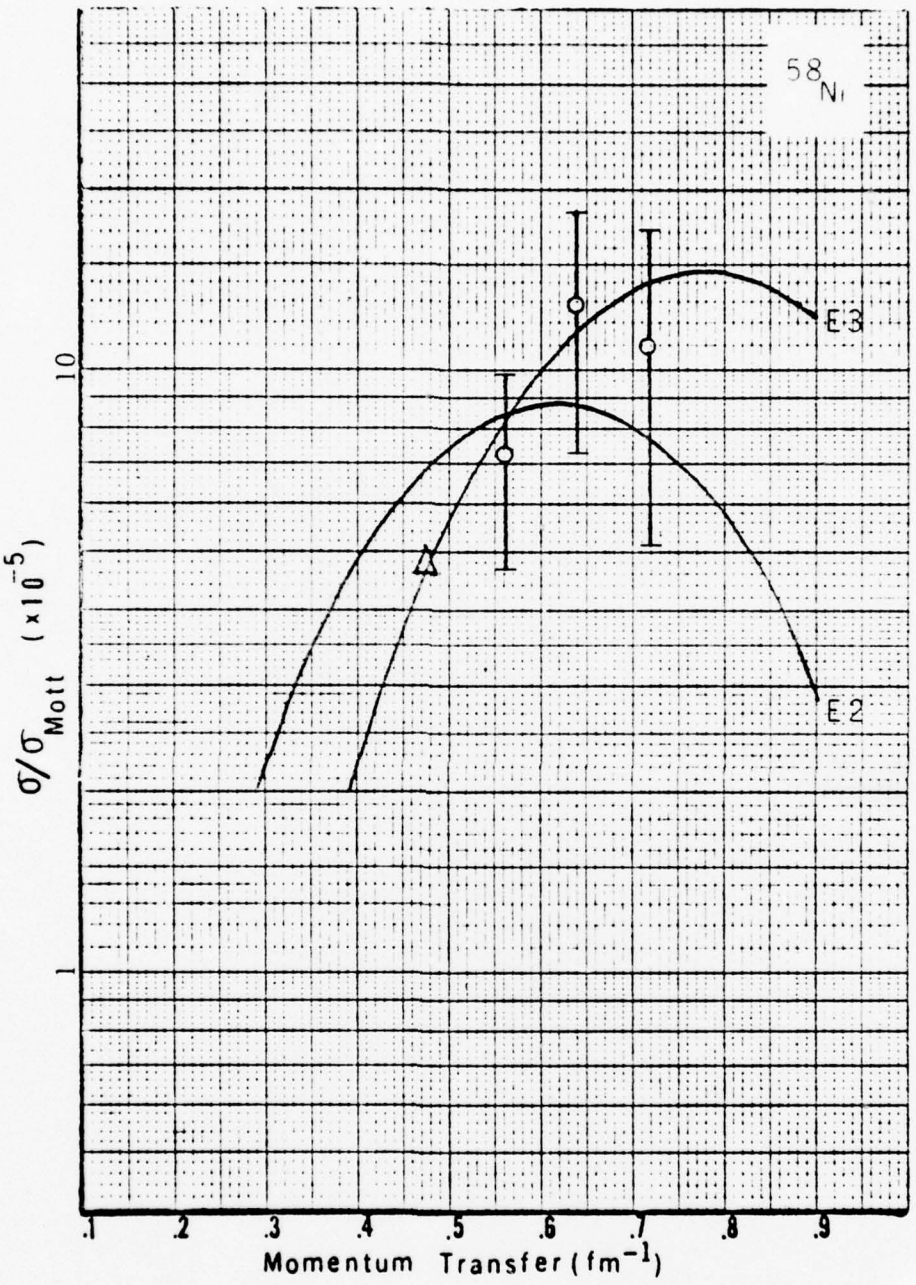


FIGURE 39. Experimental inelastic form factors squared for state at 27.0 MeV

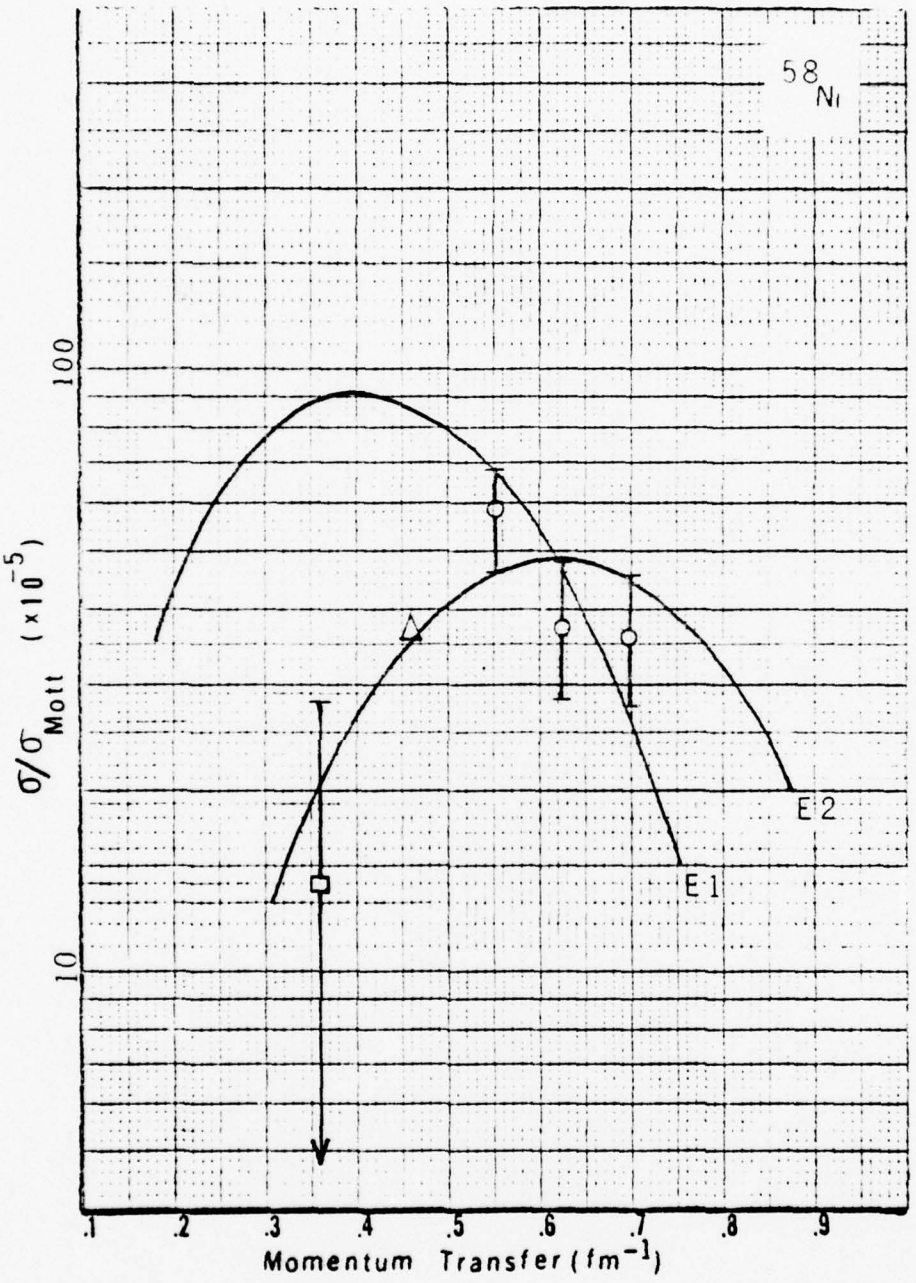


FIGURE 10. Experimental inelastic form factors squared for state at 32.0 Mev

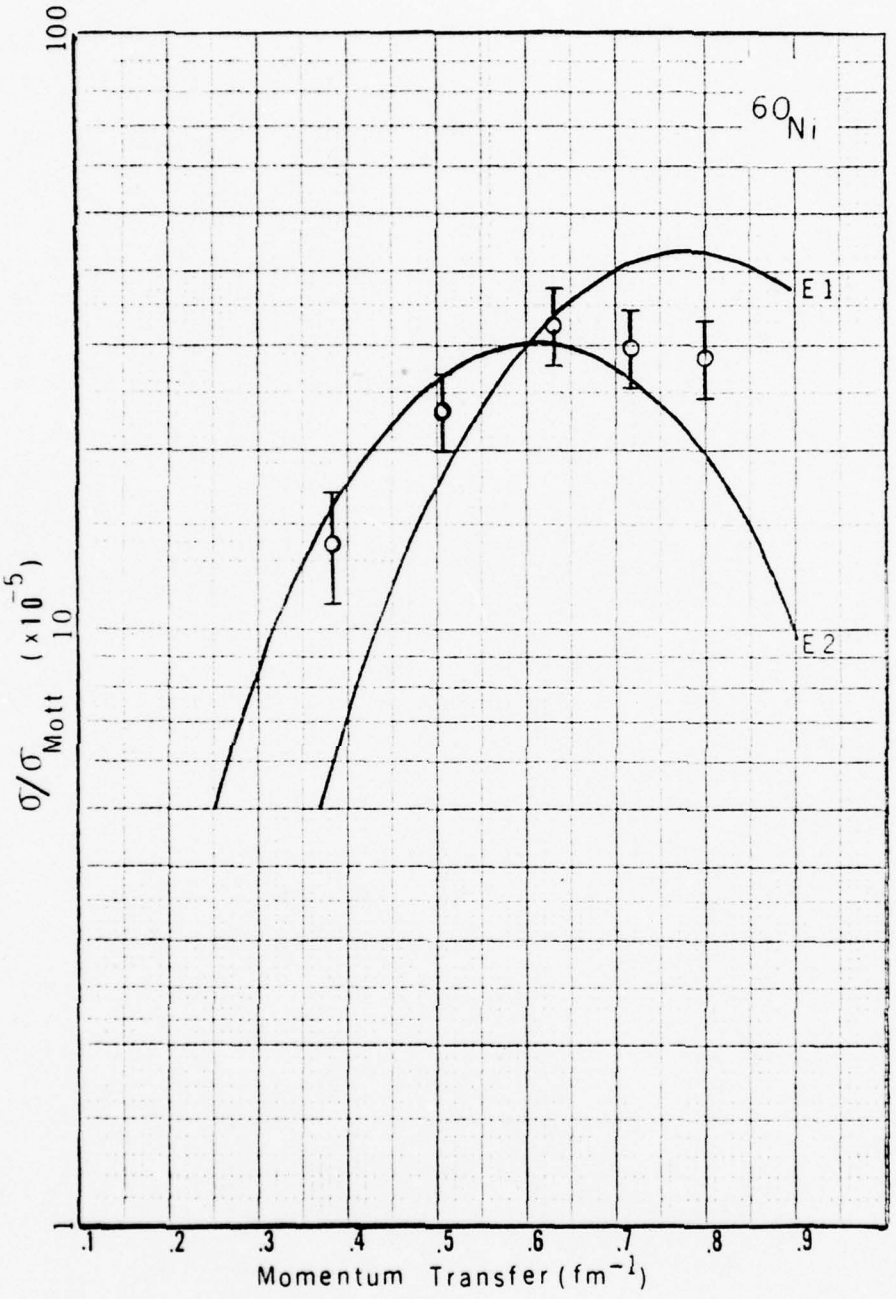


FIGURE 41. Experimental inelastic form factors squared for state at 6.12 MeV

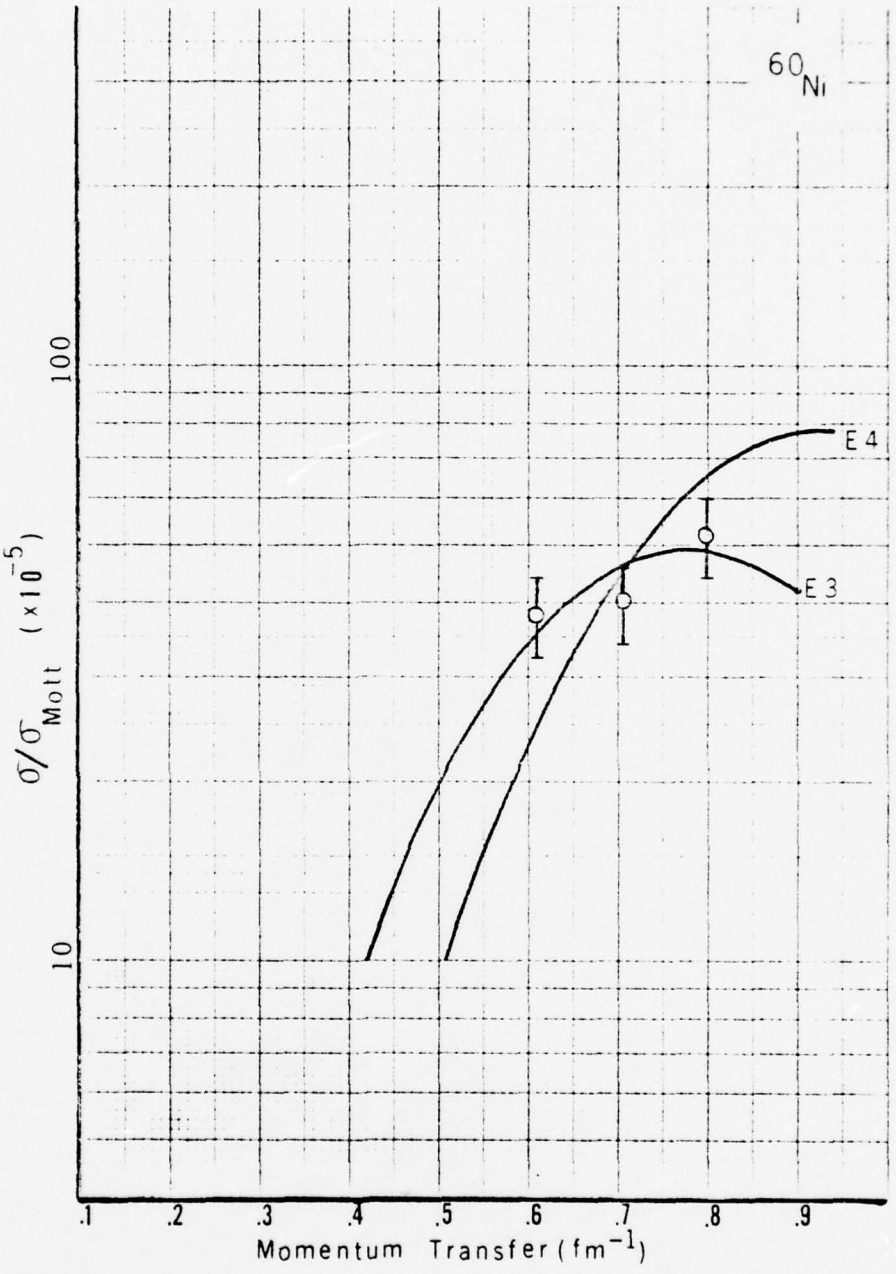


FIGURE 42. Experimental inelastic form factors squared for state at 7.0 + 7.6 MeV

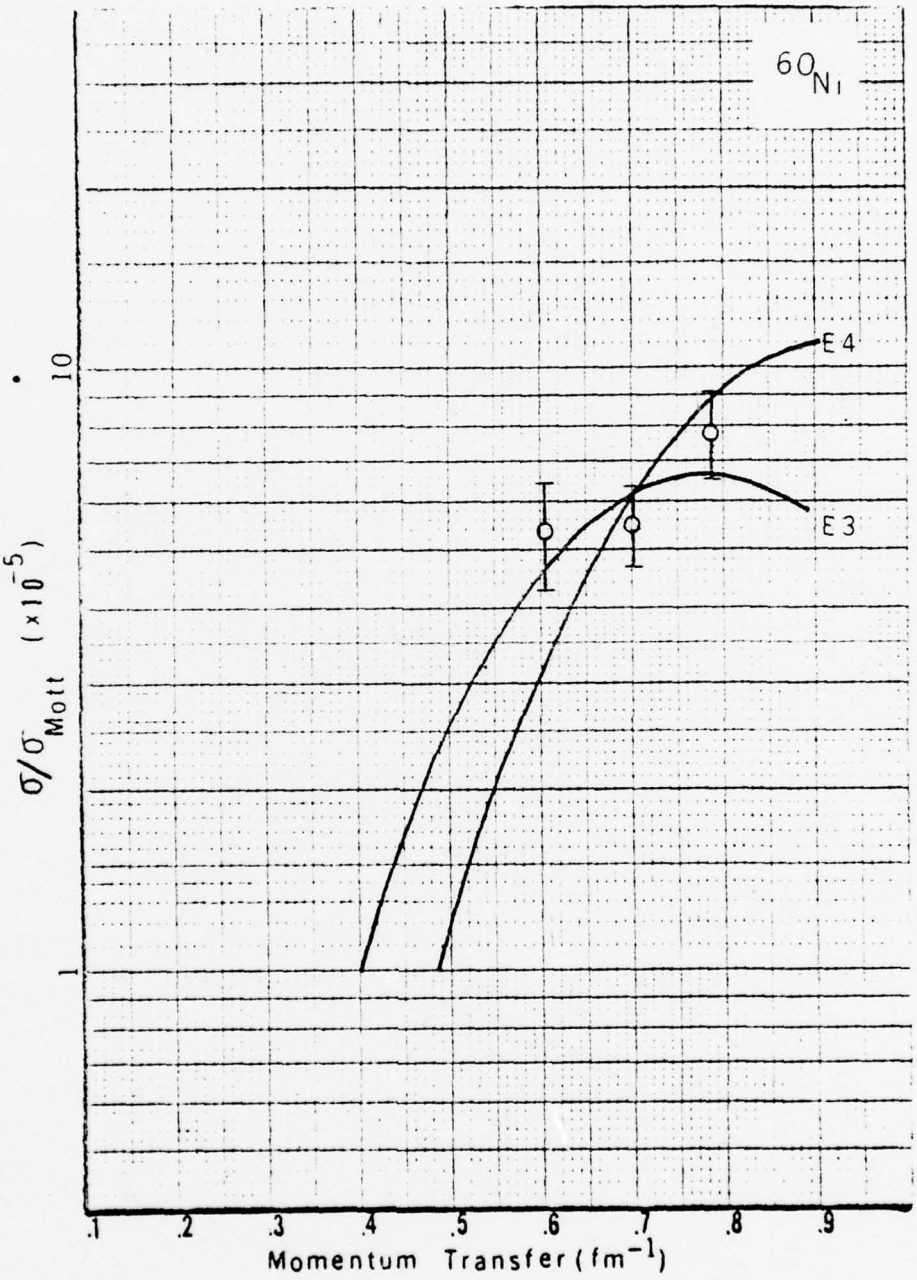


FIGURE 43. Experimental inelastic form factors squared for state at 8.7 MeV

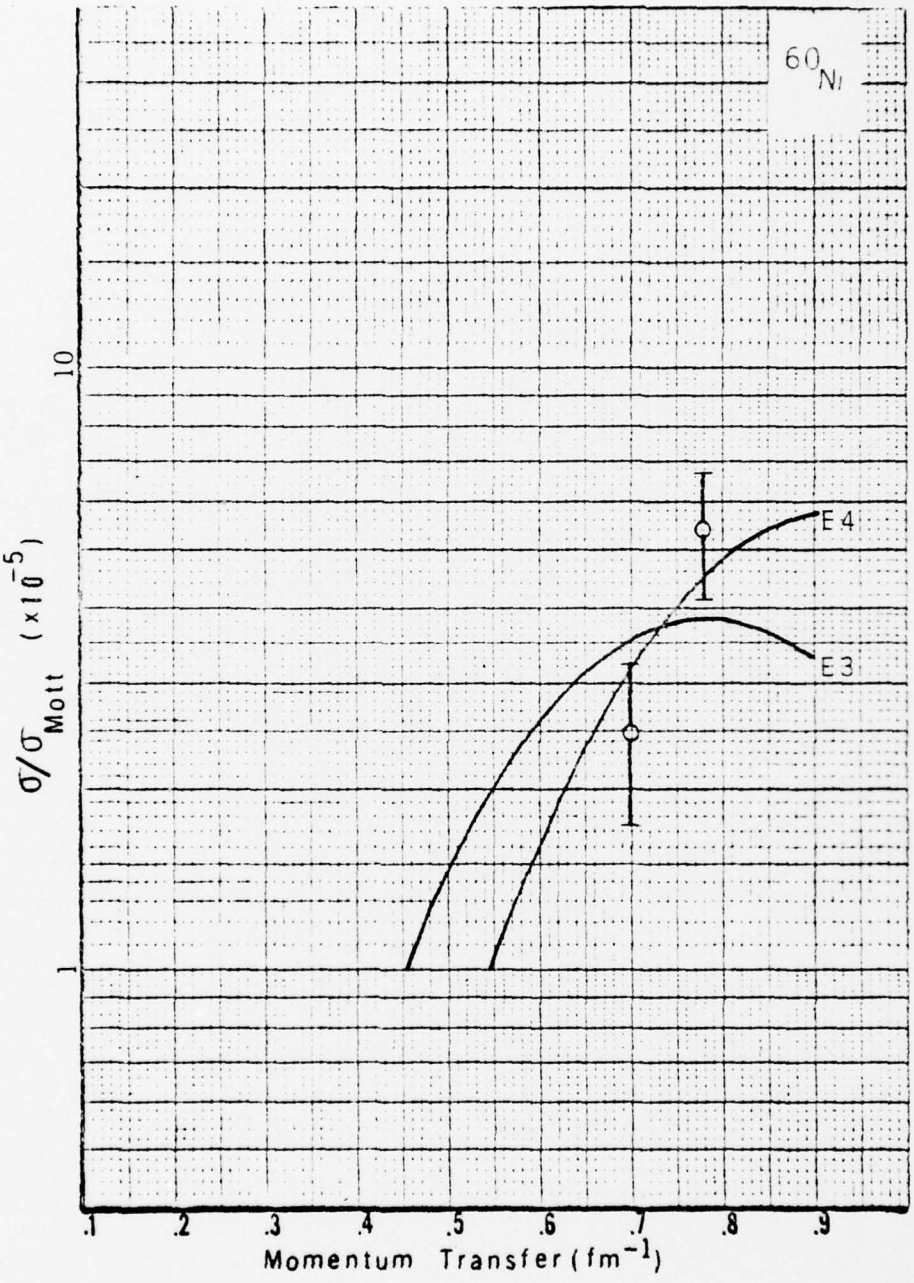


FIGURE 44. Experimental inelastic form factors squared for state at 11.4 MeV

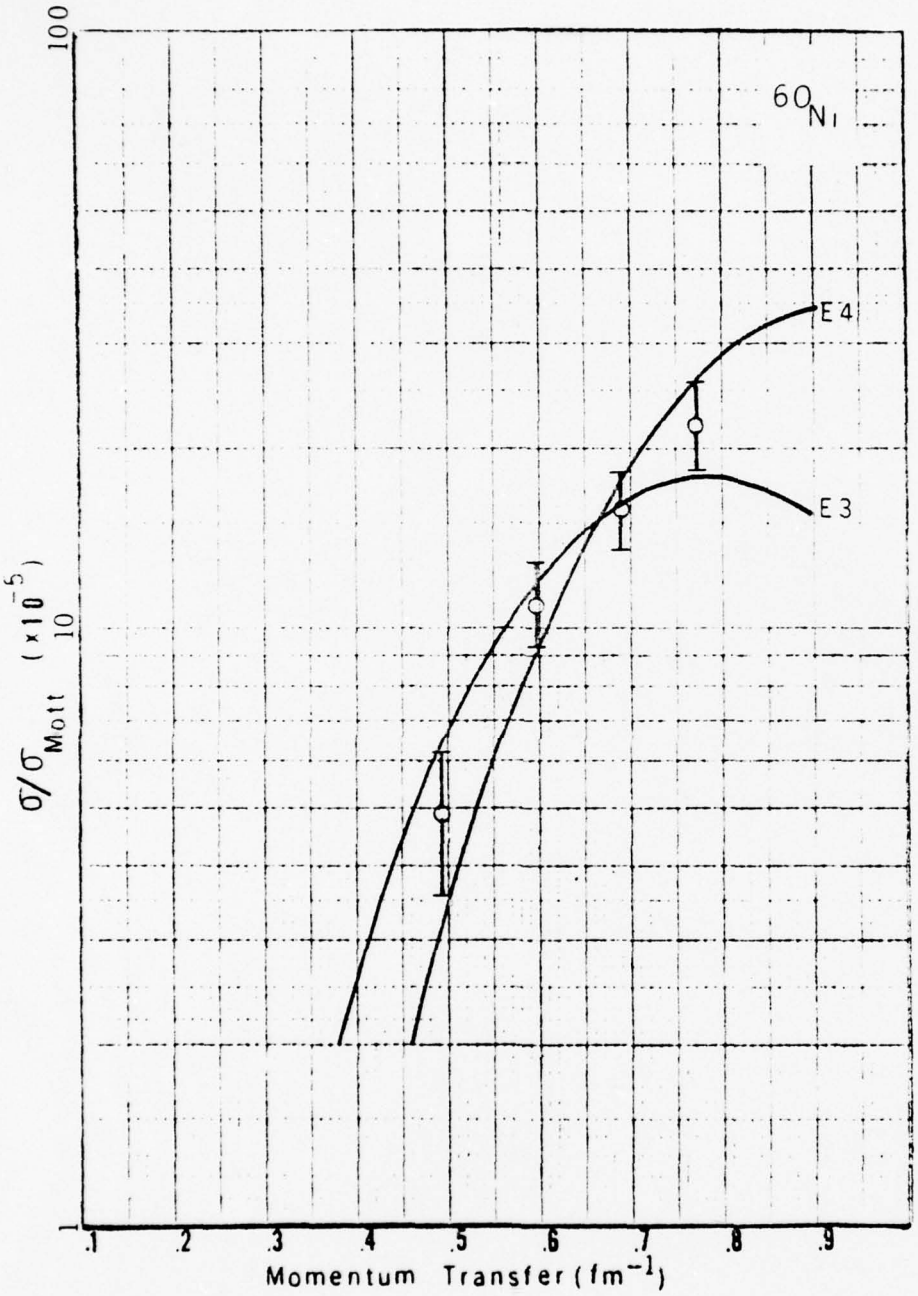


FIGURE 45. Experimental inelastic form factors squared for state at 12.8 MeV

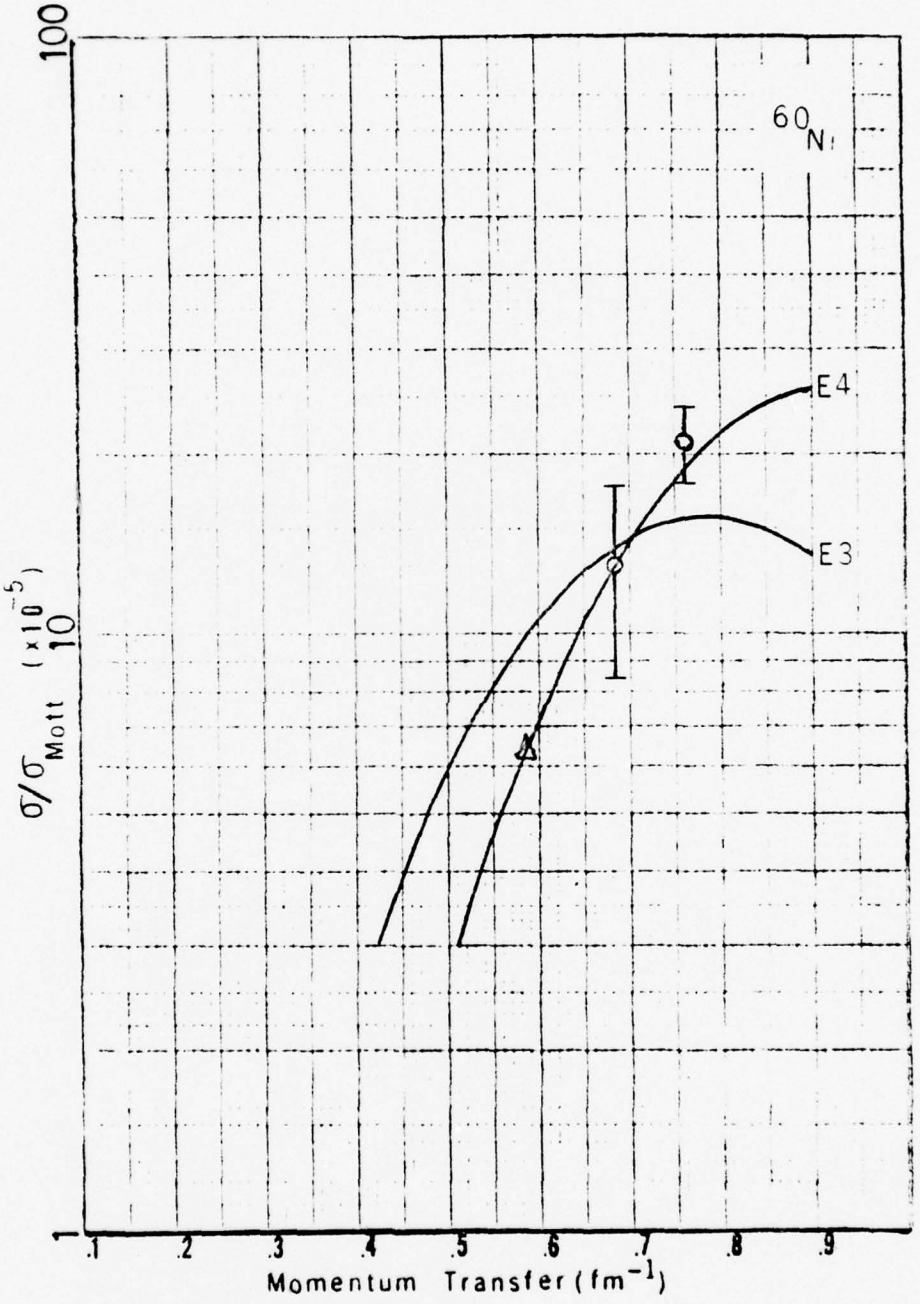


FIGURE 46. Experimental inelastic form factors squared for state at 14.9 MeV

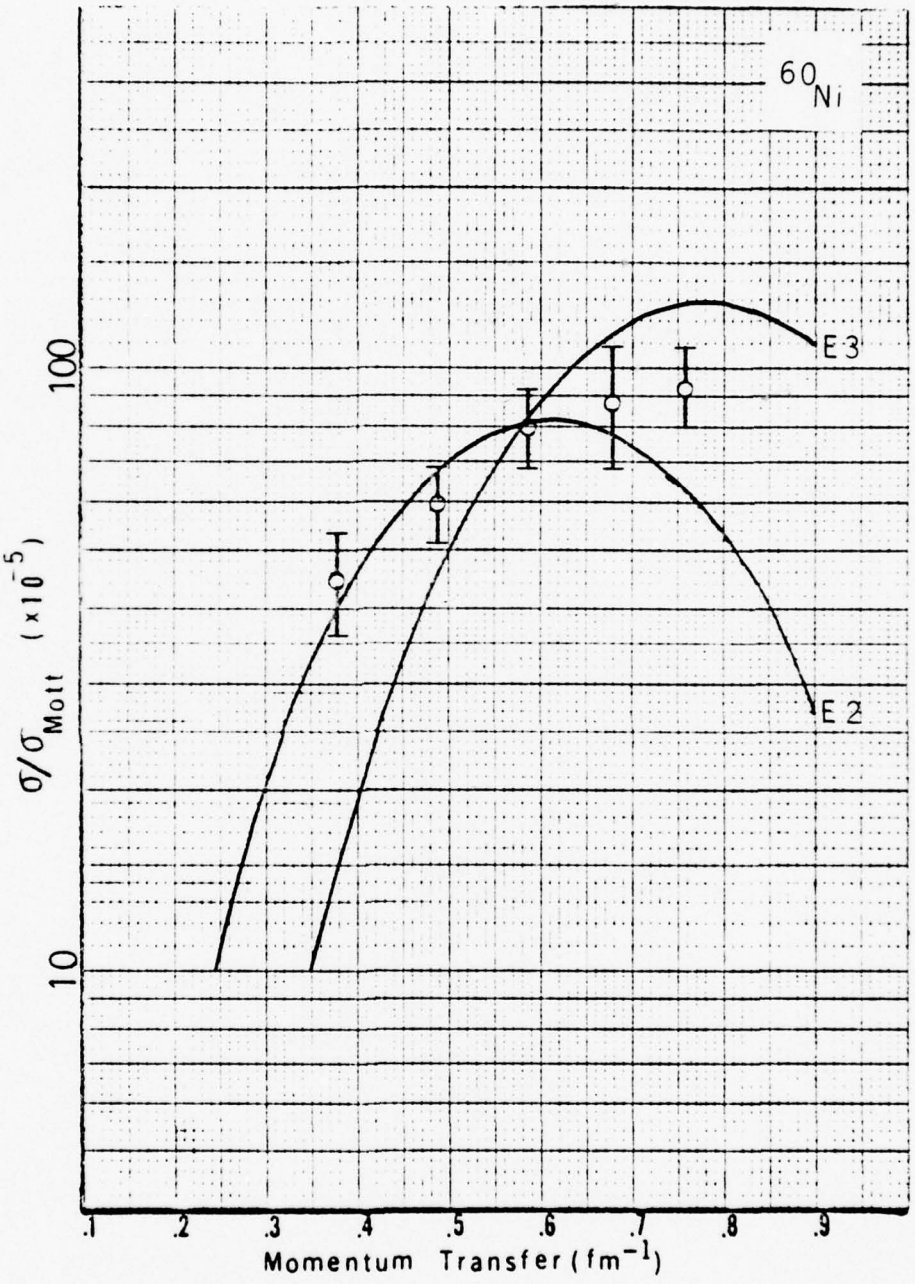


FIGURE 47. Experimental inelastic form factors squared for state at 16.2 MeV

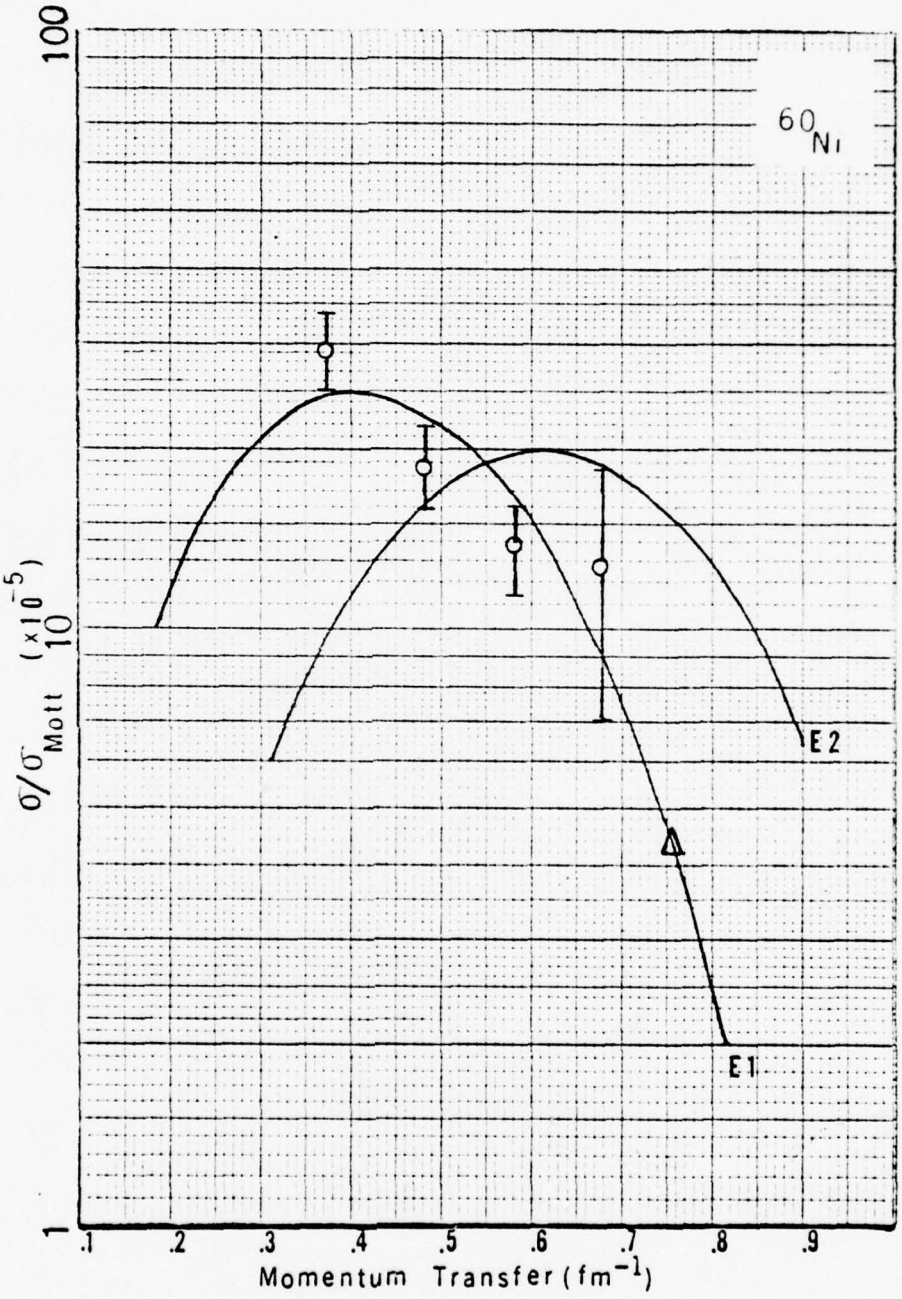


FIGURE 48. Experimental inelastic form factors squared for state at 16.7 MeV

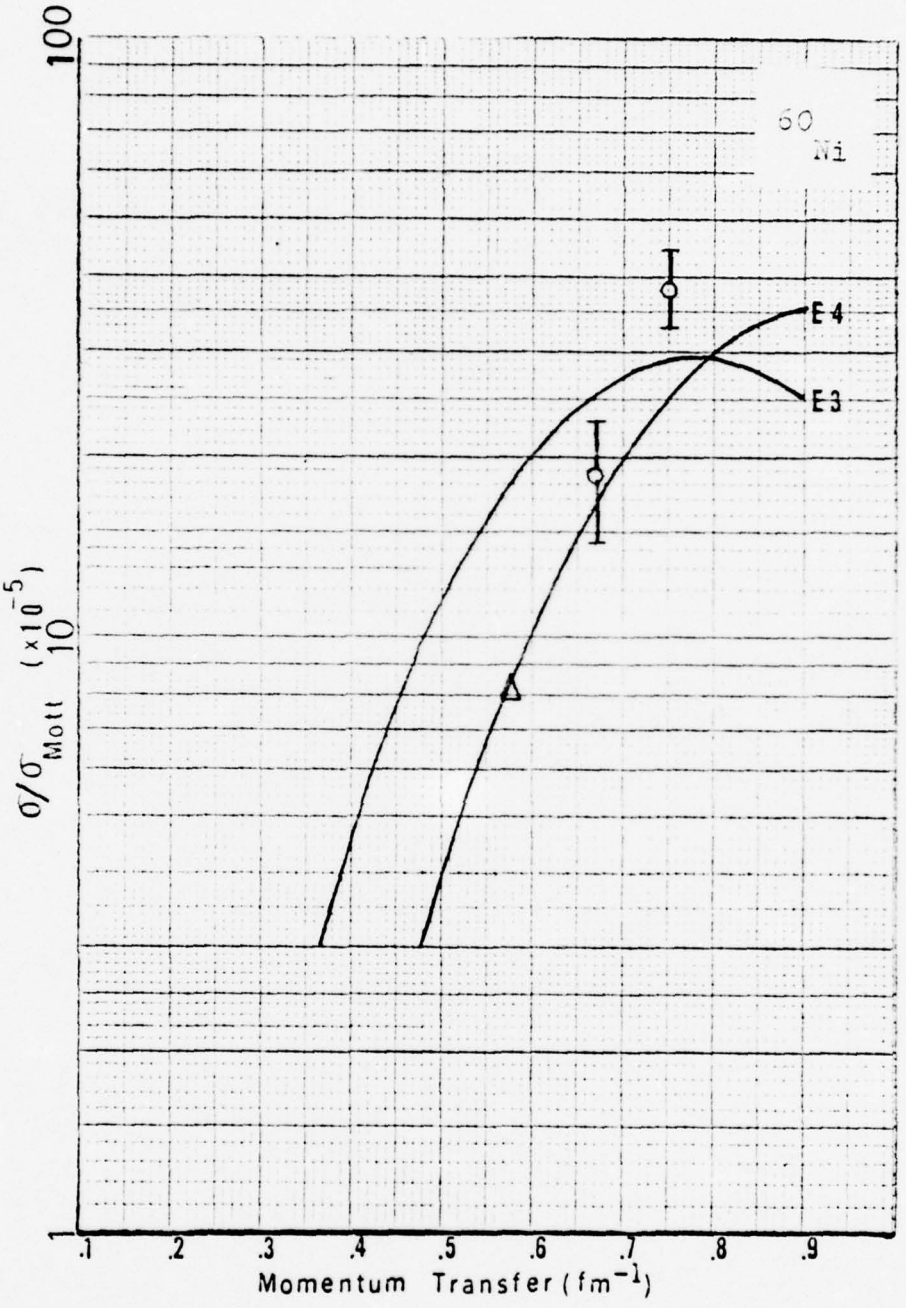


FIGURE 49. Experimental inelastic form factors squared for state at 18.6 MeV

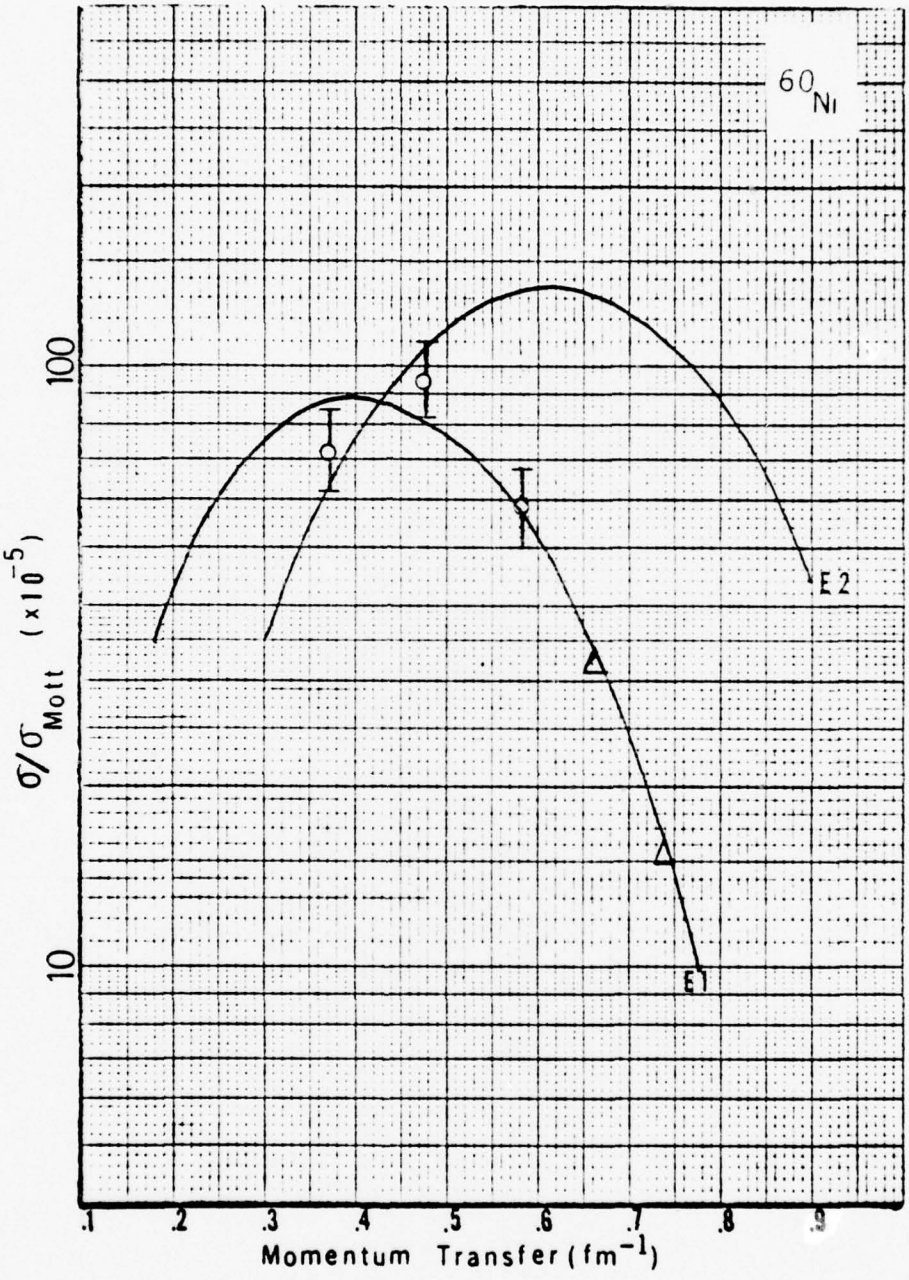


FIGURE 50. Experimental inelastic form factors squared for state at 19.2 MeV

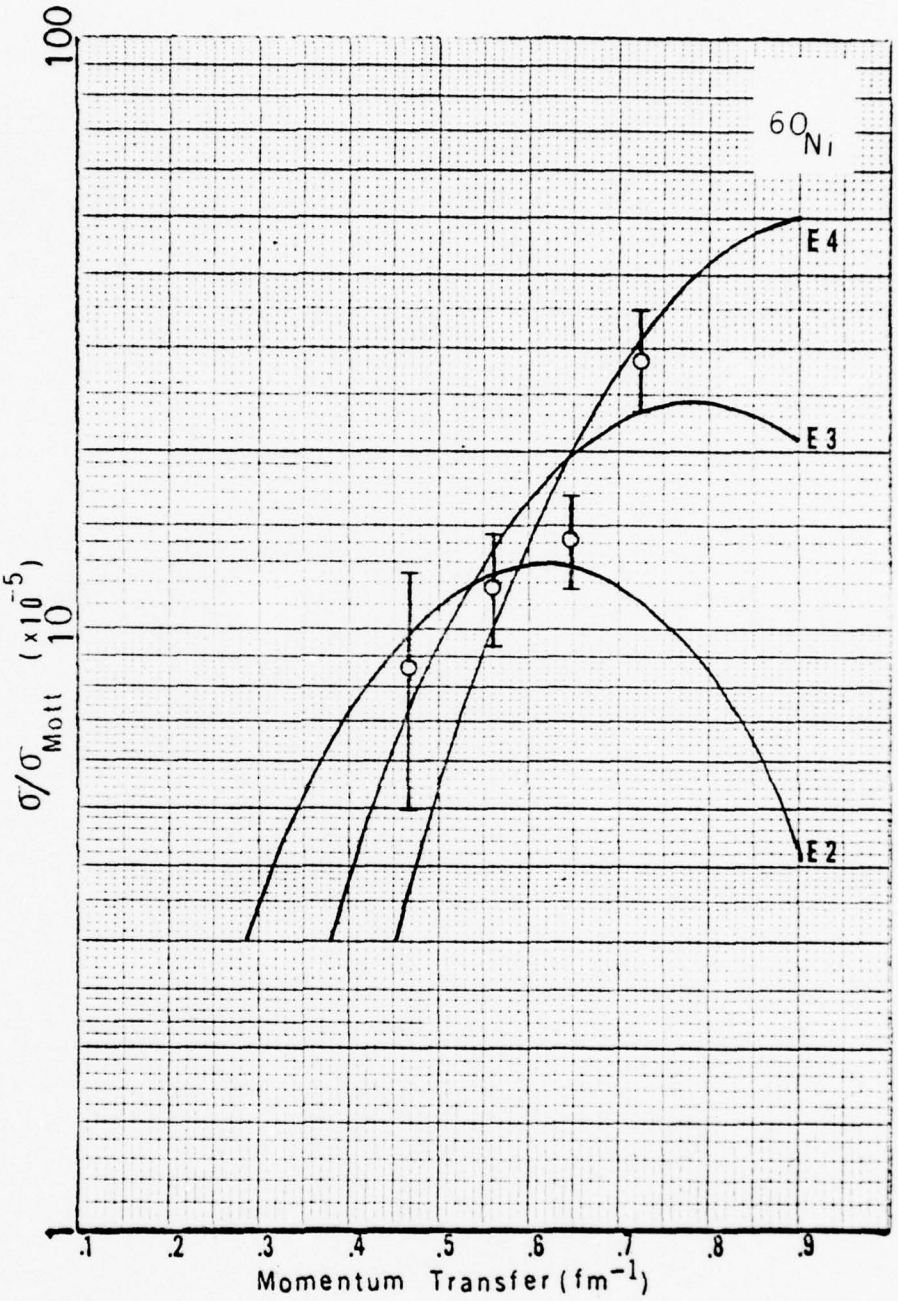


FIGURE 51. Experimental inelastic form factors squared for state at 27.1 MeV

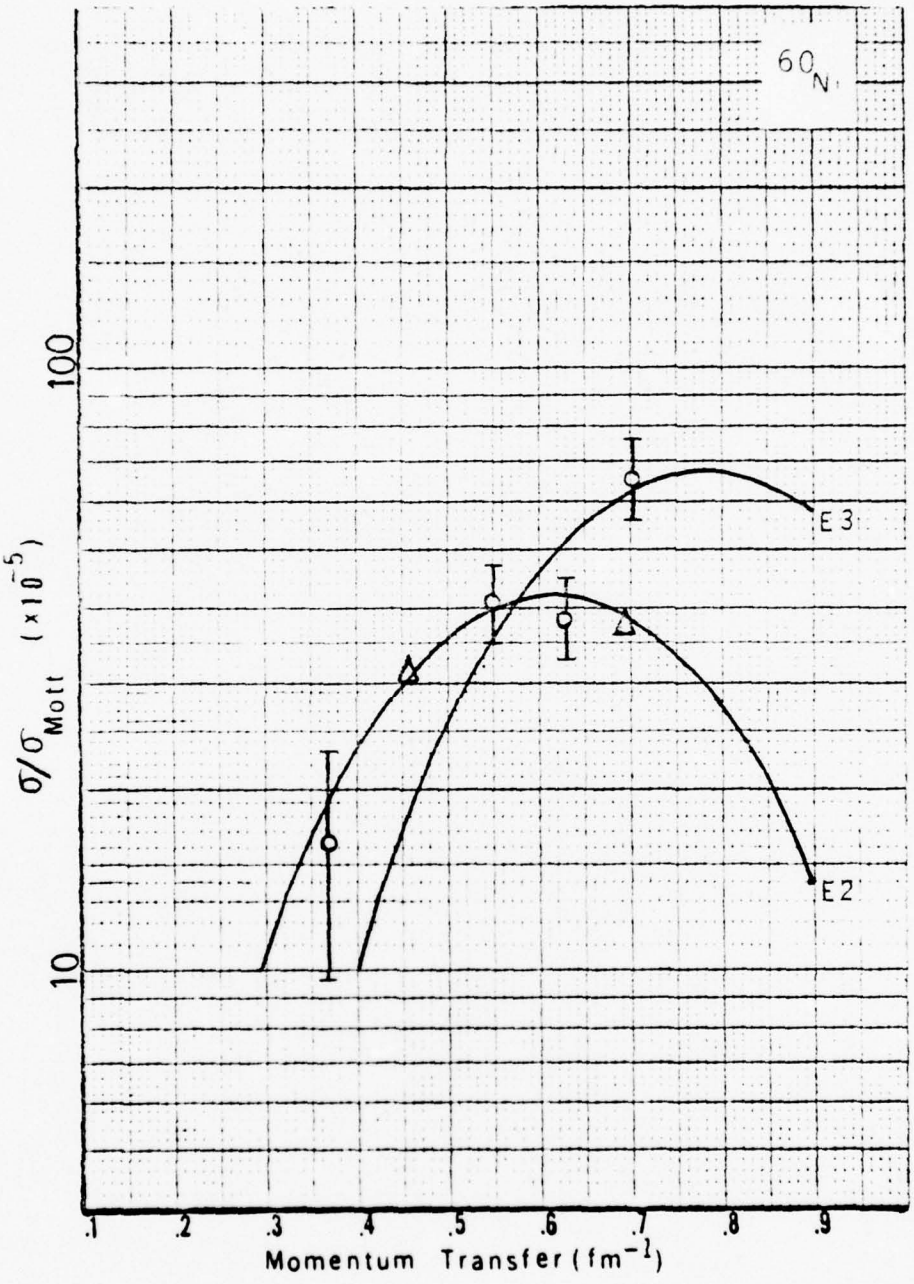


FIGURE 52. Experimental inelastic form factors squared for state at 32.0 MeV

FIGURE CAPTIONS

FIGURES 1, 3, 6, 9, 12, 14, 16, 19, 22, and 25

102.0 MeV electrons scattered inelastically from ^{58}Ni and ^{60}Ni under 45°, 60°, 75°, 90°, and 105°. The fitted background (consisting of the radiation tail and machine background) has been subtracted. The relative change in peak height with angle (momentum transfer) indicates the contribution of the various multipoles. The spectra were taken and fitted with 10 data points per MeV. For graphical purposes, the number of points for these spectra was reduced by a factor of 4. The error for the 45° data of ^{58}Ni (Figure 1) is of the size of the data points. Note the horizontally suppressed scales for the 75° spectra of ^{58}Ni and the 75° and 90° spectra of ^{60}Ni.

FIGURES 2, 4, 15, and 17

102.0 MeV electrons scattered inelastically from ^{58}Ni and ^{60}Ni under 45° and 60°. The fitted background (consisting of the radiation tail and machine background) has been subtracted. Additionally, the three-step sequence of plots indicates the removal of the ghost peak, E2 resonances, and the E3 resonances (in that order) in the GR region in order that the contribution of the GDR's to the spectra may be visualized more clearly. The spectra were taken and fitted with 10 data points per MeV. For graphical purposes, the number of points for these spectra was reduced by a factor of 4. Note the horizontally suppressed scale for the 45° spectra of ^{58}Ni (Figure 2).

FIGURES 5, 8, 11, 18, 21, and 24

102.0 MeV electrons scattered inelastically from ^{58}Ni and ^{60}Ni under 75°, 90°, and 105°. The fitted background (consisting of the radiation tail and machine background) has been included. The resonances which were used for fitting the spectra and the background as described in the results are drawn. The spectra were taken and fitted with 10 data points per MeV. For graphical purposes, the number of points for all spectra was reduced by a factor of 4. Note the suppressed vertical and horizontal scales for all spectra except the 105° spectra of ^{58}Ni where only the vertical scale is suppressed.

FIGURES 7 and 20

102.0 MeV electrons scattered inelastically from ^{58}Ni and ^{60}Ni under 75°. The fitted background consisting of the radiation tail and machine background) has been subtracted. Additionally, the three-step sequence of plots indicates the removal of the ghost peak, the E1 resonances, and the E3 resonances (in that order) in the GR region in order that the contribution of the Giant Quadrupole Resonances (both isoscalar and isovectors) to the spectra may be visualized more closely. The spectra were taken and fitted with 10 data points per MeV. For graphical purposes, the number of points for these spectra was reduced by a factor of 4. Note the suppressed horizontal scale in both Figures 7 and 20.

FIGURES 10, 13, 23, and 26

102.0 MeV electrons scattered inelastically from ^{58}Ni and ^{60}Ni under 90° and 105°. The fitted background (consisting of the radiation tail and machine background) has been subtracted. Additionally, the three-step sequence of plots indicates the removal of the ghost peak, the E1 resonances, and the E2 resonances (in that order) in the GR region in order that the contribution of the Giant Octupole Resonances (E3) to the spectra may be visualized more clearly. The spectra were taken and fitted with 10 data points per MeV. For graphical purposes, the number of points for these spectra was reduced by a factor of 4. Note the suppressed horizontal scale of the 90° spectra of ^{60}Ni (Figure 23).

FIGURES 27 and 28

Comparison of ^{58}Ni and ^{60}Ni spectra of 102.0 MeV electrons scattered inelastically under 45° and 60°. The spectra were taken with 10 data points per MeV. The background does not correspond to the real background and is only intended to guide the eye. Note the suppressed horizontal scales in both Figures 27 and 28.

FIGURE 29

DWBA cross sections for E1 to E4 transitions divided by the Mott cross section. The curves were normalized so that the first maxima are equal. The program of Tuan et al. (TuaW68) was used with a transition charge density given by equation (III-23) the Goldhaber-Teller model. The figure shows that momentum transfer covered by this experiment is selective for multipolarities 1 to 4.

FIGURE 30

Relative DWBA cross section using the Golhaber-Teller model compared to the experimental values for the state in ^{58}Ni at 6.0 MeV with a width of 1.09 MeV. The comparison favors an E2 assignment. The value for 45° was omitted since it was inconsistently higher than the remaining four values due to the effect of the ghost peak in this region of excitation energy. Error bars of 15% were assumed for all data points.

FIGURE 31

Similar to Figure 30, but for state at 6.96 MeV in ^{58}Ni, with a width of 0.8 MeV. An E3 assignment is evident from the comparison. The value at 45° was omitted since it plotted significantly higher than the remaining values. The E3 strength at 45° is insignificant and is dominated by the ghost peak in this region of excitation energy. Error bars of 15% were assumed for all data points.

FIGURE 32

Relative DWBA cross section using the Goldhaber-Teller model compared to the state in ^{58}Ni at 9.6 MeV with a width of 0.7 MeV. The comparison favors an E4 assignment. Error bars of 15% were assumed except at 75° where the statistical error was 22.5%.

FIGURE 33

Relative DWBA cross section using the Goldhaber-Teller model compared to the state in ^{58}Ni at 13.3 MeV with a width of 1.5 MeV. The comparison identifies this state as E3. The value at 45° was

fixed to a value consistent with the other four angles. This state could not assume the required strength in a free fit as should be expected for an E3 transition at 45°. Error bars of 15% were used for all points.

FIGURE 34

Relative DWBA cross section calculated with the Goldhaber-Teller model for the structure in ^{58}Ni at 15.1 MeV with a width of 4.3 MeV. An E4 assignment is favored based on the two data points available. Statistical error bars of 23% for 90° and 19% for 105° were plotted.

FIGURE 35

Relative DWBA cross sections using the Goldhaber-Teller model compared to the resonance at 16.3 MeV with a width of 4.5 MeV. Comparison identifies this resonance as E2. The free fit strength of this resonance at 45° was inconsistent at 75% EWSR and was held constant at the mean strength of the other four angles (i.e., 50% EWSR) in order not to interfere with the extraction of the E1 strength. Error bars of 15% were assumed for all data points.

FIGURE 36

Relative DWBA cross sections using the Goldhaber-Teller model compared to the resonance at 18.3 MeV with a width of 4.2 MeV. Comparison based on the three forward angles favors an E1 assignment. A free fit of this resonance at 90° produced low values of transition strength while high values were obtained at 105°. It was also noted that the

strength of this resonance at 45° increased from 64% to 72% EWSR when the E2 resonance at 16.3 MeV was fixed to 50% EWSR. This indicates a possible interdependence of the E1 and E2 resonances near this excitation energy at low momentum transfer. Error bars of 15% were estimated.

FIGURE 37

Relative DWBA cross section calculated with the Goldhaber-Teller model for the structure in ^{58}Ni at 20.0 MeV with a width of 5.0 MeV. An E4 assignment is favored based on this limited data. The statistical error of 29% and 17% was taken for 90° and 105°, respectively, because they were greater than the estimated uncertainty from background variations.

FIGURE 38

Relative DWBA cross section calculated with the Goldhaber-Teller model for the structure in ^{58}Ni at 21.75 MeV with a width of 5.0 MeV. Comparison favors an E1 assignment. Transition strength for the backward angles was fixed to the mean value of the forward angles, 25% EWSR. This is justified since an insignificant E1 contribution is expected at 90° and 105°. A free fit produced 86% EWSR at 90° and 139% EWSR at 105°. Error bars of 15% were assumed.

FIGURE 39

Relative DWBA cross section calculated with the Goldhaber-Teller model for the structure in ^{58}Ni at 27.0 MeV and a width of 6.0 MeV. Either an E2 or E3 assignment is possible in the comparison.

A free fit of this resonance at 45° produces a value of higher strength. It is also noted that fixing the strength of the E1 resonances at 90° and 105° produced lower values at these angles for the 27.0 MeV transition. Statistical errors of 36%, 45%, and 55% were obtained from the fitting program for 75°, 90°, and 105°, respectively. These errors are reflected in the error bars indicated in this figure.

FIGURE 40

Relative DWBA cross section calculated with the Goldhaber-Teller model for the structure in ^{58}Ni at 32.0 MeV and with a width of about 10 MeV. An E2 assignment was favored in the comparison. Due to the unexplained dip in the 60° spectrum between 33 and 36 MeV (see Figure 3), the strength of this resonance was inconsistently low (i.e., 25% EWSR) and was therefore, fixed to the mean value of 47% EWSR. Although this resonance could not be detected in the spectrum at 45°, the symbol "□" corresponds to a resonance with a height of one standard deviation in the count rate and is, therefore, regarded as an upper limit. The error at 45° represents one additional standard deviation. An error of 20% was estimated for the value at 75°, while statistical errors of 25% and 27% were used for the values at 90° and 105°, respectively.

FIGURE 41

Relative DWBA cross section using the Goldhaber-Teller model compared to the state in ^{60}Ni at 6.12 MeV with a width of 0.7 MeV. The comparison favors an E2 assignment. Error bars of 15% were estimated, except at 45° where the statistical error was 21%.

FIGURE 42

Similar to Figure 41 except that the comparison was made for the combined strength of the states at 7.0 and 7.6 MeV in ^{60}Ni with widths of 0.7 and 0.95 MeV, respectively. These states were considered together due to their close proximity in excitation energy and the resulting interdependence seen during the fitting process. Comparison favors an E3 assignment. Error bars of 15% were estimated.

FIGURE 43

Relative DWBA cross section using the Goldhaber-Teller model compared to the state in ^{60}Ni at 8.7 MeV with a width of 0.97 MeV. The comparison favors an E3 assignment. An error bar of 15% was estimated for the value at 90°. Statistical errors of 21% and 16% were reflected in the error bars for 75° and 105°, respectively.

FIGURE 44

Relative DWBA cross section using the Goldhaber-Teller model compared to the state in ^{60}Ni at 11.4 MeV with a width of 1.2 MeV. The comparison favors an E4 assignment based on this limited data. Statistical error bars of 30% and 23% are indicated for 90° and 105°, respectively.

FIGURE 45

Relative DWBA cross section using the Goldhaber-Teller model compared to the resonance in ^{60}Ni at 12.8 MeV with a width of 1.5 MeV. An E3 assignment is somewhat favored over an E4 assignment in

the comparison. In the case of either the E3 or E4 DWBA curve, one data point lies above and one lies below by more than the estimated error bars. However, the two central data points lie well within the error bars in the case of the E3 assignment, while the E4 curve is just contained within the error bars, passing below the data point at 75° and above the point at 90°. An error of 15% was estimated for all points except the value at 60°, where the statistical error was 27%.

FIGURE 46

Relative DWBA cross section using the Goldhaber-Teller model compared to a resonance in ^{60}Ni at 14.9 MeV with a width of 2.1 MeV. The value at 75° was fixed to the mean value obtained at 90° and 105°. Comparison favored an E4 assignment for this resonance. The statistical error of 36% in the value at 90° is indicated by the error bar. An error of 15% was estimated for the value at 105°.

FIGURE 47

Relative DWBA cross section using the Goldhaber-Teller model compared to the resonance in ^{60}Ni at 16.2 MeV with a width of 4.7 MeV. Comparison favors an E2 assignment. Error bars of 15% were estimated for the values at 60°, 75°, and 105°. The statistical errors of 20% and 22% for the values at 45° and 90°, respectively, are indicated.

FIGURE 48

Relative DWBA cross section using the Goldhaber-Teller model compared to the resonance in ^{60}Ni at 16.7 MeV with a width of 2.1 MeV. An E1 assignment is indicated by the comparison. The value at 105° was fixed due to its small contribution at this momentum transfer. Error bars of 15% were estimated for the values at 45° and 75°, while the statistical errors of 17% and 46% were used to determine the error bars for the values plotted at 60° and 90°, respectively.

FIGURE 49

Relative DWBA cross section using the Goldhaber-Teller model compared to the resonance in ^{60}Ni at 18.6 MeV with a width of 4.0 MeV. The value at 75° was fixed due to the insignificant strength of this resonance at this momentum transfer. The comparison favors an E4 assignment. A statistical error bar of 23% was plotted for the value at 90° while an error bar of 15% was estimated for the value at 105°.

FIGURE 50

Relative DWBA cross section using the Goldhaber-Teller model compared to the resonance in ^{60}Ni at 19.2 MeV with a width of 6.0 MeV. Comparison favors an E1 assignment. The values at 90° and 105° were fixed at the mean strength found in the forward angles (51% EWSR) due to the small contribution of this resonance to the total cross section at 90° and 105°. Error bars of 15% were estimated.

FIGURE 51

Relative DWBA cross section using the Goldhaber-Teller model compared to the resonance in ^{60}Ni at 21.1 MeV with a width of 6.0 MeV. Comparison favors an E3 assignment, although neither an E2 nor an E4 assignment can be discounted. Statistical error bars of 43%, 21%, and 17% were plotted for the values at 60°, 75°, and 90°, respectively. An error of 15% was assumed for the value at 105°.

FIGURE 52

Relative DWBA cross section using the Goldhaber-Teller model compared to the resonance in ^{60}Ni at 32.0 MeV with a width of about 9 MeV. The comparison favors an E2 assignment. The value at 60° was fixed since a free fit of this resonance in the 60° spectrum yielded a consistently smaller strength than that found in the adjacent angles. This is possibly due to the greater statistical fluctuations associated with this higher excitation energy and larger momentum transfer. The free fit value at 105° is plotted as well as is the fixed value to indicate the additional strength observed in this resonance at the higher momentum transfer we measured. Error bars of 15% were estimated for the plotted values except at 45° where the statistical error was 42%.

LIST OF REFERENCES

AkyF71 Akyüz, R.Ö. and Fallieros, S.: Phys, Rev. Letters 27, 1016 (1971).

BarC66 Barnett, M.T. and Cuneen, W.J.: Design and Performance of the Electron Linear Accelerator at the Naval Postgraduate School, M.S. Thesis, Naval Postgraduate School, Monterey, Ca., unpublished (1966).

BerF75 Berman, B.L. and Fultz, S.C.: Rev. Mod. Phys. 47, 713 (1975).

Berm74 Berman, B.L.: Atlas of Photoneutron Cross-Sections Obtained with Monoenergetic Photons, 2nd. Ed., Lawrence Livermore Laboratory, Livermore, Ca. (1974).

Broe63 Broek, H.W.: Phys. Rev. 130, 1914 (1963).

BusG72 Buskirk, F.R., Gräf, H.D., Pitthan, R., Theissen, H., Titze, O. and Walcher, T.: Phys. Letters 42B, 194 (1972).

ChaB75 Chang, C.C., Bertrand, F.E. and Kocher, D.C.: Phys. Rev. Letters 34, 221 (1975).

CraH61 Crannell, H., Helm, R., Kendall, H., Oeser, J. and Yearian, M.: Phys. Rev. 123, 923 (1961).

deJd74 de Jager, C.W., de Vries, H. and de Vries, C.: Atomic Data and Nuclear Tables 14, 479 (1974).

Denn70 Dennis, S.J.: Calculation of Electron Scattering Cross Sections for Carbon-Twelve and Lithium-Six using Phase Shift Analysis, M.S. Thesis, Naval Postgraduate School, Monterey, Ca., unpublished (1970).

Drec68 Drechsel, D.: Nucl. Phys. A113, 665 (1968).

DuBB76 DuBois, II, D.H. and Bates, G.M.: Electro-excitation of Giant Resonances in ^{60}Ni between 5 MeV and 30 MeV Excitation Energy, M.S. Thesis, Naval Postgraduate School, Monterey, Ca., unpublished (1976).

Fagg75 Fagg, L.W.: Rev. Mod. Phys. 47, 683 (1975).

FalG65 Fallieros, S., Goulard, B. and Venter, R.H.: Phys. Letters 19, 5, 398 (1965).

FalG70 Fallieros, S. and Goulard, B.: Nucl. Phys. A147, 593 (1970).

FerW74 Ferlic, K.P. and Waddell, R.D.: Electroexcitation of Giant Resonances between 5 MeV and 40 MeV Excitation Energy in ^{197}Au, M.S. Thesis, Naval Postgraduate School, Monterey, Ca., unpublished (1974).

FisR64 Fischer, C.R. and Rawitscher, G.H.: Phys. Rev. 135, B377 (1964).

FukT72 Fukuda, S. and Torizuka, Y.: Phys, Rev. Letters 29, 1109 (1972).

FulA74 Fultz, S.C., Alvarez, R.A., Berman, B.L. and Meyer, P.: Phys, Rev. C10, 608 (1974).

GinP64 Ginsberg, E.S. and Pratt, R.H.: Phys. Rev. 134, B773 (1964).

GolT48 Goldhaber, M. and Teller, E.: Phys, Rev. 74, 1046 (1948).

GorI70 Goryachev, B.I., Ishkhanov, B.S., Kapitonov, I.M., Piskarev, I.M., Shevchenko, V.G. and Shevchenko, O.P.: Sov. J. Nucl. Phys. 11, 141 (1970).

GulA69 Gul'Karov, I.S., Afanas'Ev, N.G., Khvastunov, I.M., Shevchenko, N.G., Afanas'Ev, V.D., Savitskii, G.A. and Khomich, A.A.: Sov. J. Nucl. Phys. 9, 274 (1969).

Gulk71 Gul'Karov, I.S.: Sov. J. Nucl. Phys. 13, 178 (1971).

Gulk73 Bul'Karov, I.S.: Sov. J. Nucl. Phys, 18, 267 (1973).

Gulk74 Gul'Karov, I.S.: Sov. J. Nucl. Phys. 18, 267 (1974).

Hama72 Hamamoto, I.: in Proc. of the Int. Conf. on Nuclear Structure Studies Using Electron Scattering and Photoreaction, ed. by K. Shoda and H. Ui, Suppl. Res. Rep. Lab. of Nucl. Sci., Tohoku Univ., Vol. 5 (1972).

Hofs63 Hofstadter, R.: Nuclear and Nucleon Structure, Benjamin, New York, N.Y. (1963).

IsaB63 Isabelle, D.B. and Bishop, G.R.: Nucl. Phys. 45, 209 (1963).

IshK70 Ishkhanov, B.S., Kapitonov, I.M., Piskarev, I.M., Shevchenko, V.C. and Shevchenko, O.P.: Sov. J. Nucl. Phys. 11, 272 (1970).

KocB73 Kocher, D.C., Bertrand, F.E., Gross, E.E., Lord, R.S. and Newman, E.: Phys. Rev. Letters 31, 1070 (1973).

LewB72 Lewis, M.B., Bertrand, F.E. and Horen, D.J.: Nucl. Phys. A196, 337 (1972).

Migd44 Migdal, A.: J. Phys. USSR 8, 331 (1944).

MinW68 Min, K. and White, T.A.: Phys. Rev. Letters 21, 1200 (1968).

Miy073 Miyase, H., Oikawa, S., Suzuki, A., Uegaki, J., Saito, T., Sugawara, M. and Shoda, K.: in Proceedings of the International Conference on Photonuclear Reactions and Applications, Asilomar, March 1973, edited by B.L. Berman (Lawrence Livermore Laboratory, Livermore, Ca., 1973), p. 553.

MoaB73 Moalem, A., Benenson, W. and Crawley, G.M.: Phys. Rev. Letters 31, 482 (1973).

Moor74 Moore, G.L.: Electroexcitation of Giant Resonances Between 5 MeV and 30 MeV Excitation Energy in ^{165}Ho, M.S. Thesis, Naval Postgraduate School, Monterey, Ca., unpublished (1974).

Mott60 Mottelson, B.R.: in Int. Conf. on Nucl. Structure, ed. D.A. Bromely and E.W. Voigt, Univ. of Toronto Press and North-Holland Publishing Company, Amsterdam, Neth. (1960).

MosY76 Moss, J.M., Youngblood, D.H., Rozsa, C.M., Brown, D.R. and Bronson, J.D.: Phys. Rev. Letters 37, 816 (1976).

NatN66 Nathan, O. and Nilsson, S.G.: in Alpha, Beta, and Gamma-ray Spectroscopy, ed. by K. Siegbahn (North-Holland Publishing Company, Amsterdam, Neth., 1966), p. 601.

NgoR71 Ngo-Trong, C. and Rowe, D.J.: Phys. Letters 36B, 553 (1971).

PauA71 Paul, P., Amann, J.F. and Snover, K.A.: Phys. Rev. Letters 27, 1016 (1971).

PitB74 Pitthan, R., Buskirk, F.R., Dally, E.B., Dyer, J.N. and Maruyama, X.K.: Phys. Rev. Letters 33, 849 (1974).

PitB77 Pitthan, R., Buskirk, F.R., Dally, E.B., Shannon, J.O. and Smith, W.H.: Giant Resonances and Bound Collective States Observed in the Scattering of 92.5 MeV Electrons from the Closed Neutron Shell Nucleus ^{89}Y Between Excitation Energies from 2.0 to 55 MeV, Naval Postgraduate School, Monterey, Ca., to be published (1977).

PitW71 Pitthan, R. and Walcher, T.: Phys. Letters 36B, 563 (1971).

Rawi58 Rawitscher, G.H.: Phys. Rev. 112, 1274 (1958).

Satc73 Satchler, G.R.: New Giant Resonances in Nuclei, Physics Report, Oak Ridge National Laboratory, Oak Ridge, Tenn. (1973).

SchF75 Schwierczinski, A., Frey, R., Spamer, E., Theissen, H. and Walcher, T.: Phys. Letters 55B, 171 (1974).

ShaS76 Shannon, J.O. and Smith, W.H.: Electroexcitation of Giant Resonances between 6.1 MeV and 38 MeV Excitation Energy in ^{89}Y, M.S. Thesis, Naval Postgraduate School, Monterey, Ca., unpublished (1976).

SkoH66 Skorka, S.J., Hertel, J. and Retz-Schmidt, T.W.: Nucl. Data A2, 347 (1966).

Tana71 Tanaka, Y.: Progr. Theoret. Phys. (Kyoto) 46, 787 (1971).

Thei72 Theissen, H.: Spectroscopy of Light Nuclei by Low Energy Electron Scattering, Springer Tracts in Modern Physics, Vol. 65, Springer-Verlag, Berlin, Heidelberg, New York (1972).

TorK69 Torizuka, Y., Kojima, Y., Oyamada, M., Nakahara, K., Sugiyama, K., Terasawa, T., Itoh, K., Yamaguchi, A. and Kimura, M.: Phys. Rev. 185, 1499 (1969).

TorK73 Torizuka, Y., Kojima, Y., Saito, T., Itoh, K. and Nakada, A.: Res. Rep. Lab. Nucl. Sci., Tohoku Univ. 6, 165 (1973).

TuaW68 Tuan, S.T., Wright, L.E. and Onley, D.S.: Nucl. Instru. and Meth. 60, 70 (1968).

Über71 Überall, H.: Electron Scattering from Complex Nuclei, New York-London, Academic Press (1971).

WarW69 Warburton, E.K. and Weneser, J.: in Isospin in Nuclear Physics, ed. by D.H. Wilkinson (North-Holland Publishing Company, Amsterdam, Neth., 1969), p. 173.

WarW73 Warshawsky, A.S. and Webber, A.M.: Giant Multipole Resonances in ^{197}Au, M.S. Thesis, Naval Postgraduate School, Monterey, Ca., unpublished (1973).

YouM76 Youngblood, D.H., Moss, J.M., Rozsa, C.M., Bronson, J.D., Bacher, A.D. and Brown, D.R.: Phys. Rev. C 13, 994 (1976).

ZieP68 Ziegler, J.F. and Peterson, G.A.: Phys. Rev. 165, 1337 (1968).

INITIAL DISTRIBUTION LIST

		No. Copies
1.	Defense Documentation Center Cameron Station Alexandria, Virginia 22314	2
2.	Library, Code 0212 Naval Postgraduate School Monterey, Calif. 93940	2
3.	Department Chairman, Code 61 Department of Physics and Chemistry Naval Postgraduate School Monterey, Calif. 93940	2
4.	Professor F.R. Buskirk, Code 61Bs Department of Physics and Chemistry Naval Postgraduate School Monterey, Calif. 93940	3
5.	Professor J.N. Dyer, Code 61Dy Department of Physics and Chemistry Naval Postgraduate School Monterey, Calif. 93940	2
6.	Professor W.R. Pitthan, Code 61Pt Department of Physics and Chemistry Naval Postgraduate School Monterey, Calif. 93940	3
7.	LCDR John S. Beachy, USN College of Naval Command and Staff Naval War College Newport, Rhode Island 02840	1
8.	LCDR Stephen J. Kowalick Jr., USN USS DALE (CG-19) c/o Fleet Post Office New York, New York 09501	1